MESOPOROUS SILICA SUPPORTED CATALYSTS FOR CARBON-CARBON BOND FORMING REACTIONS

by

SUPARB TAMUANG

A thesis submitted to
The University of Birmingham
For the degree of
DOCTOR OF PHILOSOPHY

School of Chemistry
College of Engineering and
Physical Sciences
The University of Birmingham
August 2012

ABSTRACT

The synthesis and characterisation of well-ordered mesoporous silicas, MCM-41, MCM-48, SBA-1, and SBA-2 has been carried out successfully. All of the synthesised materials possess the expected characteristic ordering as confirmed by powder X-ray diffraction. Moreover, surface modification of these mesoporous silicas had also been achieved through the incorporation of alkylamine groups and attachment of an asymmetric organometallic nickel-salen complex.

The catalytic activity of the amino and nickel complex-modified mesoporous silica materials was examined for carbon-carbon bond forming reactions; Knoevenagel condensation of benzaldehyde and ethylcyanoacetate, and Kumada-Corriu coupling reaction between an organobromide and Grignard reagent, respectively. All the NH_2-mesoporous silica catalysts result in high conversion (>95%) and can easily be reused by washing with water. Furthermore, the catalytic performances of the asymmetric nickel-salen complex bound to mesoporous silicas were found to be greater than 60% which is comparable to the homogenous nickel complex catalyst (62% conversion) but are more easily recycled.

The further modification of catalysts to capture the remaining surface silanol groups in the modified-mesoporous silicas has been carried out by using chlorotrimethylsilane to obtain the surface functionalised with trimethyl groups instead of silanols. The methylated catalysts with MCM-41 and MCM-48 as support demonstrate better recyclability, while this was not observed in the cage-like SBA-1 and SBA-2 supports catalyst as the presence of additional trimethylsilyl groups could cause more pore blocking.

ACKNOWLEDGEMENTS

Firstly, I would like to thank the School of Chemistry, University of Birmingham and especially my supervisor, Dr Ian J Shannon, for giving me the opportunity to do my PhD here and also for all his help, guidance, and patient.

I would also like to thank all the school of chemistry analytical staffs; Mr Peter Ashton, Mr Nick May, Mr Graham Burns, Mrs Lianne Hill, Mrs Cheryl Powell, Dr Chi Tseng, and Dr Neil Spencer for their time and expertise helping me analyse my samples. Thanks Dr Jacqueline Deans and Dr Louise Male for the X-ray fluorescence and X-ray diffraction technical assistance. Thanks the Advantage West Midlands (AWM) for the research facilities. And I'm really grateful to Dr Roberto Portillo Reyes and Dr Marco Antonio Lopez Martinez at the Universidad Autónoma de Puebla, Mexico, for the surface area analysis. And I would also like to express my thankfulness to the Ministry of Science and Technology, Thailand for funding.

I would like to express my gratitude to Dr Shannon's former and present members, Dr Laura Perkins, Dr Marco Antonio Lopez Martinez, Selina Omonmhenle, and Chao Zhao. And also thanks all friends on the 4^{th} and 5^{th} floor for the enjoyable time throughout the period of my study, it is a really great pleasure to work with everyone.

Finally, the sincere thankfulness to my family for all their love and mental supports, I love you all.

CONTENTS

CHAPTER 1 INTRODUCTION 1

1.1 Use of catalysts 1

1.1.1 Homogeneous catalysts 1

1.1.2 Heterogeneous catalysts 2

1.2 Mesoporous materials 4

1.2.1 Overview of mesoporous materials 4

1.2.2 General synthesis of mesoporous materials 7

1.2.2.1 Mesoporous silicas 7

1.2.2.2 Non-siliceous materials 8

1.3 Modification of mesoporous materials 9

1.3.1 Modification of mesoporous materials with organic species 9

1.3.2 Modification of mesoporous materials by inorganic species 11

1.4 Mesoporous materials in catalysis 11

1.4.1 Acid catalysts 12

1.4.2 Base catalysts 15

1.4.3 Redox catalysts 17

1.4.4 Anchored molecular catalysts for enantioselective reactions 20

1.5 Aims of the study 25

CHAPTER 2 TECHNIQUES 26

2.1 X-Ray Diffraction (XRD) 26

2.1.1 Principles 26

2.1.2 Powder XRD 28

2.1.3 Instrument and experimental procedure 29

2.2 Nitrogen physisorption 32
2.2.1 Principles 32
2.2.1.1 Type of Isotherms 32
2.2.1.2 Surface area determination 34
2.2.1.3 Pore volume and pore size distribution 37
2.2.2 Experimental procedure 40
2.3 Gas Chromatography (GC) 40
2.3.1 Principles 40
2.3.2 Instrument and experimental procedure 41
2.4 Atomic Absorption Spectroscopy (AAS) 42
2.4.1 Principles 42
2.4.2 Instrument and experimental procedure 43
2.5 X-Ray Fluorescence (XRF) 44
2.5.1 Principles 44
2.5.2 Instrument and experimental procedure 45
2.6 CHN Analysis 46
2.7 Fureir Transform Infrared Spectroscopy (FTIR) 47
2.7.1 Principle 47
2.7.2 Instrument and experimental procedure 48
2.8 Nuclear Magnetic Resonance Spectroscopy (NMR) 49
2.8.1 Principle 49
2.8.1.1 Chemical Shift 51
2.8.1.2 Spin-Spin Coupling 52
2.8.2 Instrument and experimental procedure 52

CHAPTER 3 SYNTHESIS AND CHARACTERISATION OF ORDERED MESOPOROUS SILICAS 54

3.1 Introduction 54

3.1.1 Background of ordered mesoporous silicas 54

3.1.2 Method for preparation of ordered mesoporous silicas 57

3.1.3 Method of surfactant removal 60

3.1.3.1 Calcination 60

3.1.3.2 Solvent extraction 61

3.2 Experimental 61

3.2.1 Synthesis of MCM-41 61

3.2.2 Synthesis of MCM-48 61

3.2.3 Synthesis of SBA-1 62

3.2.3.1 Synthesis of hexadecyltriethylammonium bromide (CTEABr) 62

3.2.3.2 Synthesis of SBA-1 64

3.2.4 Synthesis of SBA-2 64

3.2.4.1 Synthesis of gemini quaternary ammonium surfactant surfactant ($C_{16\text{-}3\text{-}1}$) 64

3.2.4.2 Synthesis of SBA-2 66

3.2.5 Template removal 67

3.3 Results and discussion 68

3.3.1 Template removal results 68

3.3.2 Characterisation of ordered mesoporous materials by powder X-ray diffraction 71

3.3.3 Characterisation of mesoporous silicas by nitrogen adsorption-desorption 75

3.4 Conclusion 78

CHAPTER 4 AMINO MODIFIED MESOPOROUS SILICAS 79

4.1 Introduction 79

4.1.1 Modification of ordered mesoporous silicas 79

4.1.1.1 Direct synthesis 80

4.1.1.2 Post grafting method 80

4.1.2 Modification of mesoporous silicas by the amino group 81

4.2 Experimental 82

4.2.1 Post-synthesis grafting of mesoporous silicas with 3-aminopropyltrimethoxy silane 82

4.2.2 Catalytic activity testing 82

4.2.3 The reusability of amino-modified mesoporous silica 83

4.3 Results and Discussion 84

4.3.1 Characterisation of amino-modified mesoporous silicas 84

4.3.1.1 Characterisation of amino-mesoporous silicas by powder X-ray diffraction 84

4.3.1.2 Characterisation of amino-modified mesoporous silica by Elemental Analysis 87

4.3.1.3 Characterisation of amino-modified mesoporous silica by nitrogen adsorption-desorption 88

4.3.2 Activity of the synthesised catalysts 91

4.3.2.1 Catalytic activity of amino-modified mesoporous silica in the Knoevenagel condensation reaction 91

4.3.2.2 Catalyst recycling 94

4.3.2.3 Reaction mechanism 95
4.4 Conclusion 97
CHAPTER 5 ASYMMETRIC NICKEL-SALEN COMPLEX MODIFIED MESOPOROUS SILICAS 98
5.1 Introduction 98
5.1.1 Importance of nickel-catalysed carbon-carbon bond forming reaction 98
5.1.2 Heterogeneous nickel-catalysed carbon-carbon bond forming reaction 99
5.1.3 Nickel salen-type ligand compound 100
5.2 Experimental 102
5.2.1 Synthesis of [9-(2,4-dihydroxypheny)-5,8-diaza-4-methyl-non-2,3,8-trienato](2-) nickel(II); Nickel complex (1) 102
5.2.2 Modification of mesoporous silica by asymmetric nickel-salen complex 104
5.2.3 Catalytic testing using Kumada-Corriu reaction 106
5.3 Results and discussion 107
5.3.1 Characterisation of (1)-mesoporous silicas 107
5.3.1.1 Characterisation of (1)-mesoporous silicas by powder X-ray diffraction 107
5.3.1.2 Characterisation of the (1)-mesoporous silicas by X-ray fluorescence (XRF) 110
5.3.1.3 Characterisation of (1)-mesoporous silicas by Elemental Analysis 111
5.3.1.4 Characterisation of (1)-mesoporous silicas by nitrogen adsorption-desorption 112
5.3.2 Catalytic testing 117
5.3.2.1 Catalytic testing of (1)-mesoporous silicas 117

5.3.2.2 Catalyst reusability 120
5.3.3 Post-reaction solution study 121
5.3.4 Reaction mechanism 124
5.4 Conclusion 125
CHAPTER 6 FURTHER METHYLATION ON MODIFIED MESOPOROUS SILICAS…… 126
6.1 Introduction 126
6.2 Experimental 128
6.2.1 Methylated amino-mesoporous silicas 128
6.2.2 Methylated (1)-mesoporous silicas 129
6.3 Results and discussion 129
6.3.1 Me-NH_2-mesoporous silicas 129
6.3.1.1 Characterisation of Me-NH_2-mesoporous silicas by powder X-ray diffraction (XRD) 129
6.3.1.2 Characterisation of Me-NH_2-mesoporous silicas by nitrogen adsorption-desorption 134
6.3.1.3 Characterisation of Me-NH_2-mesoporous silicas by Elemental Analysis 136
6.3.1.4 Catalytic testing of Me-NH_2-mesoporous silicas 137
6.3.1.5 Catalyst recycling 138
6.3.2 Me-(1)-mesoporous silicas 141
6.3.2.1 Characterisation of Me-(1)-mesoporous silicas by powder X-ray diffraction (XRD) 141
6.3.2.2 Characterisation of Me-(1)-mesoporous silicas by Elemental Analysis 145

6.3.2.3 Characterisation of Me-(1)-mesoporous silicas by X-ray fluorescence spectroscopy (XRF) 145
6.3.2.4 Characterisation of Me-(1)-mesoporous silicas by nitrogen adsorption-desorption 146
6.3.2.5 Catalytic testing 149
6.3.2.6 Catalyst recycling 150
6.3.2.7 Post reaction solution study 152
6.4 Conclusion 153
CHAPTER 7 CONCLUSIONS AND FUTURE WORK 155
7.1 Conclusions 155
7.2 Future work direction 156
REFERENCES 159

LIST OF FIGURES

Figure 1.1 Pore structure of MCM-41 5

Figure 1.2 Structure of MCM-48 5

Figure 1.3 Proposed assembly structure for MSU-V 6

Figure 1.4 Channel system of SBA-2 6

Figure 1.5 Most frequently used functionalised organosilanes for the modification of mesoporous silicas 10

Figure 1.6 Isomerrisation of *endo*-dicyclopentadiene 13

Figure 1.7 Production of jasminaldehyde 14

Figure 1.8 Propanesulfonic (A) and benzenesulfonic (B) -mesoporous silica catalysts 14

Figure 1.9 Knoevenagel condensation of benzaldehyde and ethyl cyanoacetate 15

Figure 1.10 Acid-base bifunctionalised mesoporous silicas 17

Figure 1.11 Deacetalisation-Knoevanegel reaction 17

Figure 1.12 One-pot deacetalisation-nitroaldol cascade reaction 17

Figure 1.13 Oxidation reaction of sulfides 18

Figure 1.14 Schematic diagram of the pathways for the immobilisation lisation of the molecular catalyst onto mesoporous silicas surface 21

Figure 1.15 Enantioselective alkylation of benzaldehyde with diethylzinc 22

Figure 1.16 Two-step hydrogenation of ethyl nicotinate to ethyl nipecotinate 23

Figure 1.17 Allylic amination of cinnamylacetate 23

Figure 1.18 Schematic representation of the pore confinement concept 24

Figure 2.1 Bragg's scattering of X-rays from parallel planes with d representing inter-planar spacing 27

Figure 2.2 Formation of the diffraction cone 28

Figure 2.3 X-ray emission spectrum of Cu....30
Figure 2.4 General layout of X-ray diffractometer....31
Figure 2.5 Types of gas adsorption-desorption isotherms....33
Figure 2.6 The BET adsorption model....34
Figure 2.7 BET plot....36
Figure 2.8 Instrumentation diagram of the typical GC....41
Figure 2.9 Diagram of the flame atomic absorption spectrometer....43
Figure 2.10 Diagram of the conventional XRF....45
Figure 2.11 Simple layouts of the vibrational modes associated to a molecular dipole moment change detectable in an IR absorption spectrum....48
Figure 2.12 Diagram of FTIR spectrometer....49
Figure 2.13 Block diagram of a typical NMR spectrometer....53
Figure 3.1 Liquid crystal templating for the synthesis of ordered mesoporous MCM-41....55
Figure 3.2. General scheme for the synthesis mechanism of mesoporous silica....56
Figure 3.3 Reaction scheme for the synthesis of CTEABr....62
Figure 3.4 NMR spectrum of CTEABr....63
Figure 3.5 FTIR spectrum of CTEABr....63
Figure 3.6 Reaction scheme for the synthesis of $C_{16\text{-}3\text{-}1}$....65
Figure 3.7 NMR spectrum of $C_{16\text{-}3\text{-}1}$ surfactant....65
Figure 3.8 FTIR spectrum of $C_{16\text{-}3\text{-}1}$ surfactant....66
Figure 3.9 FTIR spectra of a) calcined MCM-48, b) extracted MCM-48, and c) As-synthesised MCM-48....69
Figure 3.10 Powder X-ray diffraction patterns for a calcined MCM-48, extracted MCM-48, and As-synthesised MCM-48....70

Figure 3.11 Powder X-ray diffraction pattern of MCM-41 73
Figure 3.12 Powder X-ray diffraction pattern of MCM-48 73
Figure 3.13 Powder X-ray diffraction pattern of SBA-1 74
Figure 3.14 Powder X-ray diffraction pattern of SBA-2 74
Figure 3.15 Nitrogen adsorption-desorption isotherm and pore size distribution of MCM-41 76
Figure 3.16 Nitrogen adsorption-desorption isotherm and pore size distribution of MCM-48 76
Figure 3.17 Nitrogen adsorption-desorption isotherm and pore size distribution of SBA-1 ... 77
Figure 3.18 Nitrogen adsorption-desorption isotherm and pore size distribution of SBA-2 ... 77
Figure 4.1 Amino-modified mesoporous silica 82
Figure 4.2 Knoevenagel condensation reaction of benzaldehyde and ethylcyanoacetate 83
Figure 4.3 Powder X-ray diffraction pattern of NH_2-MCM-41 85
Figure 4.4 Powder X-ray diffraction pattern of NH_2-MCM-48 85
Figure 4.5 Powder X-ray diffraction pattern of NH_2-SBA-1 86
Figure 4.6 Powder X-ray diffraction pattern of NH_2-SBA-2 86
Figure 4.7 Nitrogen adsorption-desorption isotherm of NH_2-MCM-41 89
Figure 4.8 Nitrogen adsorption-desorption isotherm of NH_2-MCM-48 89
Figure 4.9 Knoevenagel condensation of benzaldehyde and ethylcyanoacetate 91
Figure 4.10 Conversion of Knoevenagel condensation reaction using NH_2-mesoporous silica as catalyst at different time 92
Figure 4.11 Reusability of the amino-modified mesoporous silica catalysts 94
Figure 4.12 Proposed mechanism of the Knoevenagel condensation reaction using NH_2-mesoporous silica as the catalyst 96

Figure 5.1 $Ni(acac)_2$-diamine anchored SBA-1 100

Figure 5.2 Synthesis scheme for [9-(2,4-dihydroxypheny)-5,8-diaza-4-methyl-non-2,3,8-trienato](2-) nickel(II) 103

Figure 5.3 NMR spectrum for compound (1) 104

Figure 5.4 Modification of mesoporous silica with the asymmetric nickel-salen complex 105

Figure 5.5 Powder x-ray diffraction patterns of MCM-41 and (1)-MCM-41 108

Figure 5.6 Powder x-ray diffraction patterns of MCM-48 and (1)-MCM-48 108

Figure 5.7 Powder x-ray diffraction patterns of SBA-1 and (1)-SBA-1 109

Figure 5.8 Powder x-ray diffraction patterns of SBA-2 and (1)-SBA-2 109

Figure 5.9 Nitrogen adsorption-desorption isotherm and pore size distribution of (1)-MCM-41 114

Figure 5.10 Nitrogen adsorption-desorption isotherm and pore size distribution of (1)-MCM-48 114

Figure 5.11 Nitrogen adsorption-desorption isotherm and pore size distrubution of (1)-SBA-1 115

Figure 5.12 Nitrogen adsorption-desorption isotherm and pore size distribution of (1)-SBA-2 115

Figure 5.13 Kumada-Corriu reaction between benzaldehyde and phenylmagnesium bromide 117

Figure 5.14 Conversion of Kumada-Corriu reaction upon recycling 121

Figure 5.15 Proposed catalytic cycle of Kumada-Corriu reaction 124

Figure 6.1 Hydrogen bond between basic site and silanol group on mesoporous silica sufrace 127

Figure 6.2 Surface modification of NH_2-mesoporous silica with TMCS 128

Figure 6.3 Powder X-ray diffraction pattern of Me-NH_2-MCM-41 131

Figure 6.4 Powder X-ray diffraction pattern of Me-NH_2-MCM-48 131

Figure 6.5 Powder X-ray diffraction pattern of Me-NH_2-SBA-1 132

Figure 6.6 Powder X-ray diffraction pattern of Me-NH_2-SBA-2 132

Figure 6.7 Nitrogen adsorption-desorption isotherm and pore size distribution of Me-NH_2-MCM-41 134

Figure 6.8 Nitrogen adsorption-desorption isotherm and pore size distribution of Me-NH_2-MCM-48 135

Figure 6.9 Catalyst recycling for Me-NH2-mesoporous silica 140

Figure 6.10 Catalyst recycling for NH_2-mesoporous silica 140

Figure 6.11 Powder X-ray diffraction pattern of Me-(1)-MCM-41 142

Figure 6.12 Powder X-ray diffraction pattern of Me-(1)-MCM-48 142

Figure 6.13 Powder X-ray diffraction pattern of Me-(1)-SBA-1 143

Figure 6.14 Powder X-ray diffraction pattern of Me-(1)-SBA-2 143

Figure 6.15 Nitrogen adsorption-desorption isotherm and pore size distribution of Me-(1)-MCM-41 147

Figure 6.16 Nitrogen aAdsorption-desorption isotherm and pore size distribution of Me-(1)-MCM-48 147

Figure 6.17 Nitrogen adsorption-desorption isotherm and pore size distribution of Me-(1)-SBA-1 148

Figure 6.18 Conversion upon recycling for Me-(1)-mesoporous silica catalysts 151

Figure 6.19 Conversion upon recycling for (1)-mesoporous silica catalysts 151

LIST OF TABLES

Table 3.1 Packing parameter in the synthesis of mesoporous silicas 57

Table 3.2 Unit cell parameter of crude MCM-48, calcined MCM-48, and extracted MCM-48 70

Table 3.3 BET Surface area, pore diameter, and pore volume of the synthesised mesoporous silicas 78

Table 4.1 Unit cell parameter, a, for amino-modified mesoporous silica 87

Table 4.2 Elemental analysis results for amino-modified mesoporous silica 87

Table 4.3 Surface area, pore size and pore volume of amino-modified mesoporous materials 90

Table 4.4 Conversion of Knoevenagel condensation reaction using NH_2-mesoporous silica as catalyst at 1 hour 92

Table 5.1 Unit cell parameter of (1)-mesoporous silicas and their corresponding pure materials 110

Table 5.2 Nickel content in (1)-mesoporous silicas determined by XRF 111

Table 5.3 Elemental analysis results for (1)-mesoporous silicas 112

Table 5.4 Surface area, pore diameter and pore volume of (1)-mesoporous silicas 116

Table 5.5 Conversion of Kumada-Corriu reaction 118

Table 5.6 Nickel leached from Kumada-Corriu reaction using nickel complex-modified mesoporous silicas catalyst 122

Table 5.7 Amount of the remained nickel in the inactive catalyst 123

Table 6.1 Unit cell parameter of pure mesoporous silica, NH_2-mesoporous silica, and Me-NH_2-mesoporous silica 133

Table 6.2 Surface area, pore size and pore volume of the Me-NH_2-mesoporous silicas 136

Table 6.3 Elemental analysis results for Me-NH_2-mesoporous silicas 137

Table 6.4 Catalytic activity of the Methylated-amino-modified mesoporous silicas..... 137

Table 6.5 Unit cell parameter of pure mesoporous silica, (1)-mesoporous silica, and Me-(1)-mesoporous silicas..... 144

Table 6.6 Elemental Analysis results for Me-(1)-mesoporous silicas..... 145

Table 6.7 Nickel content in Me-(1)-mesoporous silica determined by XRF 146

Table 6.8 Surface area, pore size, and pore volume of Me-(1)-mesoporous silicas..... 148

Table 6.9 Conversion of Kumada-Corriu reaction using Me-(1)-mesoporous silicas 150

Table 6.10 Nickel leached from Kumada-Corriu reaction using Me-(1)-mesoporous silicas..... 152

Table 6.11 Remaining nickel in the deactivated catalysts for Me-(1)-mesoporous silicas 153

ABBREVIATIONS

AAS	Atomic Absorption Spectroscopy
CTAB	Hexadecyltrimethylammonium bromide
CTEABr	Hexadecyltriethylammonium bromide
FTIR	Fourier Transform Infrared Spectroscopy
GC	Gas Chromatography
MCM-41	Mobil Composition of Matter number 41
MCM-48	Mobil Composition of Matter number 48
NMR	Nuclear Magnetic Resonance Spectroscopy
SBA-1	Santa Barbara number 1
SBA-2	Santa Barbara number 2
TEOS	Tetraethyl orthosilicate
XRD	X-Ray Diffraction
XRF	X-Ray Fluorescence

CHAPTER 1 INTRODUCTION

1.1 USE OF CATALYSTS

Catalysis is the phenomenon that takes place in a chemical reaction when a catalyst is used. A catalyst is a substance that accelerates a chemical reaction but is not consumed in the reaction and does not affect the reaction equilibrium. Catalysts cause the reactions to proceed faster than they would otherwise by somehow combining with the reactant molecules so that they are rearranged into the product molecules, and the catalyst can be regenerated and be used over and over again. Catalysts can accelerate the reaction because they provides a new and easier pathway for reactants molecule to be converted to the products, or they might be guided rapidly along an indirect pathway which is more complicated but faster[1].

Catalysis is essential in the chemical industry as well as in organisms. Most of the products consumed in daily life such as polymers, pharmaceuticals, food and drinks, combustibles, and detergents, were produced by using a catalyst at some stage in their processing. As the catalytic technologies play an important role in the global economy, the study and development of this area is of the great interest.

Catalyst systems are categorised into two main groups, which are homogeneous and heterogeneous catalysts.

1.1.1 Homogeneous catalysts

Homogeneous catalysts are usually liquid or soluble in the solvent (or reactants) used in the reaction; this leads to a homogeneous distribution of the catalyst in the system and results in the participation of all molecules in the catalytic process. Therefore, these catalysts usually provide high activity. Organometallic compounds are widely used as homogeneous catalysts

due to the variety of metal centres and organic ligands available, so a wide range of reactions can be performed. However, difficulty with separation of the catalyst from the reaction mixture, and also catalyst recovery and recycling can be major drawbacks of homogeneous catalysts, as these are time and cost consuming processes.

Examples of reactions catalysed by organometallic complexes as the homogeneous catalysts include polymerisation, addition, and oxidation of olefins.

1.1.2 Heterogeneous catalysts

Unlike homogeneous catalysts, heterogeneous catalysts are in a different phase to the reactants or, in other words, the catalysts are insoluble in the reaction mixture. Most heterogeneous catalysts are solid. In general, the chemical processes involved in the heterogeneous catalysed reaction are more complicated. The catalytic process starts with the diffusion of the reactants toward the catalyst and adsorption on the catalyst surface. The reaction normally takes place on the surface of the catalyst, then the products will be desorbed from the surface and diffused away from the catalysts. They are easier to be separated from the reaction mixture (e.g. by filtration), and also easier to handle and reuse compared to the homogeneous catalysts.

As described above, heterogeneous catalytic reactions normally take place on the catalyst surface, and the materials are more complex than the homogeneous ones. Generally, heterogeneous catalysts are composed of an active site and a support matrix. The active site is responsible for the catalyst activity whilst the support is the cast where the active site is loaded; the support materials are usually solids that provide a large surface area for the active site to be accommodated and also provide mechanical and thermal stability.

The chemical industry is in a continual search for new catalyst systems with improved properties over current technologies. While homogeneous catalysts usually demonstrate higher activity and selectivity than is found for heterogeneous catalysts, problems and expense in the recycling of the catalysts after reaction often prohibit the commercial use of the processes based on such systems. Hence, an area of particular interest is in the development of catalysts which retain desirable properties of current catalysts, but can be easily and cheaply recovered after the reaction. The immobilisation of organometallic, inorganic, and organic catalysts on the surface of solid supports, generates catalysts with a large number of accessible and well-defined active sites. According to their variety of pore architectures, porous materials which are mesoporous silicas are amongst the important solid catalyst supports and will be focused in this study.

1.2 MESOPOROUS MATERIALS

1.2.1 Overview of mesoporous materials

According to the IUPAC definition, there are three types of porous materials which are microporous (pore size <2 nm), mesoporous (pore size 2-50 nm), and macroporous (pore size >50 nm) materials[2]. Many types of porous materials such as pillared clays, carbon nanotubes and related porous carbons, and anodic alumina are widely studied[3]. Zeolites which possess a narrow and uniform pore size distribution are the best known microporous members. Zeolites can efficiently be used as the solid catalyst in the petroleum and petrochemical industries instead of liquid catalysts due to economic and environmental considerations. However, because of their micropores, limitations in terms of mass transfer cause problems when large reactant molecules are involved. Hence, the enlargement of pore size in order to allow the larger molecules to enter the pore system is of interest.

The first reported mesoporous material was synthesised in 1969[4]; however, due to lack of analysis, the characteristics of this product were not recognised. In 1990, hexagonally packed mesoporous materials synthesised by using a layered sodium silicate, Kanamite, as silica source were reported by Yanagisawa et al[5]. This material is called FSM-n; Folded Sheet Materials-n, where n is the number of carbon atom in the alkyl chain from the surfactant used in the synthesis procedure[6, 7].

The most significant breakthrough in the mesoporous materials research area arose when the scientists in Mobil Oil Corporation discovered the M41S family of materials[8, 9]. MCM-41 (Mobil Composition of Matter number 41) is the most studied member of materials in this family. This material shows a highly ordered hexagonal array of mesopores with a narrow pore size distribution but the wall characteristics are similar to amorphous silica.

Other related silica mesoporous phases were also reported by this research group such as a cubic MCM-48[10] and a lamellar MCM-50[11]. These materials possess a large pore diameter, uniform pore size distribution, high surface area and pore volume.

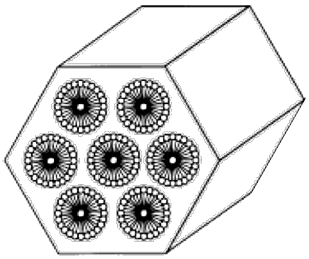

Figure 1.1 Pore structure of MCM-41[12]

Figure 1.2 Structure of MCM-48[13]

Following the discovery of M41S materials, various other families of mesoporous materials have been developed. Hexagonal mesoporous silica (HMS)[14] and Michigan State University materials (MSU)[15-17] are amongst the examples of mesoporous materials reported by Pinnavania et al. These materials were synthesised by using neutral or non-ionic surfactants such as primary amines and poly(ethylene oxides) as structure directing agent. HMS possesses a slightly disordered hexagonal structure whilst a worm-like structure is observed in MSU. Compared to MCM-41, HMS and MSU have similar surface areas and pore volumes but broader pore size distribution. In addition, their pore walls are thicker than these of MCM-41.

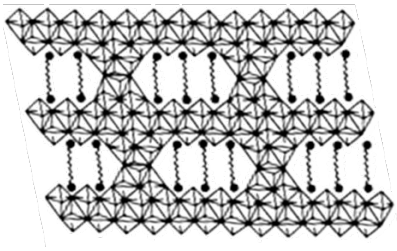

Figure 1.3 Proposed assembly structure for MSU-V[15]

In addition to the mesoporous materials mentioned above, there also another important family of such materials denoted as SBA-n (Santa Barbara-n)[18]. The hexagonal SBA-15, hexagonal SBA-3, 3-dimensional hexagonal SBA-2, and cubic SBA-1 are the members of this family. Typically, SBA materials exhibit significantly improved thermal and hydrothermal stability compared to other mesoporous silicas.

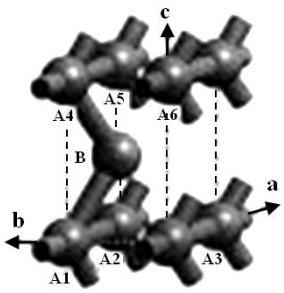

Figure 1.4 Channel system of SBA-2[19]

Another mesoporous silica known as Mesocellular Siliceous Foam (MCF)[20] materials consist of large spherical cells connected by windows to form a continuous matrix of pores, in a so called "aerogel-like" structure. The synthesis of MCF utilises triblock-copolymer stabilised oil in water as the template.

The porous materials are mostly silica based, prepared through the silica formation around the template micelles. In addition to preparation of mesoporous silicas, it is also possible to synthesise mesoporous structures from materials other than silica. Various

mesoporous metal oxides such as TiO_2, Ta_2O_5, Nb_2O_5, ZrO_2, Al_2O_3, and V_2O_5, etc., can be synthesised[21, 22].

1.2.2 General synthesis of mesoporous materials

The structural properties, morphology, and pore size engineering of the mesoporous materials are influenced by the synthesis method and also synthesis parameters.

1.2.2.1 Mesoporous silicas

Surfactant type, silica source, solvent, temperature, and also pH are the essential parameters to allow the formation of the final materials. The synthesis of materials and control of their properties can be limited by specific synthesis mechanisms and the interaction of the silica source with the surfactant molecules; therefore, fine tuning of the synthesised materials can be achieved by altering the synthesis parameters.

A general synthesis method for templated mesoporous silicas can be described as follows:

- Dissolution of surfactant in the solvent with the attention for other parameters such as pH, temperature, co-solvent, additives, etc.
- Addition of the silica source; TEOS, fumed silica, metasilicate, etc.
- Stirring at a certain temperature for a period of time to allow hydrolysis and condensation.
- Product recovery process, usually by filtration followed by washing and drying.
- Removal of the template.

When the synthesis mixture is being stirred, the temperature might be increased, sometimes combined with hydrothermal treatment or microwave synthesis, or even change of

the pH. Further details related to the synthesis of siliceous mesoporous materials will be discussed in Chapter 3.

1.2.2.2 Non-siliceous materials

In addition to the important parameters that control the structural formation discussed with the siliceous materials, special attention has to be paid to the hydrolysis rate, phase transformation, and redox reactivity. In general, the hydrolysis rate of transition metal oxides is much faster than that of silica. Therefore, the reduction of uncontrolled hydrolysis and condensation rate has to be achieved so that the good interaction between the surfactant and the inorganic source is obtained, as well as to prevent phase separation.

The main approaches to control the transition metal oxide precursor reactivity are:

- pH adjustment; hydrolysis and condensation are inhibited by acid, and this can also increase the solubility of the metal oxide[21-24].
- Retardation of hydrolysis by precursor complexation[25-27].
- Use of non-aqueous solvents and a controlled amount of water to prevent or slow down the hydrolysis[21, 22, 28, 29].

One or a combination of two or more, of these synthesis approaches can be applied to the synthesis procedure in order to gain maximum control of the final materials.

However, under thermal treatment, transition metal oxides are less stable than siliceous materials due to the possibility of redox reactions, phase transformation and also crystallisation. Therefore, solvent extraction methods to remove the surfactant are often applied to avoid structural collapse, and the formation of unwanted crystals upon calcination.

1.3 MODIFICATION OF MESOPOROUS MATERIALS

The modification of mesoporous materials has been carried out with a view to their potential use in different applications. Thermal stability of the mesoporous materials depends on the silica source and the wall thickness. In addition, hydrothermal stability is influenced by both the degree of silica polymerisation and again the wall thickness. On the other hand, mechanical stability is only slightly influenced by the nature of materials and normally enough for an application in catalysis[3, 30-32]. Since hydrothermal stability is an important factor for using mesoporous materials in various applications, a large number of studies on the modification of mesoporous materials, particularly to improve the hydrothermal stability of the resulting materials, have been carried out. However, most of these studies have been focused on MCM-41 and SBA-15 due to the easy synthesis method. Here are the methods for modification of mesoporous materials.

1.3.1 Modification of mesoporous materials with organic species

The addition of organosilanes or other organic compounds has been carried out to cover the silanol surface of the siliceous materials with a monolayer of organic material. Since the structural and hydrothermal stability are greatly influenced by the surface silanol groups, by covering those groups the surface hydrophobicity will be drastically increased and result in materials with improved hydrothermal stability[33].

This modification can be done either during or after the synthesis of the mesoporous solid. Modification during the mesoporous synthesis can be carried out by substitution of the silica source with a small amount (typically < 20%) of alkylalkoxysilane. The organosilane species will arrange themselves around the surfactant micelles along with the silicon atom from the normal silica source to form the remaining bulk of the materials. The incorporated

organic molecules can either be pendant on the wall surface[34] or incorporated as bridges between silicon atoms in the wall[35]. However, template removal from the materials modified by this method cannot be achieved by calcination as all the organic species would be destroyed at the required temperature. The modified materials prepared by this method exhibit smaller pore size and pore volume compare to the pure siliceous analogous but the surface area still remains high[33].

The grafting of organic molecules to the mesoporous solid after the synthesis of the mesoporous solid can also be achieved using organosilanes. The modification process is normally carried out under reflux conditions in dry solvent (such as dry toluene or dry THF). Pore size and surface area of the resulting materials are reduced but the moisture and compression stability are improved[36]. Moreover, this modification method has also been utilised for the addition of organometallic species to the mesoporous materials.

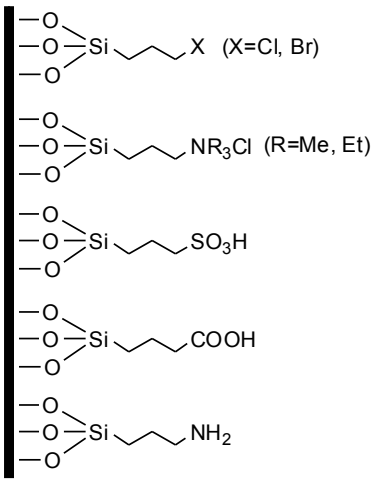

Figure 1.5 Most frequently used functionalised organosilanes for the modification of mesoporous silicas[3]

1.3.2 Modification of mesoporous materials by inorganic species

The incorporation of heteroatoms such as B, Fe, Ga, Ti, V, Sn, and particularly Al has been carried out in order to modify the composition of the mesoporous inorganic wall. As for the organic modification above, this can also be carried out either by the addition of heteroelement to the synthesis mixture containing silica source or by post-treatment of the prepared mesoporous materials. The post-treatment of synthesised materials can be achieved by solid state impregnation (grinding the surfactant-free mesoporous materials with a metal-salt followed by heating in air at 500 °C)[37] or wet impregnation (addition of a metal-salt solution to the mesoporous materials and heating at 60 °C for 3 hours, before the solvent is removed by calcination at 500 °C)[37]. Homogeneous incorporation of heteroatoms is observed when the modification has been done during the mesoporous synthesis, whilst the post-synthesis treatment primarily results in an increase of heteroatom concentration on the mesoporous solid surface.

One of the most common elements introduced is Al, to provide the acid sites to the mesoporous framework as in zeolites. Several forms of aluminium source such as aluminium isopropoxides, aluminium sulfates, sodium aluminates, and aluminium orthophosphates are utilised[38]. The Al-MCM-41 materials are normally less ordered and have a broader pore size distribution than their pure silica counterparts.

1.4 MESOPOROUS MATERIALS IN CATALYSIS

Due to their large pore diameter, pore volume, and also high surface area, mesoporous materials have been successfully applied as catalyst supports for a range of catalytic reactions, and sometimes the mesoporous materials are even used as the catalysts themselves. The

advantages of using mesoporous materials in catalysis are the high surface areas which permit high concentration of the active site, and also the relatively large pore size which allows better reactant and product diffusion. There are too many possible modifications of mesoporous materials for use as catalysts to list them all but below we discuss generally different examples of mesoporous materials used in catalysis.

1.4.1 Acid catalysts

Acid catalysts are normally used in cracking and other petrochemical conversions. The disadvantages of mesoporous materials in their use as catalysts in these processes are the low acid strength and low hydrothermal stability. However, the advantage in term of pore accessibility when large molecules are involved can be perhaps compensation. It is possible to induce activity in acid-catalysed reaction by the proper modification of mesoporous materials.

Normally, when trivalent cations such as Al^{3+}, B^{3+}, Ga^{3+}, Fe^{3+} substitute for silicon in the mesoporous silica, the framework will become negatively charged; this charge can be balanced by proton and the materials can be used in acid catalysed reactions. Amongst these trivalent cations, the highest acid strength of the modified materials achieved when Al^{3+} is incorporated, therefore the Al^{3+} is the most common element to be incorporated in the mesoporous structure; the obtained Al-mesoporous materials can imitate zeolite catalysts. The acid sites found in Al-mesoporous silica are both Brønsted and Lewis acid sites[39-41].

Al-MCM-41 has been used as catalyst in the cracking of tetralin and decalin and also the oligomerisation of n-hexane and n-heptane, it shows similar activity to amorphous silica-alumina but lower than that of β-zeolite[42-44]. In addition to petrochemical cracking reactions, Al-mesoporous materials can also be used as catalysts in reactions for fine chemical synthesis. Friedel-Crafts alkylations of electron rich aromatic compounds are successfully carried out

using Al-MCM-41 as catalyst[45-47]. The large pore opening of mesoporous materials provide the advantage of diffusion for bulky molecules that is restricted in microporous zeolites. The advantage of Al-mesoporous silica having larger pore compared with the microporous zeolites is also observed in the isomerisation of *endo*-dicyclopentadiene (Figure 1.6), when the Al-MCM-41 shows higher conversion and better coke tolerance capacity[48]. Al-MCM-41 are also found to be active in alkylation of naphthalene with propylene[49], three-component Strecker-type synthesis of alpha-aminonitriles[50], hydroisomerisation of n-dodecane[51], and esterification of acetic acid and in benzylation of anisole[52].

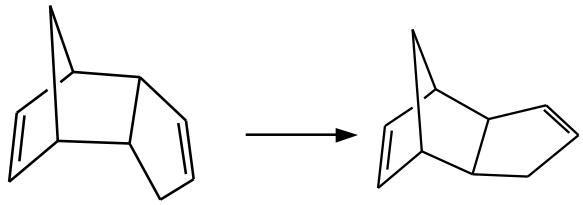

endo-dicyclopentadiene *exo*-dicyclopentadiene

Figure 1.6 Isomerrisation of *endo*-dicyclopentadiene

Acetalisation, which is one of the common reactions in the production of fine chemicals such as aromatic ketones, does not require strong acid sites and therefore mesoporous silica with weak to medium acid strength can be used as catalyst[53, 54]. This reaction is one of the steps in the one-pot, three consecutive reactions, production of α-*n*-amylcinnamaldehyde (jasminaldehyde), presented in Figure 1.7. Several catalysts, including Al-MCM-41 with various aluminium-silica ratio and β-zeolite were used. The large and uniform pore structures are required because they enable fast diffusion of the product and side reactions can be avoided[54].

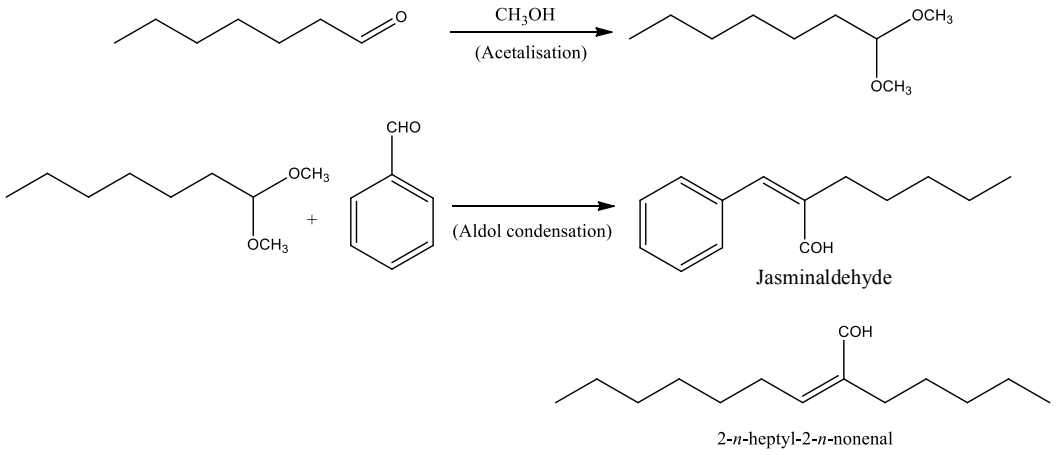

Figure 1.7 Production of jasminaldehyde[54]

Beckman rearrangement, glicosidation, and aldol condensation are further examples of mild acidity reactions which can be catalysed by the acid mesoporous materials especially when the large molecule reactants are involved[55, 56].

To enhance acidity of mesoporous silica, other functional groups such as propanesulfonic, benzenesulfonic, and phosphoric acid have also been incorporated. The propanesulfonic and benzenesulfonic-mesoporous silica catalysts (Figure 1.8) are active in the Friedel-Crafts alkylation of benzene and toluene with benzyl alcohol[57] and a one-pot Fischer indole synthesis of tryptophols[58], while phosphoric-mesoporous silica is active in the dialkylation of naphthalene with isopropanol[59].

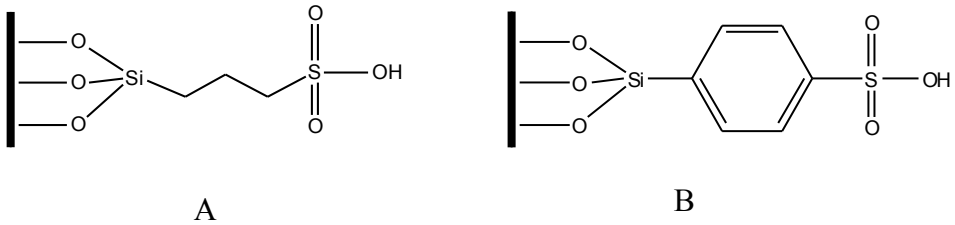

Figure 1.8 Propanesulfonic (A) and benzenesulfonic (B) -mesoporous silica catalysts

Since the ordered mesoporous aluminosilicates possess mild acidity, they are not suitable for use as catalysts in reactions that require strong acid sites such as paraffin isomerisation and isobutane/butene alkylation. In order to overcome this limitation, different methods of introducing strong acid sites to the mesoporous structure have been sought. The heteropolyacid ($H_3PW_{12}O_{40}$) was utilised as the strong acid sites[60, 61]; other than mesoporous silica, this heteropolyacid can also be incorporated into alumina and carbon supports[62].

1.4.2 Base catalysts

Mesoporous aluminosilicates can also be used as base catalysts when the negative charge is compensated by an alkaline ion[63, 64]. Following the same idea as with zeolites, the negative charge of each aluminum atom in Al-MCM-41 was balanced by Na^+ and Cs^+ ions and the resultant materials were found to be active for the base-catalysed Knoevenagel condensation reaction of benzaldehyde and ethyl cyanoacetate (Figure 1.9). The smaller the charge to radius ratio of the alkaline cation, the stronger basicity is; therefore the Cs^+ exchanged sample is more basic and hence more active than the Na^+ exchanged sample [65].

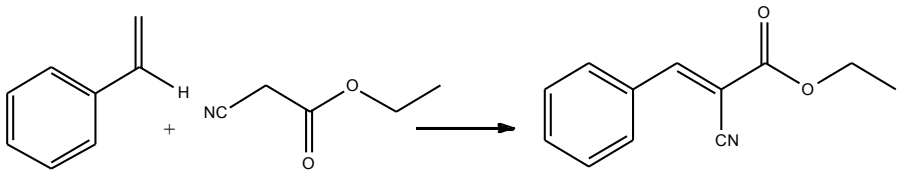

Figure 1.9 Knoevenagel condensation of benzaldehyde and ethyl cyanoacetate

Na^+-MCM-41 was also shown to be active in the more base demanding reaction of the condensation of benzaldehyde with diethylmalonate, but the reaction rate was very slow (6% conversion in 3 hours at 150 °C). When excess alkali is introduced, Na_2O and Cs_2O species can be formed, and the materials formed exhibit stronger basicity, which are active in

reactions demanding very strong base sites. However, difficulties in preparation process which requires no CO_2 and H_2O can be an inconvenience.

CaO was also incorporated to mesoporous silicas, MCM-41 and SBA-15, the obtained materials were used as catalyst in the base-catalysed transesterification for biodiesel production which are the reaction between ethylbutyrate [66] or sunflower oil [67] with methanol. The Ca-mesoporous silica catalysts in both reactions exhibited high conversion (>90%).

Base-catalysed reactions requiring less demanding conditions can also be catalysed by amines with different basicities[68, 69]. The heterogenisation of mesoporous silicas has been achieved with a range of amino functional groups, and the amine-mesoporous silicas are active in a range of reactions such as the Knoevenagel condensation and transesterification. The Knoevenagel condensation reaction catalyzed by amino-mesoporous silicas will be discussed in further detail in Chapter 4.

The acid-base bifunctionalised mesoporous silicas were synthesised[70-73] and found to be useful in one-pot sequential synthesis of organic molecules that require both acid and base-catalysed reactions in their synthesis steps. Amine with different basicity and sulfonic acid (Figure 1.10) are incorporated to mesoporous silicas MCM-41 and SBA-15. The NH_2-SO_3H-MCM-41 (Figure 1.10A) catalyst shows high activity in the one-pot deacetalisation-Knoevenagel reaction for the synthesis of benzylidene ethylcyanoacetate from ethylcyanoacetate with benzaldehyde dimethylacetate, the reaction scheme is shown in Figure 1.11 [74]. On the other hand, NNH-SO_3H-MCM-41 (Figure 1.10B) is found to be active in the one-pot deacetalisation-nitroaldol cascade reaction of (Figure 1.12), 95% conversion is observed[75].

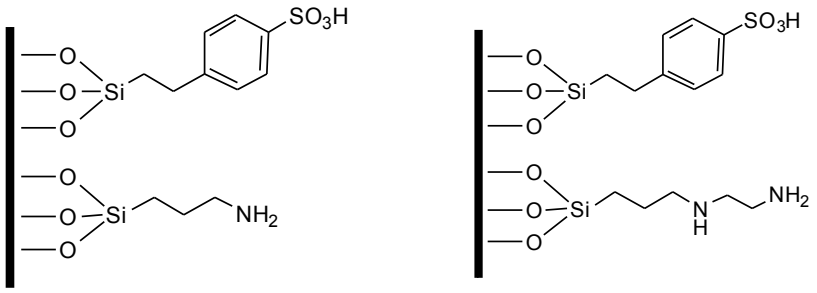

A B

Figure 1.10 Acid-base bifunctionalised mesoporous silicas

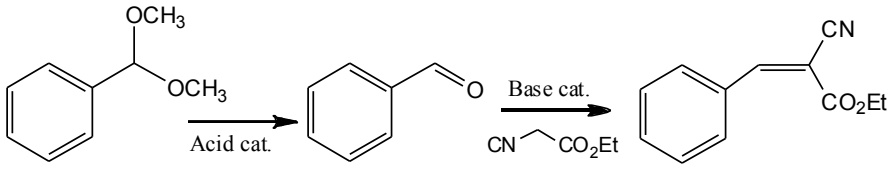

Figure 1.11 Deacetalisation-Knoevanegel reaction

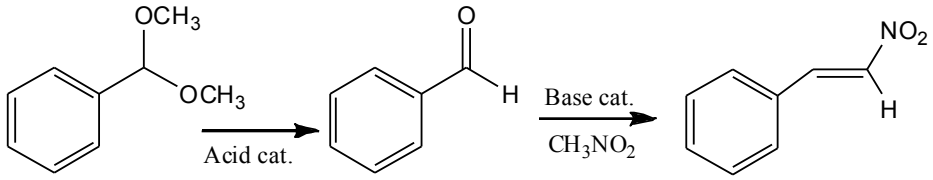

Figure 1.12 One-pot deacetalisation-nitroaldol cascade reaction

1.4.3 Redox catalysts

Selective oxidation of olefins and alcohols using Ti-silicalite[76-78] and Ti-β zeolite[79-81] have been reported. However, zeolites are less versatile due to structural strain on the size of transition metal incorporated. Therefore, the incorporation of Ti to mesoporous materials is believed to provide an advantage when larger substrate molecules that cannot diffuse through the microporous zeolites are involved.

Ti-MCM-41 was reported to be active in the epoxidation reaction of small linear olefins with H_2O_2 as oxidant but the observed activity was lower than that of Ti-β zeolite[82]. However, Ti-MCM-41 exhibited much higher activity than Ti-β zeolite when larger reactant molecules were utilised. As shown in Figure 1.13, the oxidation reaction of sulfides to sulfoxides and sulfones, Ti-MCM-41 shows higher activity in reaction B while Ti-β zeolite is more active to reaction A[83]. In addition, by using Ti-MCM-41 as catalyst, organic hydroperoxide can be used as oxidant while this is not possible in case of Ti-β zeolite due to size restriction[82].

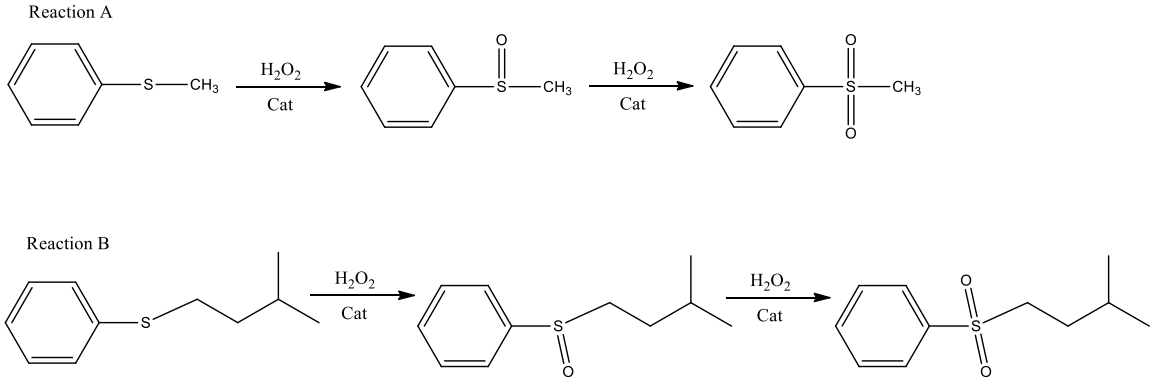

Figure 1.13 Oxidation reaction of sulfides[83]

Ti has also been introduced to the HMS structure[84], the resulting material was used as catalyst in the hydroxylation of phenol, but the activity was found to be lower than that of Ti-MCM-41. However, when the Ti-HMS was prepared by using a non-ionic surfactant, the activity in the liquid phase peroxide oxidation of methylmethacrylate, styrene, and 2,6-di-*tert*-butylphenol was higher than that obtained using Ti-MCM-41[85]. Since the structure of MCM-41 and HMS are analogous, the wall environment around Ti is assumed to be much the same, but what makes the difference in activity has been attributed to the greater mesoporosity observed in Ti-HMS which facilitates substrate transport and access to the framework. In

addition, Ti-MCM-41 and Ti-HMS were used in the oxidation of amines; the obtained products are of interest in chemical and pharmaceutical industries.

Owing to the success of the incorporation of Ti and its good activity in selective oxidation reactions, other transition metal with potential catalytic activity such as Cr, V, Mn, Nb, Co, Ni, and Sn were also incorporated into the walls of MCM-41 and also other related siliceous mesoporous materials[3].

Some examples of other transition metal incorporated mesoporous materials which have been used as catalysts in oxidation reactions are Co-MCM-41[86], Ni-MCM-41[87], Nb-MCM-41[88], NbCo-MCM-41[88], Ag-HMS[89], V-SBA-15[90], Co-SBA-15[91]. These were used as catalyst in the liquid phase oxidation of aromatic hydrocarbons such as styrene and benzene to benzaldehyde and phenol. Further examples are Fe-MCM-41[92], Cr-MCM-41[93], Co-MCM-41[94], and Mo-MCM-41[95, 96] whose use was demonstrated in the liquid phase oxidation of cyclohexane with H_2O_2 or organic hydroperoxide as oxidant, V-incorporated to mesoporous silica with different structure which are HMS, SBA-16, SBA-15, and MCM-48 for the oxidative dehydrogenation of propane and n-butane using molecular oxygen as an oxidant[97].

In addition to the examples mentioned above, CuO supported different type of mesoporous silicas SBA-15, MCM-41, MCM-48, and KIT-6 were prepared and the catalytic activity for the reduction of NO with CO was examined. CuO-MCM-41 and CuO-SBA-15 show the higher activity in this reaction than CuO-MCM-48 and CuO-KIT-6 due to the better dispersion of CuO species over mesoporous support found for MCM-41 and SBA-15[98]. Gold nanoparticles were also found to be capable to intercalate into the wall of mesoporous silica[99, 100], the obtained gold nanopartilce-mesoporous silica is active for the reduction of p-nitrophenol and methylene blue with $NaBH_4$ as reducing agent[99].

1.4.4 Anchored molecular catalysts for enantioselective reactions

The large pore diameter of mesoporous materials allows the immobilisation of molecular catalysts such as chiral metal complexes and organometallic catalysts to their surface. One of the most interesting types of catalyst that can be heterogenised by immobilisation on mesoporous material supports is enantioselective catalysts. The attachment of molecular catalysts to the mesoporous materials to be used as heterogeneous enantioselective catalyst can be done either by the immobilisation of ligands to the mesoporous support followed by subsequent reaction with the required metal centre, or by the attachment of the surface functional group, such as an alkoxysilane, with the metal complex first and this alkoxy functional group can then be the link to react with the mesoporous surface.

Figure 1.14 shows two possible pathways for the immobilisation of Pd-1,1'-bis(diphenylphosphino)ferrecene onto the mesoporous silica surface; pathway A is accomplished by the synthesis of a silane functionalised ferrocene ligand complexed with $PdCl_2$ and then this grafting reagent was loaded to the mesoporous silica surface[101], whilst pathway B involves the attachment of a phosphine modified ferrocene to the mesoporous silica surface which was previously grafted with bromopropylsilane followed by reaction with $PdCl_2$ to form the complex with phosphine group[102].

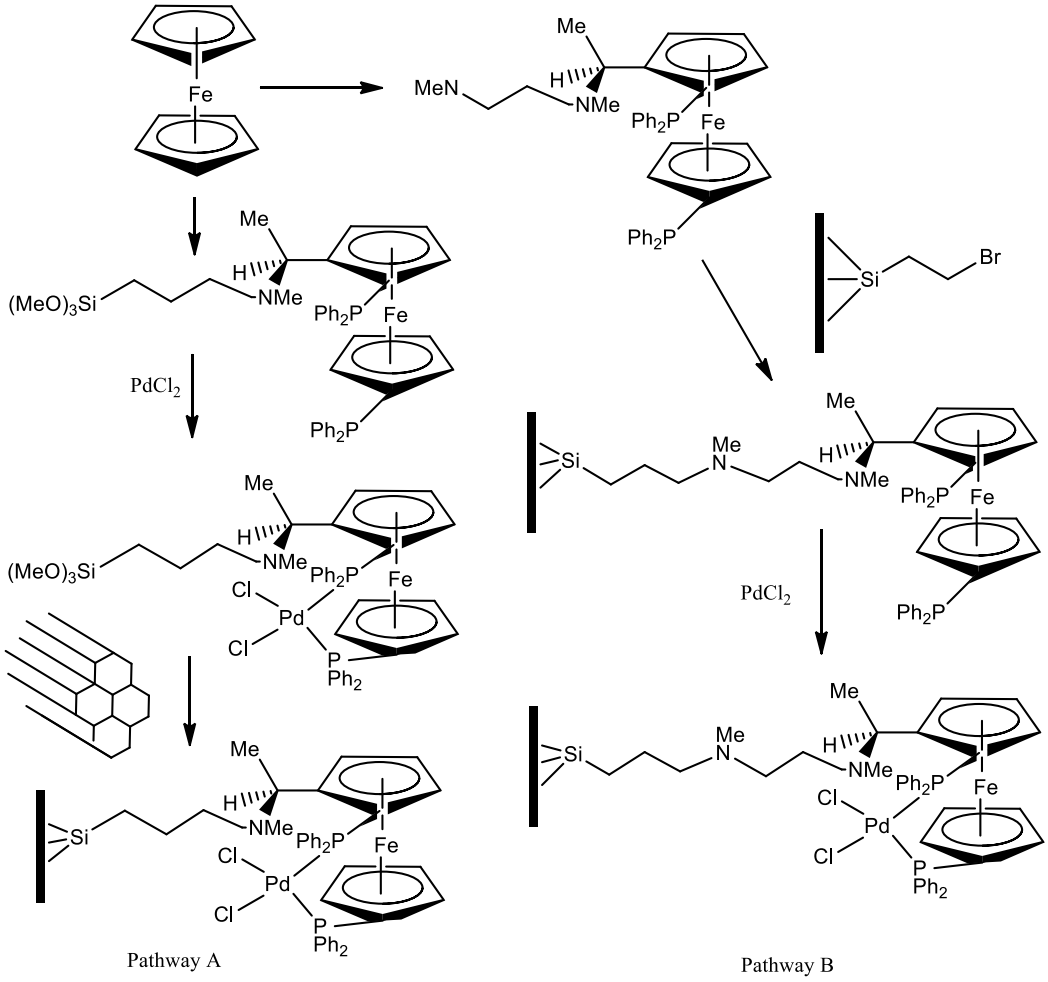

Figure 1.14 Schematic diagram of the pathways for the immobilisation lisation of the molecular catalyst onto mesoporous silicas surface[101, 102]

Mesoporous silicas have been successfully utilised as supports for a number of enantioselective catalysts. An early study of this type of catalyst supported on mesoporous silica was the immobilisation of β-aminoalcohol for use as a catalyst in the enantioselective alkylation of benzaldehyde with diethylzinc (Figure 1.15)[103, 104].

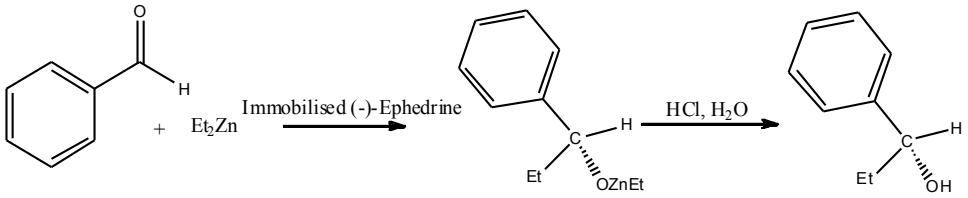

Figure 1.15 Enantioselective alkylation of benzaldehyde with diethylzinc

This reaction was previously catalysed by ephedrine anchored on silica and alumina surfaces but low activity and enantioselectivity were observed[105, 106]. However, the results from this β-aminoalcohol immobilised mesoporous support showed much lower enantioselective excess than the analogous homogeneous catalysts. Several factors related to the silica surface, such as unwanted side reactions caused by silanol groups, size of the mesoporous silica support as well as the more selective ligand and the addition of excess metal reagent, have been taken into account. A new chiral heterogeneous catalyst for the above reaction was reported by Bae et al [107], who immobilised a proline-derived ligand on MCM-41 and SBA-15. The supported SBA-15 exhibited higher enantioselectivity due to the larger pore diameter (89 Å compared to 31 Å for MCM-41). The addition of butyl lithium and also capping of the silanol surface by trimethylsilane improved the enantioselectivity in both supported MCM-41 and SBA-15 catalysts.

The metal (Pd(II)) bonded chiral chelate ligand 1,1'-bis(diphenylphosphino)ferrocene (dppf) tethered mesoporous silicas (Fig 1.14, pathway A) were demonstrated to be suitable for enantioselective hydrogenation of ethyl nicotinate to ethyl nipecotinate (Figure 1.16)[101].

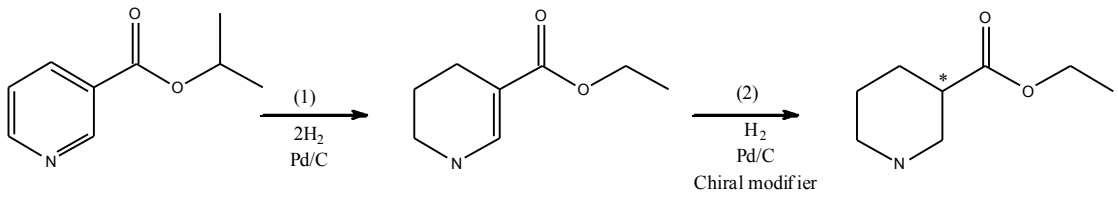

Figure 1.16 Two-step hydrogenation of ethyl nicotinate to ethyl nipecotinate

A significant increase in the activity and enantioselectivity compared to the homogeneous catalyst and non-porous supported catalyst was observed. The Palladium-phosphine complex-MCM-41 (Figure 1.14, pathway B) has also been used in the allylic amination of cinnamylacetate (Figure 1.17)[102], and showed greater regioselective and enantiomeric excess compared to the homogeneous counterparts and the catalyst-bound non-porous silica.

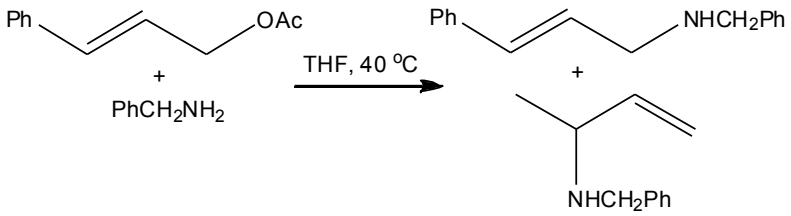

Figure 1.17 Allylic amination of cinnamylacetate

Further examples of mesoporous materials in enantioselective reactions include a Mn-Salen complex, (R,R)-(-)-N,N'-bis(3,5-di-*tert*-butylsalicylidene)-1,2-cyclohexadiamine, immobilised on Al-MCM-41 for the enantioselective epoxidation of cis-stilbene, 70% e.e. were observed[108], the Mn complexes with different salen type ligands immobilised mesoporous silica were also found to be active as enantioselective catalyst in different reactions, mainly for the epoxidation of olefins[109-114]. Immobilised dichloro-(S)-6,6'-dimethyl-2,2'-diaminophenyl-ruthenium complex onto MCM-41 was used for the

hydrogenation of α-acetamidocinamic acid[115], while another Ru complex, $RuCl_2(PPh_3)_2$(S,S-DPEN), is active for the hydrogenation of aromatic ketone[116]. The chiral copper(II)bisoxazoline-MCM-41 catalysts have been shown to be suitable for asymmetric Diels-Alder, Friedel-Crafts reactions[117, 118], and also for the cyclopropanation reaction[119].

There are many more examples that are not mentioned here, but the immobilisation of enantioselective catalysts onto mesoporous materials is still of interest, and research in this area is still open due to the enormous variety of ligand and metal centre that can be incorporated.

The improvement of enantioselectivity in the mesoporous supported catalysts might be explained by the pore confinement effect[120]. As presented in Figure 1.18, the reaction must occur in the restricted space between catalytic centre, chiral ligand, and pore wall. The orientation of the substrates relative to the active catalyst centre is strongly influenced by the limitation of the substrate in the mesopores which does not happen in homogeneous catalysts.

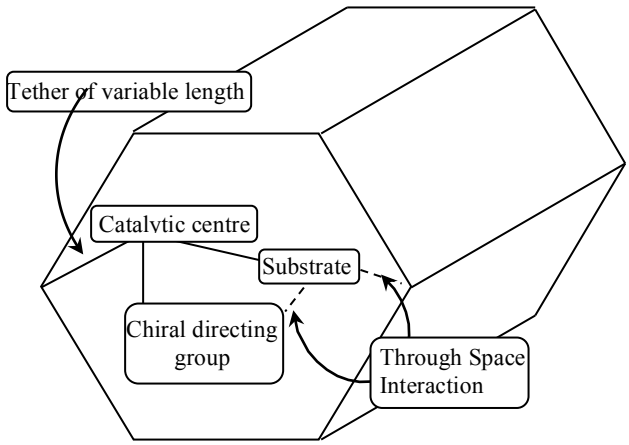

Figure 1.18 Schematic representation of the pore confinement concept[120]

1.5 AIMS OF THE STUDY

The aims of this study are to synthesise mesoporous silicas with different pore structures, which are hexagonal MCM-41, cubic MCM-48, cage-like cubic SBA-1, and cage-like hexagonal SBA-2. The resulting mesoporous silicas will be functionalised with the amino groups and organometallic asymmetric nickel-salen complexes via post grafting methods to be used as heterogeneous catalysts in carbon-carbon bond forming reactions; the Knoevenagel condensation for amino-mesoporous silicas and Kumada-Corriu reaction for nickel complex-mesoporous silicas. The catalytic activity as well as the reusability of the catalysts will be investigated. In addition, the effect of mesopore structure and surface hydrophobicity on the catalytic activity will also be examined.

CHAPTER 2 TECHNIQUES

2.1 X-RAY DIFFRACTION (XRD)

2.1.1 Principles

An X-ray is type of radiation that has short wavelength (0.1-100 Å) and high energy. It was first discovered by Wilhelm Conrad Röntgen in 1895[121]. The X-ray wavelength covers the range of the same order as typical molecular bond (0.8-3.0 Å), and therefore they are able to interact with the arrangement of atoms and molecules in crystals, enabling crystallographic experiments to be performed.

X-ray diffraction is one of the most important techniques in revealing the crystal structure. Max von Laue and co-workers first reported the X-ray diffraction in crystal in 1912[121]; they envisaged the crystals in three dimensional network of rows of atoms and the analysis was based on the notion that crystals behaved as a three dimensional diffraction grating. However, due to dealing with three dimensions, this approach is rather impractical. On the other hand, W. L. Bragg successfully applied X-ray diffraction of crystal structures by a simpler approach; based on the reflection of X-ray by the planes of atoms, known as Bragg's law[121]. The orientation of particular family of planes is identified by its Miller indices (h, k, l). Figure 2.1 shows the schematic representation of the Bragg's law.

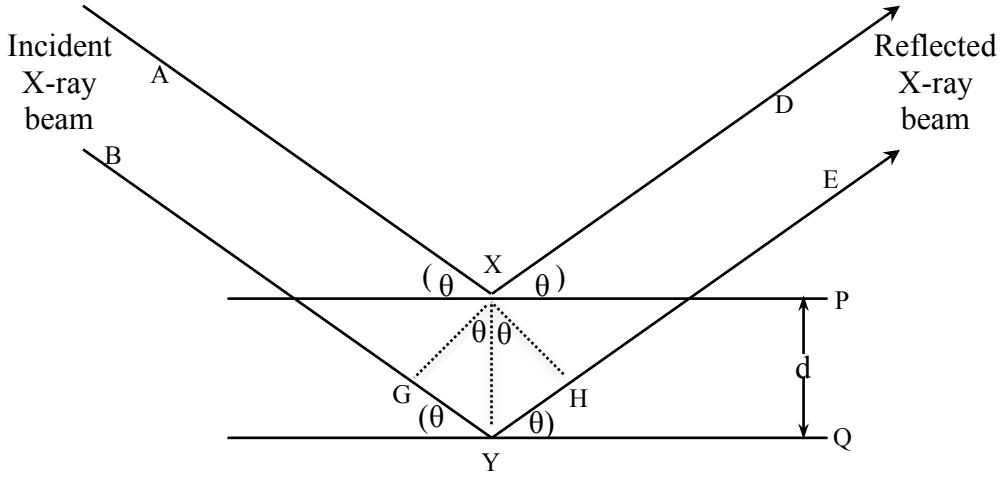

Figure 2.1 Bragg's scattering of X-rays from parallel planes with d representing inter-planar spacing

As seen in the figure, the monochromatic X-ray beam is incident on the surface of the crystal at an angle of θ. P and Q are the edges of a family of planes which are a distance d apart. Plane P reflects AX in XD, similarly plane Q reflects BY in YE at the same angle, θ. Since Q is lower than P, the beam path BYE is longer than AXD by the amount GY+YH, this value is called path difference.

$$\text{From } \Delta \text{ GXY, } \sin\theta = \frac{GY}{d} \qquad \therefore \; GY = d\sin\theta$$

$$\text{From } \Delta \text{ YXH, } \sin\theta = \frac{YH}{d} \qquad \therefore \; YH = d\sin\theta$$

$$\therefore \text{ Path difference } (GY + YH) = 2d\sin\theta$$

The two reflected rays XD and YE will constructively interfere when the path difference is equal to the wavelength (λ) or a multiple of it. Therefore the conditions for X-ray diffraction for Bragg's law are summarised in the following equation:

$$n\lambda = 2d \sin\theta$$

Where n is an integer called the order of reflection.

2.1.2 Powder XRD

Powder X-ray diffraction techniques were developed by Debye and Scherrer and independently by Hull in the period 1914-1919[121]. This technique may be classified as a 'fixed λ, verifying θ' technique. A family of planes of atoms in a crystal will only reflect X-ray beam when the Bragg equation is fulfilled. If the single crystal is placed in the X-ray beam then it would be only small chance that a particular family of planes is in the correct position to satisfy the Bragg equation. Making the powder sample would create more possibility for the small crystals to be oriented in all possible directions and there will be at least a few of those planes at the appropriate Bragg angles for reflection.

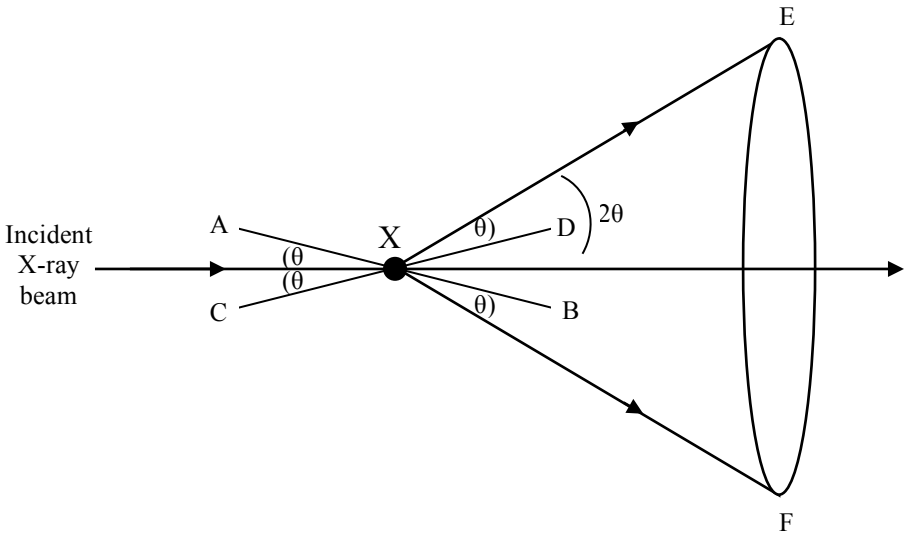

Figure 2.2 Formation of the diffraction cone

The X-ray diffraction of powder crystal is shown in Figure 2.2. The powder crystals (X) irradiated with the monochromatic X-ray beam, AB and CD represent the particular family of

planes in a crystal that satisfy Bragg equation so part of the X-ray beam is reflected along XE and XF. These two crystals have the planes orient at θ to the beam and the sample will also contain crystals having the same family of planes that orient at θ to the incident beam, thus if all possible orientation of this family of plane presented then the cone of reflected X-rays of semi- angle 2θ is generated, as shown in Figure 2.2.

2.1.3 Instrument and experimental procedure

There are three basic elements in X-ray diffractometer, which are the X-ray tube, sample holder, and X-ray detector.

The X-rays generated from X-ray tube usually have two components, one is the broad continuous of wavelength known as white radiation, or bremsstrahlung (German for 'breaking radiation'), and another is a fixed or monochromatic wavelength generated by the transition of electron from upper energy level to the vacant lower energy level. Each element emits characteristic X-ray wavelength, for example, the 2p→1s electron transition in Cu is called K_α with the wavelength of 1.5418 Å and the 3p→1s transition is K_β with the wavelength 1.3922 Å (Figure 2.3). In the diffraction experiment the monochromatic wavelength from Cu K_α is normally used. In order to get the K_α, Ni foil is used as the filter to absorb Cu K_β and the white radiation.

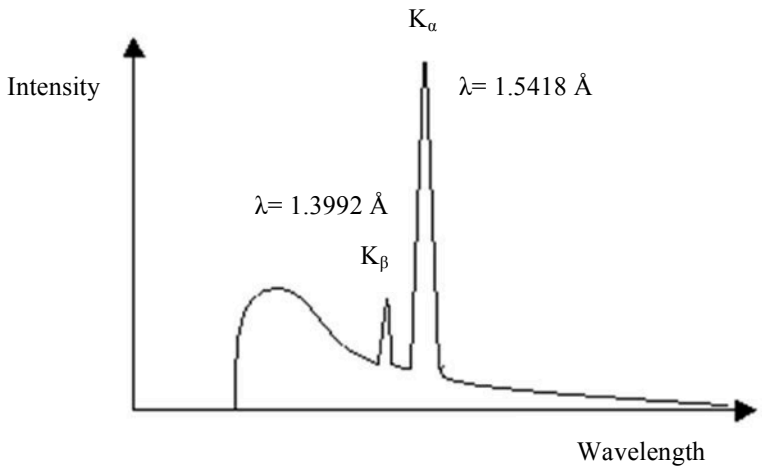

Figure 2.3 X-ray emission spectrum of Cu

Figure 2.4 shows the layout of typical diffractometer for the powder sample. A flat sample specimen is mounted on a turntable around which moves a detector. The angle θ between sample and the incident beam changes as the sample rotates, and when the Bragg condition is fulfilled, X-rays are diffracted and detected by the detector. The detector is connected to the specimen table in a way that when the table rotates by θ degrees, the detector will rotates by 2θ degrees, therefore the detector always being in the correct position to receive the reflected X-ray.

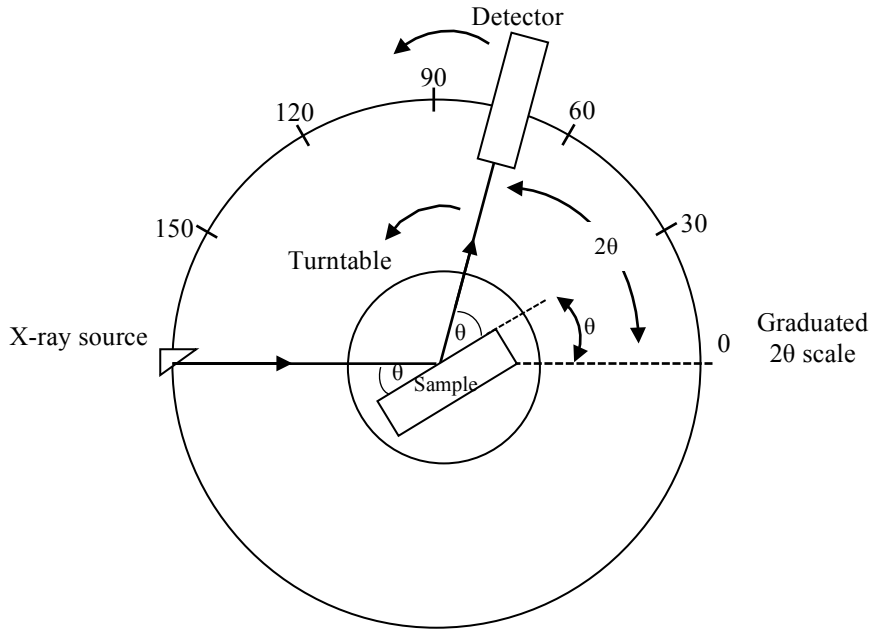

Figure 2.4 General layout of X-ray diffractometer

The X-ray diffractometer can be operated in both transmission and reflection geometry. For most crystalline materials, the diffraction pattern recorded between *2θ* of typically 10-90 degrees provides all information needed for the detail of structural order and can also permit refinement of the data to obtain information about molecular packing and interatomic distances. According to the Bragg's equation the lower angle the larger interplanar spacing, *d*. For mesoporous materials which have much larger *d*-spacing than the typical crystalline materials, the diffraction patterns only show peaks at low angle, generally between *2θ* of 2-8 degrees. In addition, the mesoporous materials only have a regular arrangement of pores but no short-range interatomic order as the structure of pore wall is amorphous. Therefore, the structural information that usually obtained from X-ray diffraction for mesoporous materials is the *d*-spacing and the symmetry or packing arrangement of the pores relative to each other.

In this work, powder X-ray diffraction data were recorded at an ambient temperature on a Bruker D8 diffractometer operating in the reflection geometry from 2θ of 1 to 8° with a step size of 0.01°.

2.2 NITROGEN PHYSISORPTION

2.2.1 Principles

The term adsorption is defined as an increase in concentration of gas molecules at a solid surface or an increase in concentration of a dissolved substance at the interface of solid and liquid phase; the reverse process is called desorption. The substance that is adsorbed is the adsorbate and the underlying material is the adsorbent.

Gas adsorption measurements are widely used for the determination of surface area and pore size distribution of solid materials such as catalysts, pigments, ceramics, industrial adsorbent, etc.

2.2.1.1 Type of Isotherms

The majority of gas adsorption-desorpton isotherms are catagorised into six types as shown in Figure 2.5 [2], and the explanations for each type of isotherm are as follows[2, 122].

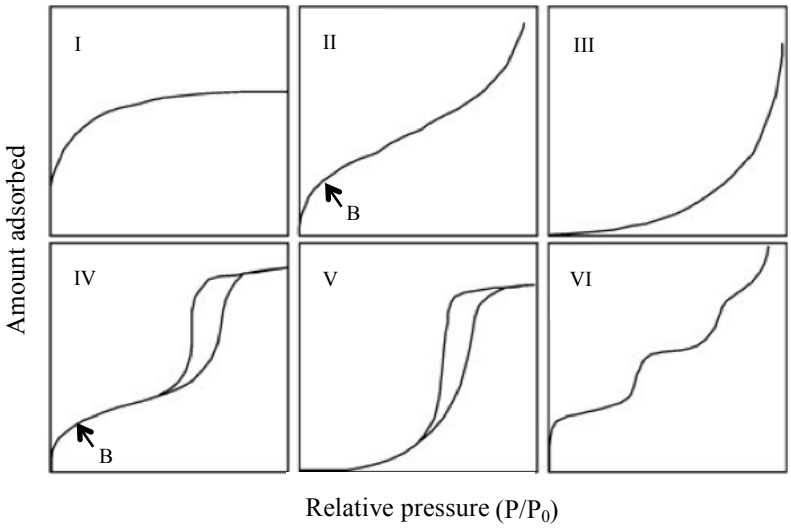

Figure 2.5 Types of gas adsorption-desorption isotherms

- Type I isotherm, sometime refers to Langmuir isotherm, is given by microporous solids having relatively small external surface. The limiting amount of gas adsorbed being governed by the accessible micropore volume rather than the internal surface area.
- Type II isotherm is the normal form of isotherm obtained with a non-porous or macroporous adsorbent. This isotherm shows unrestricted monolayer-multilayer adsorption, point B (i.e. the beginning of the almost linear middle section of the isotherm) indicates the stage at which monolayer coverage is completed and multilayer adsorption about to begin.
- Type III is convex to the P/P_0 axis over its entire range, this type of isotherm is not common but there are a number of systems (e.g. nitrogen on polyethylene which the adsorbate-adsorbate interactions play an important role) to give this type III isotherm.
- Type IV isotherm is given by mesoporous adsorbent. The initial part of isotherm is attributed to monolayer-multilayer adsorption since it follows the same path as the

corresponding part of the type II isotherm, and the sharp increase of amount adsorbed at higher relative pressure is associated with capillary condensation in the mesopores.

- Type V isotherm is related to the type III isotherm in that the interaction between adsorbate-adsorbate is weak; this is uncommon but can be obtained with certain porous adsorbent.
- Type VI isotherm represents stepwise multilayer adsorption on a uniform non-porous surface. The sharpness of the steps depends on the system and the temperature; step-height represents the monolayer capacity for each adsorbate layer. Type VI isotherm is given from certain system such as argon or krypton on graphitized carbon blacks at liquid nitrogen temperature.

2.2.1.2 Surface area determination

The BET[123] (Brunauer, Emmett, and Teller who explained the adsorption of gas on a solid surface) gas adsorption method is the widely used standard procedure for the evaluation of surface area of finely divided and porous materials. The adsorption process in the BET approach is viewed as a layer-by-layer process, as presented in Figure 2.6.

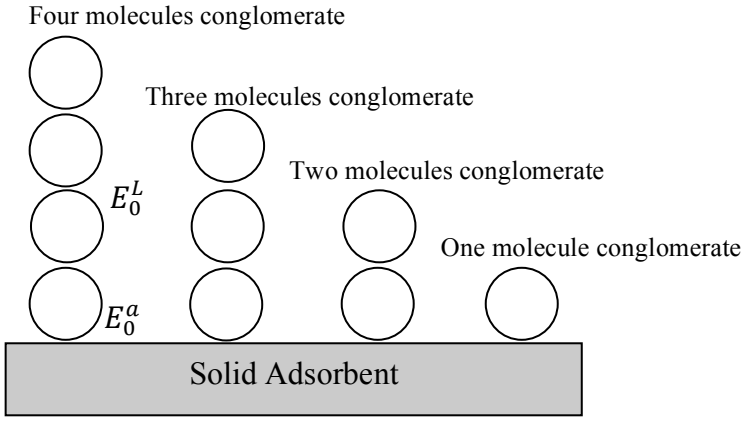

Figure 2.6 The BET adsorption model [124]

The adsorbent is assumed to be energetically homogeneous therefore the adsorption field is the same in any place of the surface. In the adsorption process, each molecule is adsorbed in a solid adsorption site. The first layer of adsorbed molecules has a heat of adsorption, E_0^a, and the vertical interaction between molecules after the first layer (liquefaction heat of adsorbate) is E_0^L. In addition, there is no lateral interaction between adsorbed molecules. Following these hypotheses, it can be summarised to the corresponding mathematical equation:

$$\frac{1}{n^a\left[\left(\frac{P_0}{P}\right)-1\right]} = \frac{1}{n_m^a C} + \frac{(C-1)P}{n_m^a C P_0}$$

$$C = exp\left(\frac{E_0^a - E_0^L}{RT}\right)$$

where:

P = equilibrium pressure of adsorbate at the temperature of adsorption

P_0 = saturation pressure of adsorbate at the temperature of adsorption

n^a = amount of gas adsorbed at the relative pressure $\frac{P}{P_0}$

n_m^a = the monolayer capacity

C = BET constant

E_0^a = heat of adsorption at the first layer

E_0^L = heat of adsorption for the second and higher layer (heat of liquefaction)

According to the experiment results, a plot between $\frac{1}{n^a[(P_0/P)-1]}$ and $\frac{P}{P_0}$ gives a straight line called the BET plot (Figure 2.7). The range of linearity is restricted to the limited part of isotherm, typically in the $\frac{P}{P_0}$ range of 0.05-0.30. In addition, the monolayer capacity, n_m^a, and BET constant, *C*, can be calculated from the slope (m) and y-intercept (b) of the BET plot, by using the following equations.

$$n_m^a = \frac{1}{m+b}$$

$$C = 1 + \frac{m}{b}$$

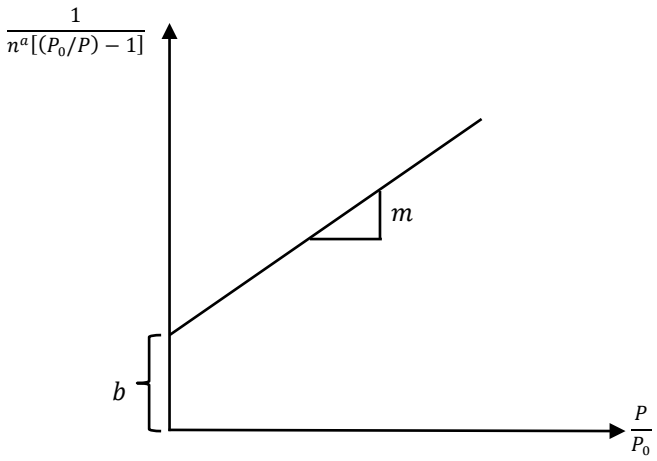

Figure 2.7 BET plot

Moreover, the total and specific surface area can be evaluated from the monolayer capacity using the following equation:

$$S_{total} = n_m^a L a_m$$

$$S = \frac{S_{total}}{m}$$

where:

S_{total} = total surface area

S = specific surface area

n_m^a = monolayer capacity

a_m = molecular cross-sectional area

m = molecular mass of adsorbed species

L = Avogadro's number

2.2.1.3 Pore volume and pore size distribution

The determination of pore size distribution and pore volume is based on the physical adsorption and a capillary condensation in the pores. The pore condensation represents a confinement-induced shifted gas-liquid phase transition, which generally occurs at a pressure, P, which is lower than the saturation pressure, P_0, of the fluids. The $\frac{P}{P_0}$ value at which the condensation takes place varies by the pore geometry, liquid-interfacial tension, strength of the interaction between the fluids and the pore walls, and the pore size. The pore condensation mechanism can be described by a Kelvin-Cohen equation[124], which gives the correlation between the pore diameter and pore condensation pressure. The Kelvin-Cohen equation predicts that when pore diameter and temperature are increased, the pore condensation shifts to higher relative pressure. Consequently, this equation serves as the basis for the methods

applied for mesoporous analysis such as BJH[125] (Barrett-Joyner-Halenda) method, which is widely used for the pore size distribution and pore volume determination.

The BJH method, in addition to the Kelvin-Cohan equation assumption, assumes that the desorption process starts at the relative pressure in the range of 0.9-0.95, which is close to the unity and all the pores are filled with the adsorbed fluids. So, the first step of desorption process only involves the removal of capillary condensate. However, both removal of condensate from the cores of a group of pores and the thinning of the multilayer in the larger pores are involved in the next desorption step. In addition, the BJH method is normally related to the desorption of nitrogen at 77 K.

At the first desorption step (j=1), when the relative pressure is reduced from $\left(\frac{P}{P_0}\right)_1$ to $\left(\frac{P}{P_0}\right)_2$, a volume $\Delta V(1)$ will be desorbed from the pore, which results in the reduction of the thickness of the physically adsorbed layer by an amount of Δt_1. Across the relative pressure reduction, the average change of the thickness is $\frac{\Delta t_1}{2}$, therefore the pore volume may be expressed as:

$$V_{p1} = \Delta V(1)\left[\frac{r_{p1}}{r_{K1} + \frac{\Delta t_1}{2}}\right]^2$$

where:

r_p = pore radius

r_K = inner capillary radius

When the relative pressure is further reduced to $\left(\frac{P}{P_0}\right)_3$, the volume, V_{p2}, desorbed from the pore is given by:

$$V_{p2} = \left[\frac{r_{p2}}{r_{K2} + \frac{\Delta t_2}{2}}\right]^2 [\Delta V(2) - \Delta V_t(2)]$$

where:

$$\Delta V(2) = \Delta V_k(2) + \Delta V_t(2)$$

and the volume desorbed from multilayer is:

$$\Delta V_t(2) = \Delta t_2 A c_1$$

Ac_1 is an area exposed by the previously emptied pore from which physically adsorbed gas is desorbed. The previous equation can be summarised to symbolise the step of desorption by:

$$\Delta V_1(n) = \Delta t_n \sum_{j=1}^{n-1} Ac_j$$

By substitution of the general value of $\Delta V_t(n)$ to the equation defining V_{p2}, the calculation of the pore volume at various relative pressure may be summarised in the following equation:

$$V_{pn} = \left[\frac{r_{pn}}{r_{Kn} + \frac{\Delta t_n}{2}}\right]^2 \left[\Delta V(n) - \Delta t_n \sum_{j=1}^{n-1} Ac_j\right]$$

2.2.2 Experimental procedure

Prior to the determination of adsorption isotherm, surface area, and pore size distribution, all the physisorbed species must be removed from the adsorbent surface. This is typically carried out by outgassing at low pressure and, normally, elevated temperature. The analysis is performed at 77 K (e.g. under liquid nitrogen). The small amounts of adsorbate gas are admitted in the step into the evacuated sample chamber.

In the work carried out here, nitrogen adsorption-desorption isotherms were recorded in collaboration with Dr M. A. Lopez Martinez and Dr R. Portillo Reyes at the Universidad Autónoma de Puebla, Mexico on a Quantachrome Autosorb1 instrument. Samples were degassed at 100 °C for 4 hours prior to analysis.

2.3 GAS CHROMATOGRAPHY (GC)

2.3.1 Principles

According to the IUPAC, chromatography is a physical method of separation in which the components to be separated are distributed between two phases, one of which is stationary (stationary phase) while the other (mobile phase) moves in a definite direction. The components of the sample are separated from one another based on their relative vapour pressure and affinities for the stationary phase[126].

Various chromatographic processes are named according to the physical state of the mobile phase. Therefore, in gas chromatography (GC) the mobile phase is a gas, and in liquid chromatography (LC) the mobile phase is a liquid.

GC is one of the most important techniques for the separation and analysis of volatile compounds such as gases, liquids, and the dissolved solid in the volatile solvent.

The carrier gas used as mobile phase in GC is usually an inert gas such as helium or a non-reactive gas such as nitrogen. The stationary phase can be either liquid or solid. Liquid are more common, however, in order to use the liquid as the stationary phase, the liquid must be held in the column by coating on a high surface area and inert solid support. The separation of the mixture is based on the vapour pressure differences.

2.3.2 Instrument and experimental procedure

The instrumentation for GC incorporates the mobile phase, stationary phase, and detection system, as shown in Figure 2.8.

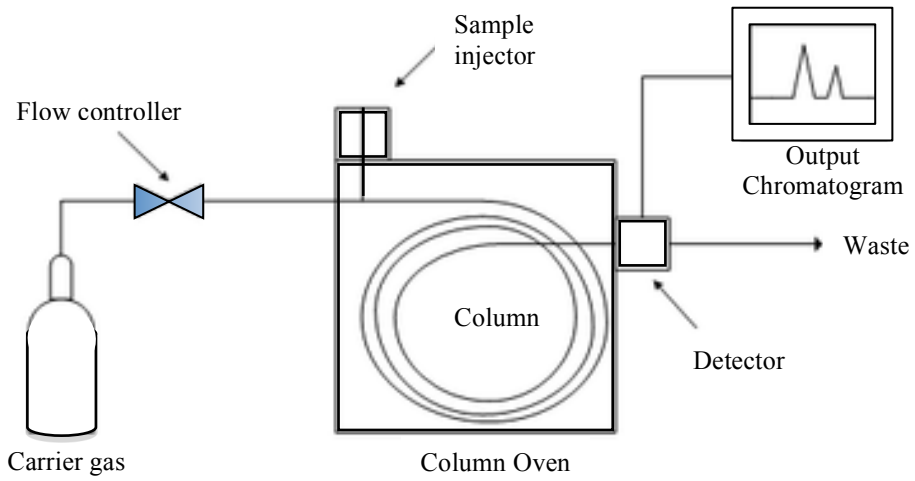

Figure 2.8 Instrumentation diagram of the typical GC

The known volume of sample is evaporated and carried by the carrier gas (the mobile phase) through the column packed with stationary phase. The column is placed inside the oven where the gas temperature can be controlled. Sample equilibrates into the stationary phase based on their solubilities at the given temperature. In addition, the rate that molecule

pass through the column depends on the type of molecule and the stationary phase materials. For example, if a sample contains A and B, and component A has a greater distribution in the mobile phase, as a consequence it is carried through the column faster than component B, which spends more time in the stationary phase. Therefore, the separation occurs as A and B travel through the column in a different time (retention time)[126].

The detector is used to monitor the outlet stream from the column, so the amount of component and the time that each component reaches the outlet are detected. The output signal of the detector gives rise to a chromatogram.

In this study, samples were analysed on a Shimadzu GC2010 with a DB225 capillary column and FID detector, start at 60 °C with a heating rate of 10 °C/minute until the temperature reaches 280 °C and remain at this temperature for 15 minutes.

2.4 ATOMIC ABSORPTION SPECTROSCOPY (AAS)

2.4.1 Principles

This technique is used to determine the concentration of a specific metal in a solution. If atoms in the ground state are illuminated by a source, they will absorb the radiation at the characteristic wavelength. Since the wavelength of the source is practically constant and specific to a particular electron transition in a particular element, the excitation process of atoms will result in the decrease of radiation energy, which can be measure. This measurement can be quantitatively related to the concentration of the analysed atom type in the absorbing medium.

The law by which the absorption of light is related to the concentration is Beer-Lambert law:

$$A = \varepsilon cl$$

where:

A = absorbance of radiation at a particular wavelength; $A = \log\left(\frac{I_0}{I}\right)$

I_0 = intensity of the incident radiation

I = intensity of the transmitted radiation

ε = proportionality constant (molar absorptivity; $Lmol^{-1}cm^{-1}$)

c = concentration of the absorbing species ($molL^{-1}$)

l = path length of light beam (cm)

From the Beer-Lambert law, the absorbance and concentration have a linear relationship; therefore, if the path length is known and the absorbance is measured then the concentration of the interested species can be calculated.

2.4.2 Instrument and experimental procedure

A sample has to be atomised before analysed by AAS. The atomisation process is normally achieved by the flame, especially when the sample is in the solution form. The instrument diagram is shown in Figure 2.9

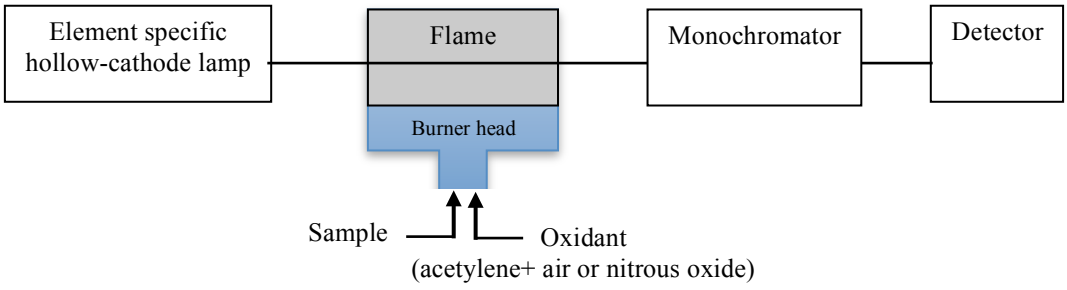

Figure 2.9 Diagram of the flame atomic absorption spectrometer

As seen from the diagram, a light beam of specific wavelength related to the particular metal is directed through a flame. The flame atomises the sample to produce atoms in their ground state. These atoms are capable of absorbing radiation from the lamp, and the absorbance can be measured.

Determination of nickel leached in this study was carried out using the Perkin-Elmer AAnalyst200 AA spectrometer.

2.5 X-RAY FLUORESCENCE (XRF)

2.5.1 Principles

XRF is an elemental analysis technique used in both qualitative and quantitative analysis. This technique is based on the principle that an electron can be ejected from its atomic orbital by the absorption of sufficient energy. When an electron from the inner orbital is ejected from an atom, an electron from the higher energy orbital will be transferred to fill the lower energy level vacancy. During this transition, a photon with a characteristic wavelength may be emitted from the atom.

The energy of the emitted photon is specific and always the same for the particular element (i.e. characteristic of the particular element), therefore by determining such energy it is possible to identify that element. In addition, the number of photons per unit time (generally mentioned as the peak intensity or count rate) is related to the amount of that element in the sample, so that the quantity can be evaluated as well.

2.5.2 Instrument and experimental procedure

Although XRF can be applied for both qualitative and quantitative analysis, in this study it was used for the determination of nickel content in the mesoporous supports therefore the quantitative analysis by XRF will be discussed.

An X-ray spectrometer consists of three main sections which are the specimen chamber where the sample is excited by the primary X-ray beam, the monochromator where the fluorescing radiation is dispersed, and the detector (incorporate with the computer system) where the dispersed radiation is detected and displayed.

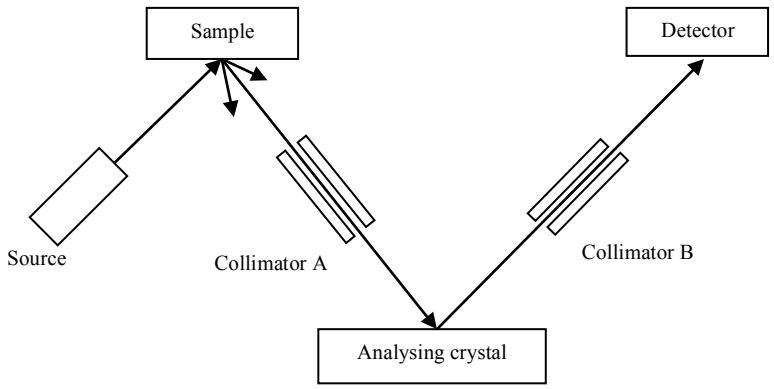

Figure 2.10 Diagram of the conventional XRF

A primary X-ray beam from the source irradiates the sample, causing the fluorescence with the characteristic wavelength, and then part of the radiation is collimated by a collimator A onto the analysing crystal. For quantitative analysis, the analysing crystal is fixed at the appropriate angle to reflect one of the element's characteristic lines. Part of the beam from the collimator A is reflected by the crystal and the reflected beam passes through another set of collimator (collimator B) and enters the detection system.

The sample for XRF analysis could be the bulk solid, powder, liquid, or gas. To ensure homogeneity and to eliminate particle size effects for the powder sample, powders are normally milled to about 300 mesh and they may then be compacted into a pellet (with or without binder), loosely packed into a cell, or supported on a substrate such as Mylar film, filter paper, or Scotch tape. If the sample is a heterogeneous solid, or the solid has a strong matrix effect, fusion with borax or lithium tetraborate to produce a glass disk can be useful. On the other hand, liquid samples are homogeneous and free of surface or particle size effect, but there can be the problem with evaporation, leakage, and precipitation of the analyte.

In this work the XRF data were recorded on a Bruker S8 TIGER instrument using the solid powder sample. The calibration curve was made using the known amount of nickel oxide standard mixed with mesoporous silica (SiO_2), the Ni/Si ratio from XRF were plotted against the actual known Ni/Si ratio, therefore the actual Ni in the mesoporous samples can be evaluated.

2.6 CHN ANALYSIS

This technique is used for the determination of carbon, hydrogen, and nitrogen content in the given sample. The results are presented as percentage of these elements against total weight. The sample is combusted under oxygen at high temperature, the end product from the combustion would be in the gas form of oxide of the concerned element which are water, carbon dioxide, and oxide of nitrogen. Oxide of nitrogen will then be converted to N_2. The mixed gases is carried by the inert gas to the detection unit and the amount of each gas is measured by three pairs of thermal conductivity cell (each thermal conductivity cell is responsible for each element). Alternatively the mixed gases are separated by chromatography before being measured by thermal conductivity detector, depending on how the machine is

designed. The conductivity signals are integrated and the data related to percentage of carbon, hydrogen, and nitrogen. The limitations of this technique are the difficulties handling volatile, very low melting point, or readily sublimating compounds[127].

In this work, CHN analysis was carried out on a Carlo-Erba EA1110 instrument, operated by Lianne Hill.

2.7 FUREIR TRANSFORM INFRARED SPECTROSCOPY (FTIR)

2.7.1 Principle

Infrared spectroscopy can be described as the technique that measures the ability of matter to absorbed or transmit infrared radiation (λ=750nm-1mm) it is the non-destructive type of analysis and can be used for almost any type of samples as long as the molecules have the permanent dipole moment (i.e. the material is composed of or contains compound rather than pure element).

In infrared spectroscopy, both vibrational and rotational energy of the molecule are considered. The model to describe the absorption process pictures as a molecule in which the individual atoms held together by chemical bonds are in vibratory motion along those bonds, while the whole molecule is rotating. When the energy of a specific vibration is equivalent to the frequency of the IR radiation directed on the molecule, the molecule absorbs the radiation. Different type of bond (i.e. different functional group) absorbs IR radiation in different wavelength.

The major type of molecular vibration are stretching and bending as shown in Figure 2.11. IR radiation is absorbed and the associated energy is converted into these types of motions. The absorption involves discrete, quantised energy level. However, the individual

vibrational motion is usually accompanied by other rotational motions, these combinations lead to the absorption band not the discrete line[128, 129].

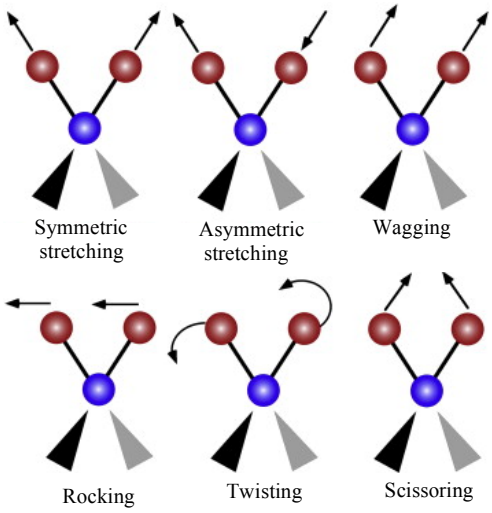

Figure 2.11 Simple layouts of the vibrational modes associated to a molecular dipole moment change detectable in an IR absorption spectrum. In addition to the two stretching modes, the four different bending vibrations are showed[130]

2.7.2 Instrument and experimental procedure

FTIR spectrometer main components are a source, interferometer, and detector. Source generates light and all the source energy will be sent through an interferometer and onto the sample. The light passes through a beam-splitter, which sends the light in two directions at right angles; one beam goes to a stationary mirror then back to the beam-splitter, the other goes to a moving mirror. The motion of the mirror makes the total path length variable versus that taken by the stationary-mirror beam. When the two meet up again at the beam-splitter, they recombine, but the difference in path lengths creates constructive and destructuive interference. The recombined beam passes through the sample. The sample absorbs all the different wavelengths characteristic of its spectrum, and this subtracts specific

wavelengths from the interferogram. The detector reports variation in energy versus time for all wavelengths simultaneously. Intensity versus time spectrum is converted into intensity versus frequency by a mathematical function called a Fourier transform. Diagram of FTIR spectrometer is shown in Figure 2.12.

In this study, FTIR spectra are recoded using the Perkin Elmer Spectrum 100 FT-IR Spectrometer.

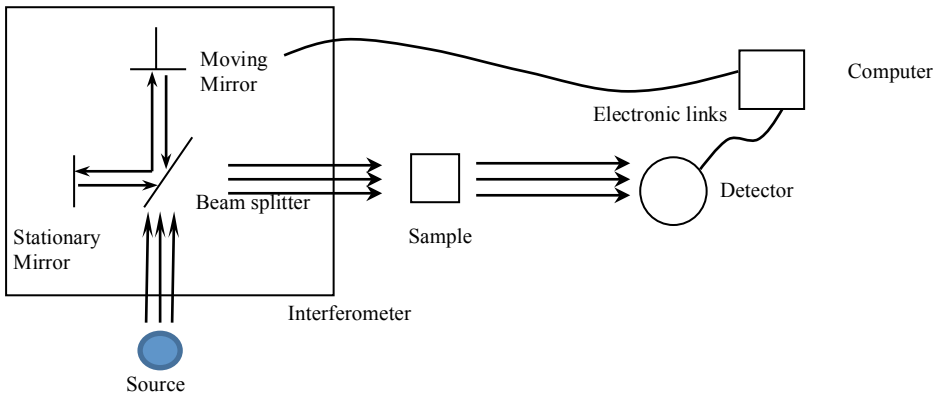

Figure 2.12 Diagram of FTIR spectrometer[131]

2.8 NUCLEAR MAGNETIC RESONANCE SPECTROSCOPY (NMR)

2.8.1 Principle

Nuclear magnetic resonance spectroscopy (NMR) is the important tool for the chemical structural analysis as, in theory, nucleus of any isotope possessing a magnetic moment (μ) such as ^{1}H, ^{11}B, ^{13}C, ^{15}P, ^{19}F, can show a nuclear magnetic resonance effect. The fundamental property of the atomic nucleus involved in nuclear magnetic resonance is the nuclear spin (I) which has values of 0, ½, 1, 1½, etc., in the unit of h/2π (where h is the Plank's constant). The nuclear magnetic moment (μ) is directly proportional to the spin, i.e.

$$\mu = \frac{\gamma I h}{2\pi}$$

where γ is the proportionality constant called magnetogyric ratio and is constant for each particular nucleus.

When a magnetic field is applied, the nuclear moments orient themselves with only certain allowed orientation, a nucleus of spin I has 2I+1 possible orientations, which are given by the value of the magnetic quantum number m_I. m_I has values of -*I*, -*I*+1, …, *I*-1, *I*. The energy of interaction is proportional to the nuclear moment and the applied field.

$$E = -\frac{\gamma h}{2\pi} m_I B$$

where B is the applied field.

The selection rule for NMR transition is that m_I can only change by one unit, i.e. $\Delta m_I = \pm 1$. Therefore the transition energy is given by

$$\Delta E = \frac{\gamma h B}{2\pi}$$

For the detection of this transition energy, radiation given by ΔE = hν must be applied, results in the fundamental resonance condition for all NMR experiment:

$$\nu = \frac{\gamma B}{2\pi}$$

When a nucleus of magnetogyric ratio γ is placed in the magnetic field B, the resonance is satisfied when the frequency of the applied radiation, ν, is given by the equation above[128, 132].

2.8.1.1 Chemical Shift

When a molecule containing nuclei under observation is placed in the magnetic field, the electrons within the molecule shield the nuclei from the external applied field. Therefore, the field at the nucleus is not equivalent to the applied field. The difference, which is called the nuclear shielding, is proportional to the applied field.

The chemical shift is defined as the nuclear shielding divided by the applied field. It is only a function of the nucleus and its environment, i.e. it is a molecular quantity. It is always measured from the suitable compound, this may be an external reference or more commonly the reference compound is added to the solution investigated (internal reference). The chemical shift is defined as

$$\delta = \frac{B_{reference} - B_{sample}}{B_{reference}} \times 10^6 \; ppm$$

where $B_{reference}$ is the magnetic field of the reference nuclei and B_{sample} is the field at the sample nuclei, then the above equation can be written as:

$$\delta = \frac{(\nu_{sample} - \nu_{reference})}{oscillator\ frequency\ (Hz)} \times 10^6$$

For ^{1}H NMR, the recommended reference is tetramethylsilane ($Si(CH_3)_4$, TMS), the TMS peak appears at 0 in the δ-scale. TMS is also the recommended reference for ^{13}C NMR, giving rise to only one peak under normal operation.

2.8.1.2 Spin-Spin Coupling

The chemical shift bands are always found to consist of several component peaks. This multiplet splitting arises from interaction between the spin systems of the differently shielded nuclei. The multiplicity of the bands is n+1, where n is the number of interacting nuclei and the separation between the lines are equal and correspond to the spin-spin coupling constant, *J*. If the spectrum is recorded at different radio frequency, chemical shift will be changed while the coupling constant is independent of field strength. Spin-spin splittings are observed because the energy of the nucleus if affected by the orientation of the nuclei in other non-equivalent groups of magnetic nuclei.

As the multiplicity of a band indicates the number of nuclei in the interacting group, therefore this is an aid in the structural determination of the compound and the magnitude of the coupling constant can give information on the relative positions of the interacting nuclei.

2.8.2 Instrument and experimental procedure

A block diagram of a typical MNR spectrometer is shown in Figure 2.13. A magnet of suitable field strength and stable is required. Either electromagnets or permanent magnets can be used for this purpose. A source of radiofrequency power and the means of conveying this to the sample are also needed, i.e. the transmitter and transmitter coil. The absorbance of energy by the sample may be detected as an induced e.m.f. either in a separate coil (receiver coil) which is orthogonal to the first or in the transmitter coil itself. The signal is amplified, detected, and displayed.

In common with other spectroscopic technique, a means of scanning a particular spectral region is required. This is commonly affected by an extra set of coils around the sample which sweep the magnetic field linearly when current is passed through them, and the scanning may be achieved also by weeping the frequency.

In this study, ^{1}H NMR spectra are recorded using Bruker AVIII300 spectrometer with TMS as reference and the deuterated solvent used are chloroform-d and DMSO-d_6.

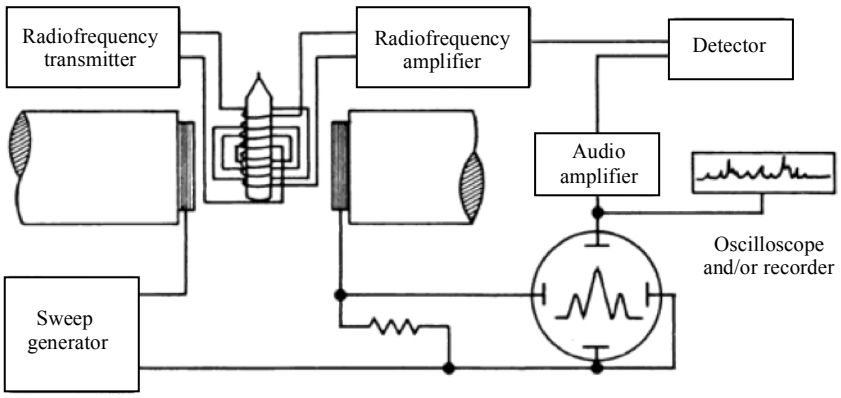

Figure 2.13 Block diagram of a typical NMR spectrometer[133]

CHAPTER 3 SYNTHESIS AND CHARACTERISATION OF ORDERED MESOPOROUS SILICAS

3.1 INTRODUCTION

3.1.1 Background of ordered mesoporous silicas

Highly ordered silica materials which possess pore sizes in the mesoporous range (2-50 nm) and show outstanding properties such as high surface area, tailored pore size, and functionalised pore surface are known as ordered mesoporous silicas.

Mobil Composition of Matter No.41, No.48 and No.50 (MCM-41, MCM-48, and MCM-50), discovered in 1990s[8, 9], are the most well-known mesoporous silica materials. The pore systems of these materials are hexagonal (*P6mm*), cubic (*Ia3d*), and lamellar for MCM-41, MCM-48, and MCM-50, respectively. They are widely used in several applications, but mostly as catalyst supports and absorbents due to their uniform pore size and high surface area. In this study, MCM-41 and MCM-48 are of interest and will be discussed in more detail.

After the discovery of ordered mesoporous silicas, M41S materials, researchers at University of California, Santa Barbara, developed another family of ordered mesoporous silicas, so called SBA-n materials[18]. Of particular interest amongst these materials are the cage-like cubic mesoporous silica SBA-1 (*Pm3n*) and cage-like hexagonal SBA-2 ($P6_3/mmc$), because their pore structures are 3-dimensional, which is believed to be advantageous due to the ability to facilitate molecular diffusion and provide better accessibility to catalytic functional sites.

Hexagonal MCM-41, cubic MCM-48, cage-like cubic SBA-1, and cage-like hexagonal SBA-2 are chosen in this study due to their different pore structure but comparable pore size (in the range of 2-4 nm[134-137]) to eliminate pore size effect.

The synthesis mechanism of mesoporous silicas can be described as a liquid crystal templating (LCT) where surfactant molecules act as the template[8]. This mechanism can be explained by the formation of hexagonal arrays of micellar rods, followed by the incorporation of the inorganic silicate species; these silicate species will occupy the space between the rod-like structure. The final step is the removal of surfactant template, resulting in the hollow cylinders of the hexagonal inorganic silicate materials. As an example of this, Figure 3.1 illustrates the liquid crystal templating mechanism for the synthesis of MCM-41.

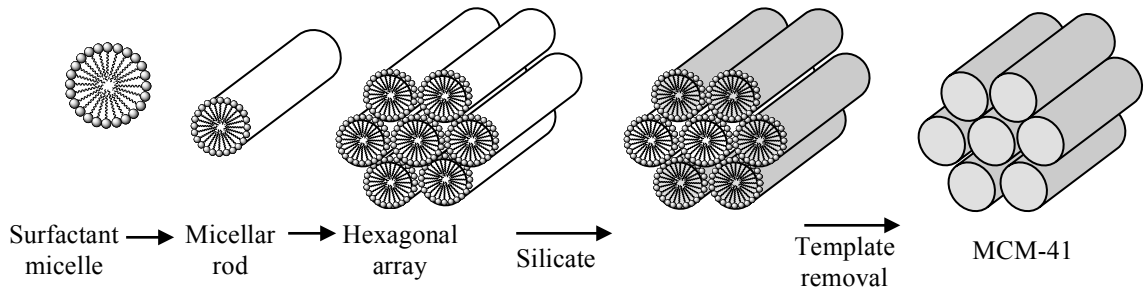

Figure 3.1 Liquid crystal templating for the synthesis of ordered mesoporous MCM-41

However, this synthesis mechanism pathway requires a high surfactant concentration to form the hexagonal micellar array, which is not applicable in practice therefore an alternative pathway has also been proposed[138]. At low surfactant concentration, no hexagonal micelle array is present, but only randomly oriented rod-like micelles are formed. However, the additional of silicate species leads to the formation of silica encapsulation around the external surface of surfactant micelles and spontaneous assembly of the long-range ordered hexagonal structure.

In both discussed mechanisms, cooperative organisation of organic surfactant and inorganic silicate species via charge density matching at the interface controls the assembly process, and results in the final structure. Based on this electrostatic assembly, Stucky and coworkers[139] have proposed the pathway to synthesise mesostructured surfactant and inorganic biphase arrays for the whole series of these materials through this assembly mechanism.

Here, we are going to discuss the mechanism for the formation of siliceous mesostructures. MCM-41 and MCM-48 are often synthesised in a basic medium, known as a S^+I^- mechanism, where S^+ and I^- stand for cationic surfactant and soluble anionic inorganic species. Mesoporous silicas can also be synthesised in an acidic medium, via a $S^+X^-I^+$ route, where S^+, X^- and I^+ are surfactant, halide and inorganic species, respectively. These synthesis routes result in lamellar, hexagonal, or cubic *Pm3n* phase as shown in Figure 3.2[139] .

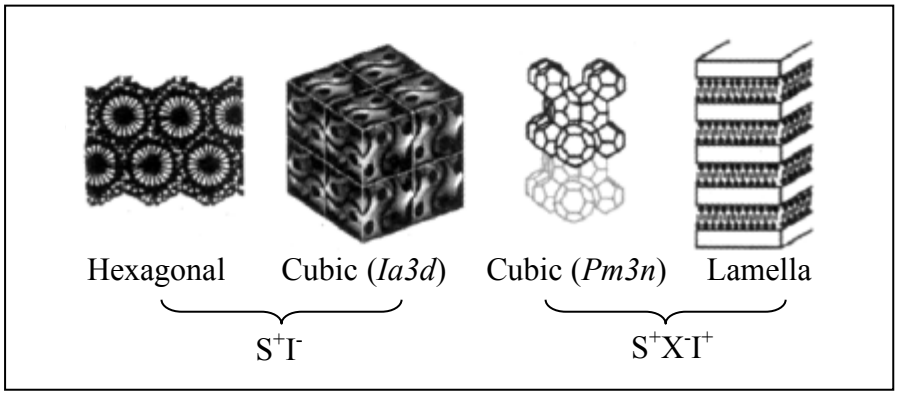

Figure 3.2. General scheme for the synthesis mechanism of mesoporous silica[139]

Normally, alkyltrimethylammonium halides $[C_nH_{2n+1}(CH_3)_3N]^+X^-$ with alkyl chain length n = 8-22 carbon atoms have been used as the cationic surfactant. These cationic surfactants play an important role for the formation of the mesoporous phase in term of

packing parameter, *g*. The value of this packing parameter is given by the equation $g = V/a_0 l$, where V is the total volume of the surfactant chains plus co-solvent organic molecule between the chains, a_0 is the effective head group area at the micelle surface, and l is the kinetic surfactant chain length or the curvature elastic energy. The expected mesophase structure in terms of packing parameter is shown in Table 3.1.[140, 141]

Table 3.1 Packing parameter in the synthesis of mesoporous silicas

g	Mesophase
⅓	Cubic (*Pm3n*)
½	Hexagonal (*P6mm*)
½-⅓	Cubic (*Ia3d*)
1	Lamella

However, it should be noted that the packing parameters are also influenced by the solution condition e.g. pH, temperature, concentration of co-surfactant so that it is not constant for the given surfactant.

3.1.2 Method for preparation of ordered mesoporous silicas

In general, the four main components in the synthesis of mesoporous silicas are:

i) alkyltrimethylammonium halide, alkyltriethylammonium halide, triblock copolymer, or double-headed surfactants as the structure-directing agent;

ii) a silica source to be precipitated;

iii) water as the solvent;

iv) sodium hydroxide (NaOH), ammonium hydroxide (NH_4OH), tetramethylammonium hydroxide (TMAOH), H_2SO_4, or HCl as pH regulator.

Several synthesis routes had been reported for MCM-41[142-147]. One synthesis proceeds via hydrothermal restructuring, using hexadecyltrimethylammonium bromide (CTAB) and Cab-O-Sil M-5 silica as the structure-directing agent and silica source, respectively, under basic conditions. The hydrothermal restructuring was carried out by hydrothermal treatment without stirring in a Teflon-line autoclave at 343 K for three days, followed by post-synthetic heat treatment in the oven for one day. This method is an easy way to synthesise high quality and large pore MCM-41 (6 nm) by using a simple commercial surfactant; however, this method is a fairly time consuming procedure[148]. By using the same silica source, Cab-O-Sil M-5, but different surfactant, the synthesis of MCM-41 using hexadecyltrimethylammonium chloride (CTACl) as the template gave a lower intensity of XRD patterns than when using CTAB. In addition, when aging time was increased, the crystallinity of materials also increased and reached a maximum at 20 hours[149].

MCM-41 can be formed not only at high temperature but also at room temperature; highly ordered MCM-41 materials can be synthesised by using TEOS as the silica source and CTAB as the surfactant at room temperature. The very low surfactant concentration and short synthesis time, 2 hours, brought about highly ordered MCM-41 materials[134]. For another synthesis approach, Mokaya et al[150] reported a seed recrystallisation route for the synthesis of large crystals of MCM-41. Primary MCM-41 was synthesised by using fumed silica as the silica source at 420 K for 48 hours, and then this primary MCM-41 was used as silica source for the secondary synthesis. The secondary product showed higher ordered materials and also

showed a change of morphology to plate-like particles. Although MCM-41 can be formed at room temperature, further heat treatment can lead to more ordered materials.

The classical surfactants, alkyltrimethylammonium halides, have been found to be most favourable for the formation of the hexagonal and lamellar phase. For the synthesis of cubic MCM-48 more specialist procedures and, sometimes, special surfactants are needed in order to attain the *g* value that cubic *Ia3d* prefers. The addition of ethanol, a small molecule alcohol, as a co-solvent into the synthesis mixture can increase the effective surfactant volume, resulting in the increased of *g* value, hence enabling a phase transformation from the hexagonal to cubic phase to occur. The role of alcohol as the co-solvent was also studied by Liu et al[151]. They suggested that the amount of alcohol needed for phase transformation is increased with decreasing carbon chain length of the alcohol. This is because with increasing alkyl chain length the alcohol's molar volume is also increased, therefore, more alcohol was needed for the shorter chain alcohol. Normally, high surfactant to silica ratio was required for the formation of MCM-48[152], otherwise a longer aging time period was needed instead[18].

For the synthesis of SBA-1, a larger head group surfactant, such as hexadecyltriethylammonium bromide (CTEABr), is required. This CTEABr surfactant tends to form spherical micelles which possess high surface curvature; consequently, a high effective head group area is observed and results in the appropriate *g* value and cubic *Pm3n* materials can be formed. In addition, according to the synthesis mechanism ($S^+X^-I^+$ route for SBA-1), the synthesis has to be carried out under acidic condition at a pH below the isoelectronic point of silica in order to obtain the cationic inorganic silicate species.

The synthesis of SBA-2 requires divalent quaternary ammonium, Gemini, surfactant $C_nH_{2n+1}N^+(CH_3)_2(CH_2)_sN^+(CH_3)_2C_mH_{2m+1}$ (designated as $C_{n\text{-}s\text{-}m}$) with m = 1 such as $C_{12\text{-}3\text{-}1}$,

$C_{16\text{-}3\text{-}1}$, $C_{16\text{-}6\text{-}1}$, $C_{18\text{-}3\text{-}1}$, as the template under basic conditions[136]. The coupling of the head group and molecular spacer controls the effective head group area (a_0) of the surfactant. In addition, the double charged surfactant with separated charge centres can either act as a chelating group to a given cluster surface, or provide the orientation of cluster with respect to each other, therefore the packing parameter of the surfactant-inorganic cluster can be adjusted to form the 3-dimensional hexagonal cage structure of SBA-2.

3.1.3 Method of surfactant removal

In order to obtain the completely porous solid, it is necessary to remove the surfactant template from the as-synthesised materials. The surfactant removal method can have an effect on the resulting materials. There are several methods to remove the surfactant from the structure such as calcination, solvent extraction, ozone treatment, microwave-assistance, and extraction with supercritical CO_2. Amongst these, the calcination and solvent extraction method are the main ones used due to their less complicated apparatus; therefore they will be discussed in more detail.

3.1.3.1 Calcination

Surfactant removal from mesoporous silicas is conventionally achieved by calcination. This normally involves heating at high temperature under oxygen flow to burn out the surfactant. Typically, the solid is heated to the desired temperature, higher than 500 °C, under an inert atmosphere to char the surfactant before burning out. A slight shrinkage (i.e. 2-5% [148, 153]) of pore size compared to the starting material is usually observed in the obtained calcined solid materials. In addition, greater condensation of silanol groups is also observed. However, calcination is considered as a harsh method; it is not suitable for the organically

modified materials. In some cases, calcination can cause pore collapse especially for materials with the larger pore size[154].

3.1.3.2 Solvent extraction

Solvent extraction is simply removal of the organic surfactant template, carried out using acidic solution, alcohol, neutral salt solution, or mixture of these. This is the only method that can be applied to remove the template from organically modified mesoporous materials prepared by a one-pot synthesis. Pore shrinkage is not observed, meaning that this method could be suitable for less stable structures and larger pore materials.

3.2 EXPERIMENTAL

3.2.1 Synthesis of MCM-41[134]

0.4 g CTAB (98%, Sigma Aldrich) was dissolved in 54.0 ml water, then 41.0 ml NH_4OH (30% ammonia in water, Acros Organics) was added and stirred until surfactant was completely dissolved. 2.0 ml TEOS (98%, Sigma Aldrich) was added into the surfactant solution, and stirring continued for 2 hours. The white precipitate formed was filtered, washed with water and then dried at room temperature. About 1.5 g crude MCM-41 was obtained.

3.2.2 Synthesis of MCM-48[135]

5.2 g CTAB (98%, Sigma Aldrich) was dissolved in a mixture of 100 ml ethanol (laboratory reagent grade, Fisher Scientific) and 240 ml water. 24 ml NH_4OH (30% ammonia in water, Acros Organics) was then added to the surfactant solution followed by the addition of 6.8 g TEOS (98%, Sigma Aldrich). After 5 minutes, a colloidal suspension was formed,

and the stirring was continued at room temperature for 10 hours. After 10 hours, the white solid was filtered and washed with water. The crude MCM-48 was dried at room temperature.

3.2.3 Synthesis of SBA-1

3.2.3.1 Synthesis of hexadecyltriethylammonium bromide (CTEABr)[137]

152.6 g of 1-bromohexadecane (97%, Sigma Aldrich) and 50.6 g triethylamine (99%, Riedel-deHaën) were added in into a flask with 400 ml of acetone (laboratory reagent grade, Fisher Scientific). The mixture was stirred under reflux conditions for 7 days. The white product was filtered and recrystallised from acetone solution 3 times, before finally being filtered and dried at 60 °C. The structure of CTEABr is shown in Figure 3.3.

Yield: 87.3%

^{1}H NMR ($CDCl_3$, 300 MHz, TMS): δ_H 3.45 (6H, N($\underline{CH_2}CH_3)_3$), 3.20 (2H, CH_2-N), 1.35 (9H, CH_3), 1.25 (28H, CH_2), 0.85 (3H, CH_3).

Elemental analysis: calculated for $C_{22}H_{48}NBr$: 65.03% C, 3.44% N, and 11.82% H; found 64.73% C, 3.70% N, and 12.50% H

FTIR: C-N stretching peak appears at 1309 cm^{-1}.

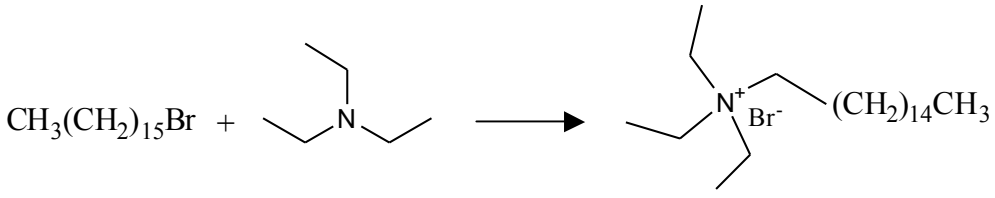

Figure 3.3 Reaction scheme for the synthesis of CTEABr

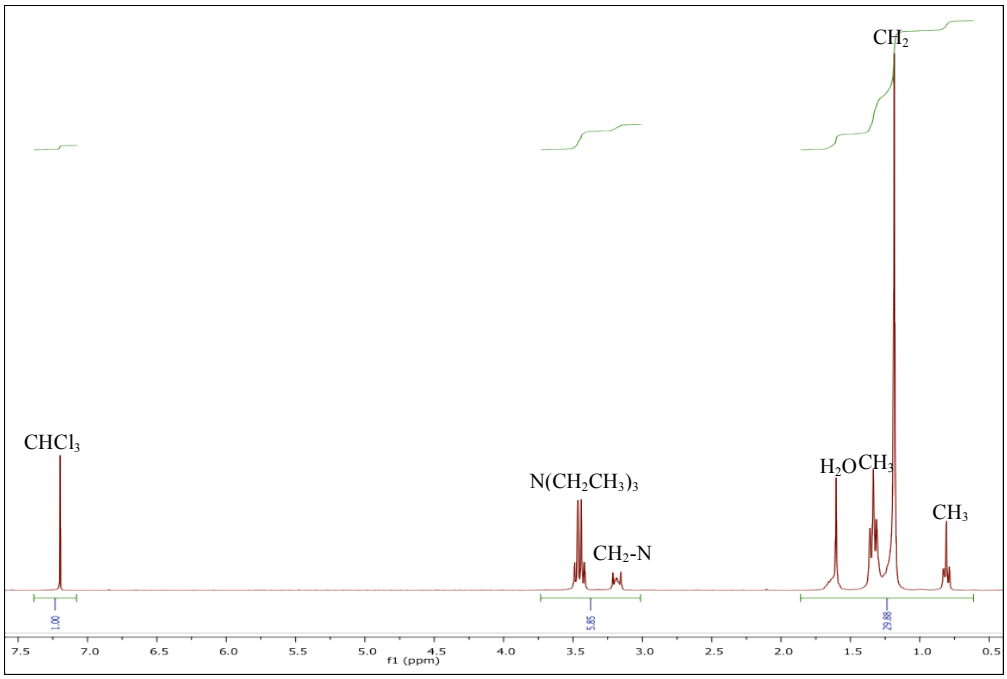

Figure 3.4 NMR spectrum of CTEABr

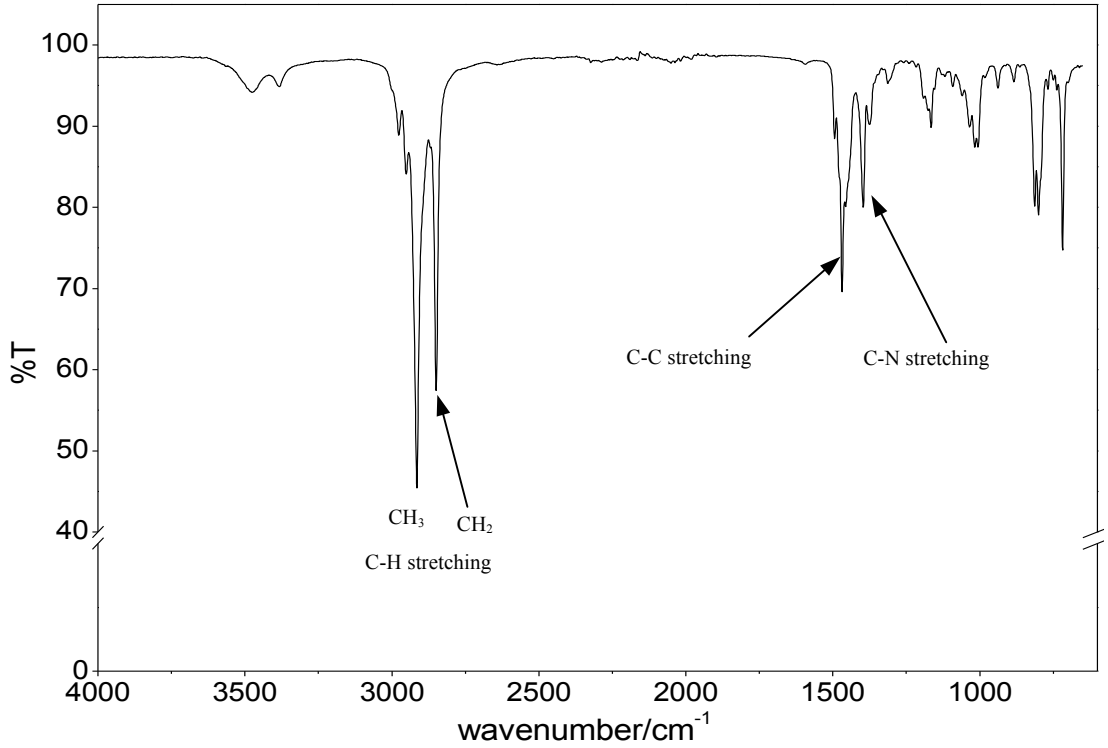

Figure 3.5 FTIR spectrum of CTEABr

3.2.3.2 Synthesis of SBA-1

Synthesis procedure of SBA-1 was modified from the literature [137]. It was carried out at 0 °C, prior to heating up to 100 °C. 1.0 g CTEABr was dissolved in a mixture of 72.8 ml HCl (37% solution in water, Acros Organics) and 107.1 ml water; this surfactant solution and 2.5 g TEOS (98%, Sigma Aldrich) were cooled down to 0 °C. TEOS was added into the surfactant solution, with continuous stirring at 0 °C for 4 hours. Then the reaction mixture was heated up to 100 °C while being stirred for 1 hour. SBA-1 was filtered without washing and dried at 60 °C in air.

3.2.4 Synthesis of SBA-2

3.2.4.1 Synthesis of gemini quaternary ammonium surfactant surfactant ($C_{16\text{-}3\text{-}1}$)[136]

The gemini surfactant was synthesised by the reaction between dimethylhexadecylamine (DMHDA) and an equimolar amount of (3-bromopropyl)trimethylammoniumbromide in dry ethanol under reflux conditions. 8.43 ml of DMHDA (95%, Sigma Aldrich) were dissolved in 50 ml of ethanol. 5.22 g of (3-bromopropyl)trimethylammonium bromide (97%, Sigma Aldrich) was added to the solution while being stirred. The reaction mixture was heated under reflux for 48 hours. After refluxing, the solvent was removed *in vacuo* to obtain a white solid. The white solid was purified by dissolution in a minimum amount of ethanol followed by the addition of ethyl acetate until a white solid precipitate was obtained. This white solid was filtered and dried before used. Figure 3.6 represents the $C_{16\text{-}3\text{-}1}$ structure.

Yield: 92.4%

^{1}H NMR ($CDCl_3$, 300 MHz, TMS): δ_H 3.75 (4H, $N\underline{CH_2}CH_2\underline{CH_2}N$), 3.45 (9H, $N(CH_3)_3$), 3.30 (6H, $-N(CH_3)_2-$), 3.0 (6H, $(CH_2)_3$), 2.55 (2H, $N(CH_2)$-R), 1.30 (2H, $NCH_2\underline{CH_2}CH_2N$), 1.20 (22H, $(CH_2)_{11}$), 0.80 (3H, CH_3).

Elemental analysis: calculated for $C_{23}H_{52}N_2Br_2$: 54.36% C, 5.28% N, and 10.21% H; found: 54.70% C, 5.60% N, and 10.50% H

FTIR: C-N stretching peak appears at 1235 cm^{-1}.

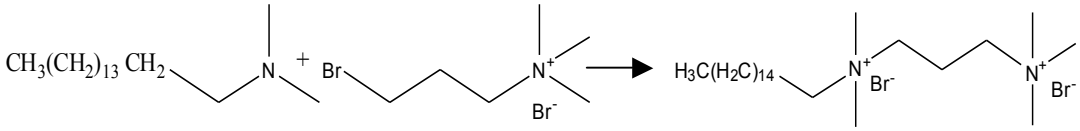

Figure 3.6 Reaction scheme for the synthesis of $C_{16\text{-}3\text{-}1}$

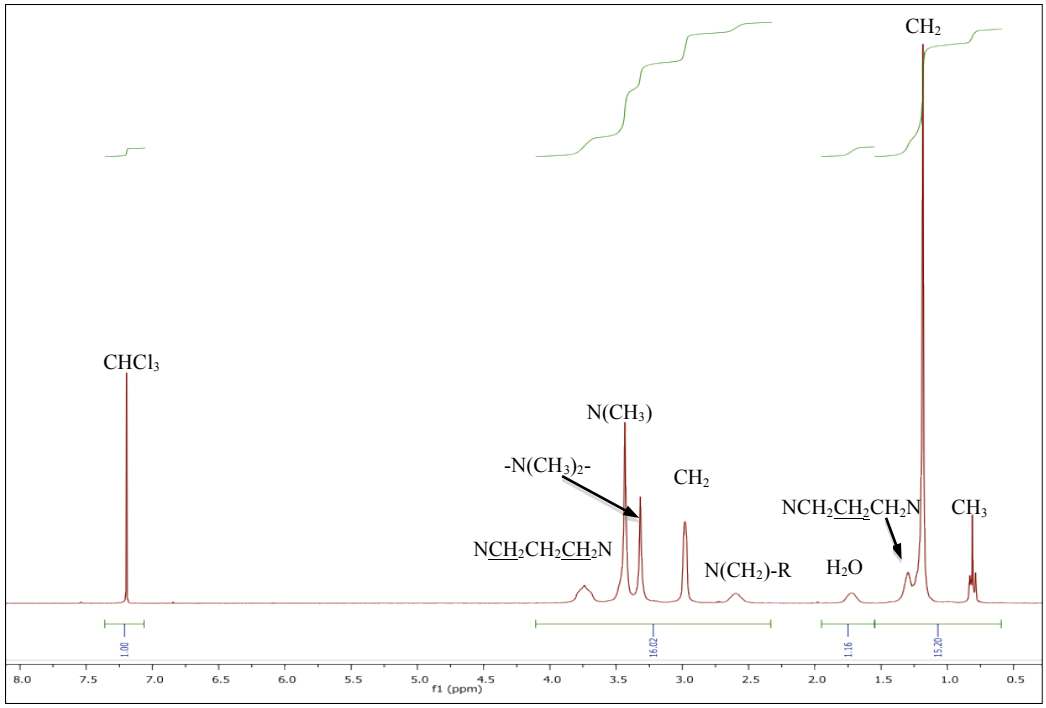

Figure 3.7 NMR spectrum of $C_{16\text{-}3\text{-}1}$ surfactant

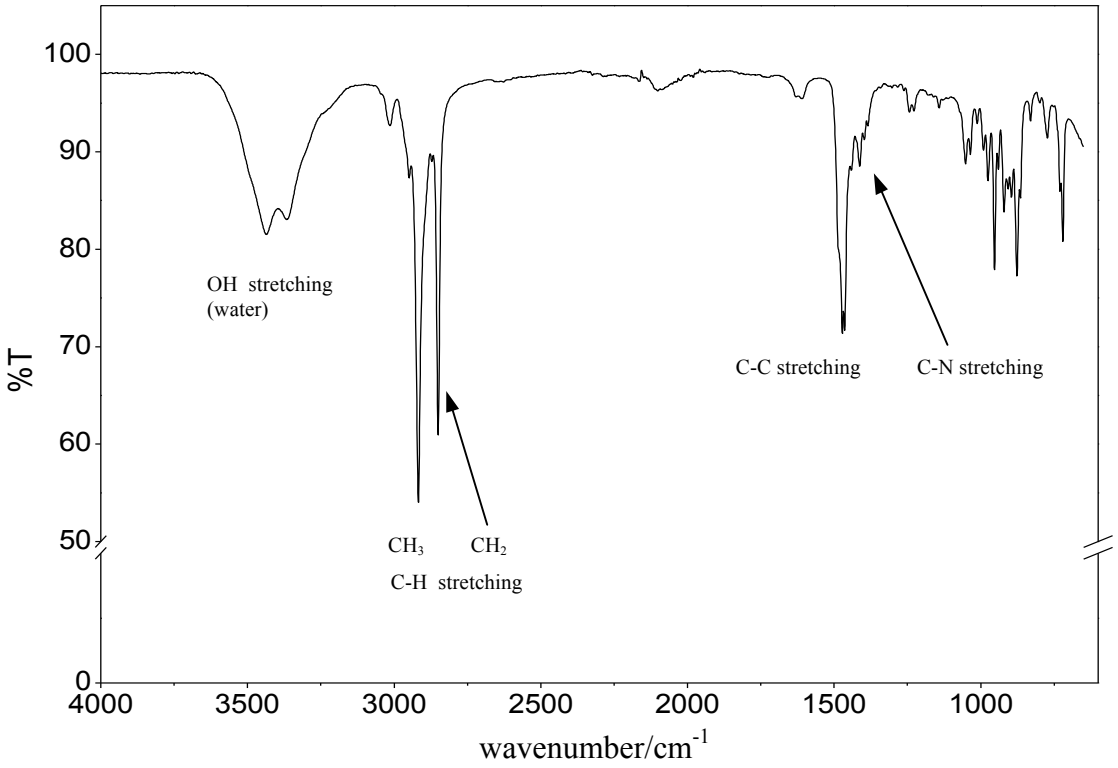

Figure 3.8 FTIR spectrum of $C_{16\text{-}3\text{-}1}$ surfactant

3.2.4.2 Synthesis of SBA-2[136]

For the synthesis of SBA-2 mesoporous silica, the synthesised Gemini surfactant, $C_{16\text{-}3\text{-}1}$, was used as the structure directing agent. 2.6 g of $C_{16\text{-}3\text{-}1}$ were dissolved in the mixture of 270 ml water and 18.3 g tetramethylammonium hydroxide (TMAOH) (25% in water, Avocado) and stirred until completely dissolved. 20.8 g TEOS was added dropwise and the pH was adjusted to 10.5 by addition of concentrated HCl. The reaction mixture was stirred for 4 hours at room temperature, followed by aging at 100 °C for 1 hour. The white precipitate was filtered, washed with water and dried at 160 °C for 4 hours.

3.2.5 Template removal

In this study surfactants as the template, were removed from the mesostructure by solvent extraction. Typically, 1.0 g of mesoporous silica was extracted in 300 ml of 1M HCl in ethanol under reflux condition for 24 hours, and then washed with ethanol. Finally the template-free mesoporous silicas were dried at room temperature before being characterised by X-ray diffraction, and pore analysis by nitrogen adsorption-desorption.

3.3 RESULTS AND DISCUSSION

3.3.1 Template removal results

As the cationic surfactant was used as the structure directing agent in the synthesis of mesoporous silicas, the surfactants are still in the inner pores when the mesostructure has completely formed. Therefore, template removal was performed to remove the template and result in the porous structure which allows molecules to diffuse through the pore without blockage by the surfactant. Two methods to remove the structure-directing agent, calcination and acid extraction were carried out here; the different results between these two methods are discussed.

The FTIR spectra of surfactant-free mesoporous silica and as-synthesised mesoporous silica with surfactant in Figure 3.9 shows that the both calcination and solvent extraction are an efficient method to remove surfactant from the mesoporous silica confirmed by the disappearance of CH_2 asymmetric and symmetric vibration bands at 2925cm^{-1} and 2852cm^{-1}, respectively[155] and the elemental analysis results show neither carbon nor nitrogen in both calcined and extracted samples.

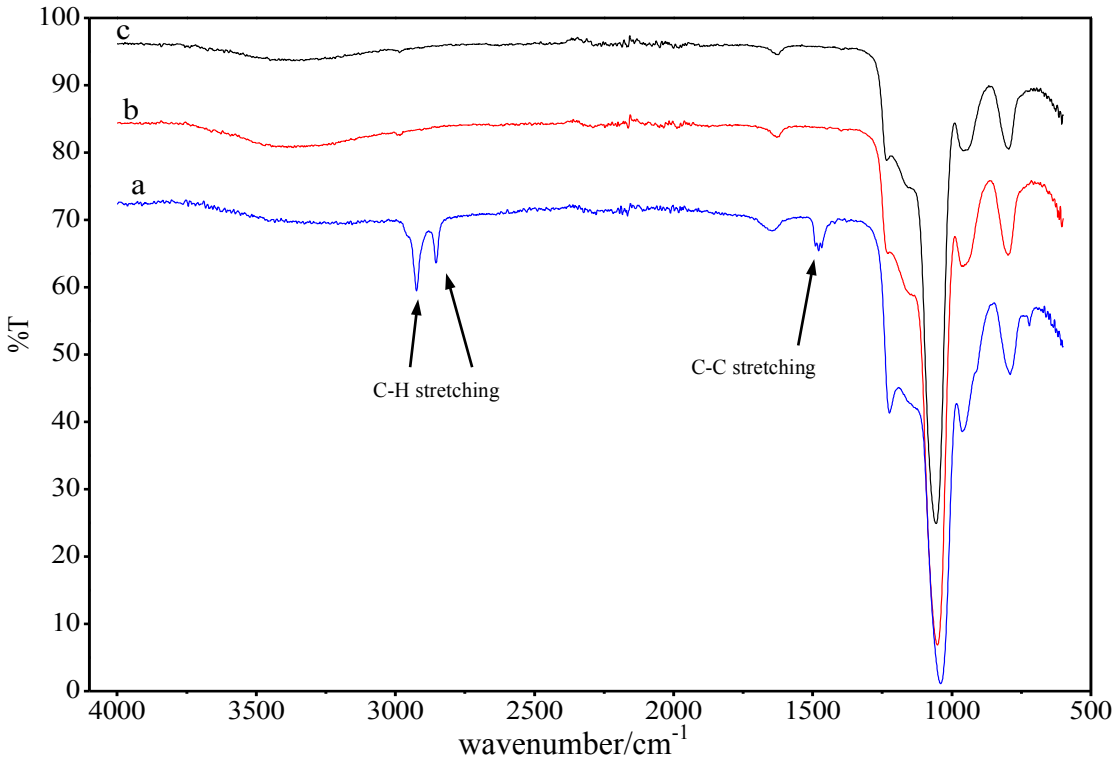

Figure 3.9 FTIR spectra of a) calcined MCM-48, b) extracted MCM-48, and c) As-synthesised MCM-48

Figure 3.10 shows the X-ray diffraction patterns for MCM-48 from which the structure-directing agent has been removed by calcination and acid extraction. As shown in the figure, the peaks for the calcined sample shift toward higher 2θ angle. This basically reveals that the calcined sample possesses a smaller lattice parameter than the extracted sample due to partial structural collapse during calcination at high temperature. In addition, high calcination temperature also results in condensation of silanol groups and shrinkage of the unit cell, as the d-spacing values show in Table 3.2.

For all the mesoporous silicas used in this study the template was removed by solvent extraction.

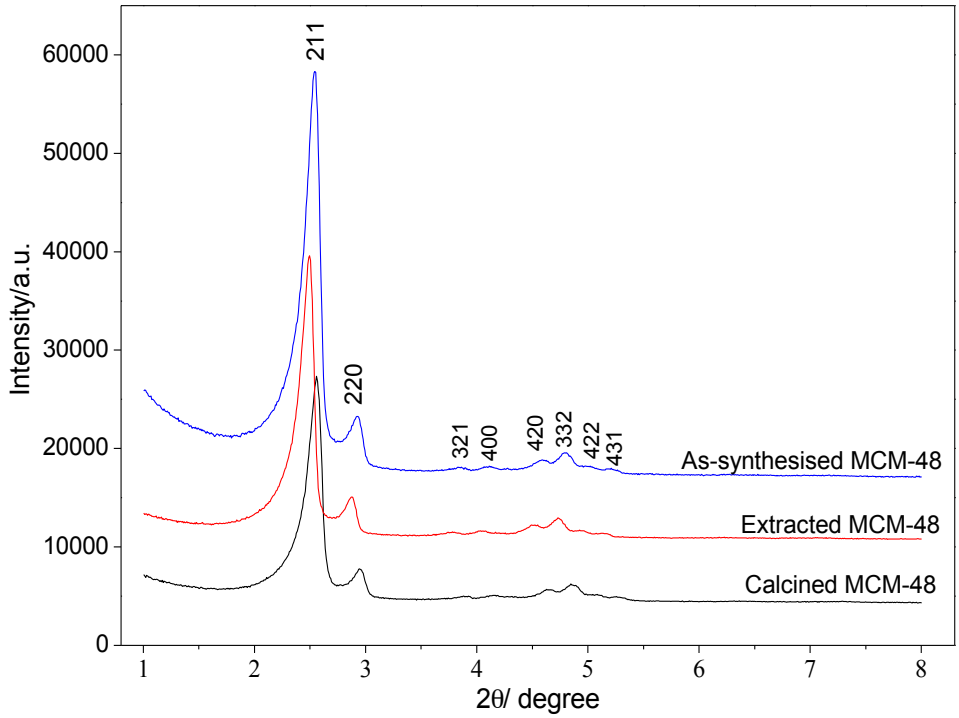

Figure 3.10 Powder X-ray diffraction patterns for a calcined MCM-48, extracted MCM-48, and as-synthesised MCM-48

Table 3.2 Unit cell parameter of crude MCM-48, calcined MCM-48, and extracted MCM-48

Material	$2\theta_{211}$	$2\theta_{220}$	Unit cell parameter, a (Å)
As-synthesised MCM-48	2.52	2.91	85.5
Calcined MCM-48	2.55	2.95	84.8
Extracted MCM-48	2.49	2.86	87.7

3.3.2 Characterisation of ordered mesoporous materials by powder X-ray diffraction

As-synthesised and template extracted mesoporous silicas were characterised by powder X-ray diffraction at ambient temperature at low angle (2θ of 1° to 8°), step size: 0.01°, using a Bruker D8 diffractometer operating in reflection geometry. XRD patterns for as-synthesised and extracted samples are shown in the corresponding figure for comparison. In general, the XRD patterns of extracted mesoporous silicas show a small shift of the peak to lower 2θ angle indicating a larger d-spacing in the extracted samples.

The XRD pattern in Figure 3.11 shows that synthesised MCM-41 possesses the characteristic of a hexagonal *P6mm* cell with the unit cell parameter of ca. 37.7 Å. There is a sharp peak at 2θ = 2.36°, indexed to the (100) reflection and there are also weaker peaks at higher 2θ angle, in the region of 4.0-6.5°, that can be assigned to the (110), (200), and (210) reflections indicating that the synthesised MCM-41 possesses a highly ordered mesostructure.

The XRD pattern of MCM-48 is shown in Figure 3.12. The first and second most intense peaks at 2θ = 2.57° and 2.95° are indexed to be the (211) and (220) reflections and these are distinctive features of cubic space group *Ia3d*, MCM-48. The weak peaks at higher angle also indicate that MCM-48 possesses highly ordered mesostructure. The unit cell parameter of MCM-48 is ca. 86.9 Å.

Figure 3.13 shows the XRD pattern of SBA-1. Three well-resolved XRD diffraction peaks at 2θ of 2.2º, 2.5º, and 2.7º are presented, which are indexed to the (200), (210), and (211) reflections, respectively. These diffraction peaks are characteristic of the cubic *Pm3n* space group. The unit cell parameter of the synthesised SBA-1 is ca. 80.7 Å. In addition, some weak peaks in the range of 3.5º to 6º indicate that the SBA-1 sample has a high order cubic mesostructure.

The XRD pattern of SBA-2 (Figure 3.14) shows the most intense peak at 2θ of 2.08° which can be indexed to the (002) reflection, characteristic of the cage-like hexagonal structure with space group *$P6_3/mmc$* as shown in Figure 3.10. The weaker peaks at higher 2θ angle, (100) and (112), also indicate that SBA-2 possesses highly ordered mesostructure as mentioned in the MCM-41, MCM-48, and SBA-1 section earlier. The unit cell parameter of SBA-2 is ca. 47.6 Å.

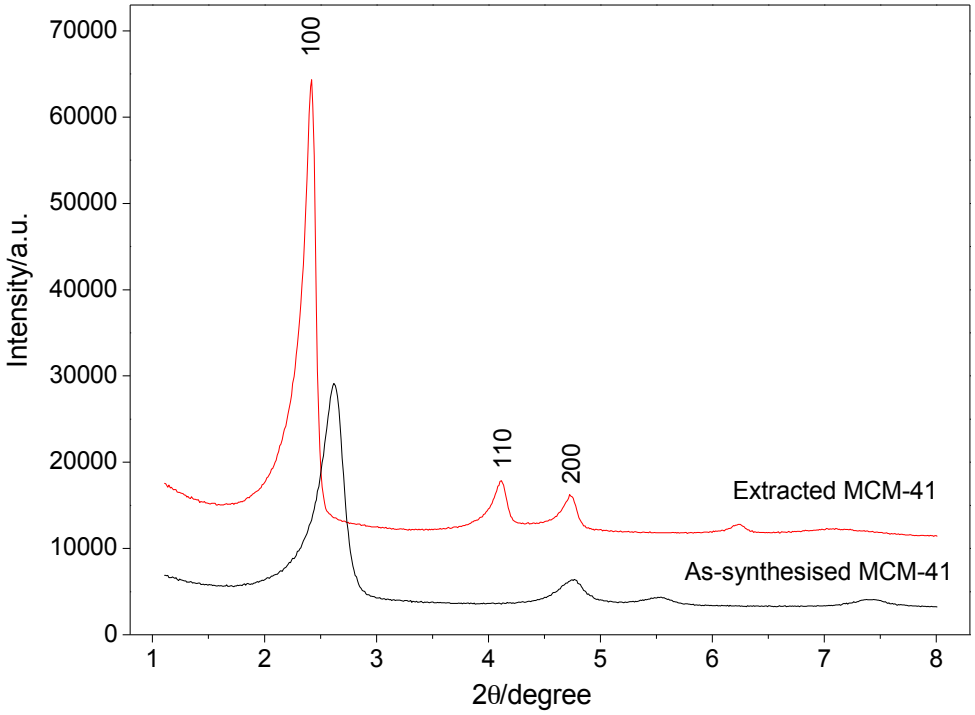

Figure 3.11 Powder X-ray diffraction pattern of MCM-41

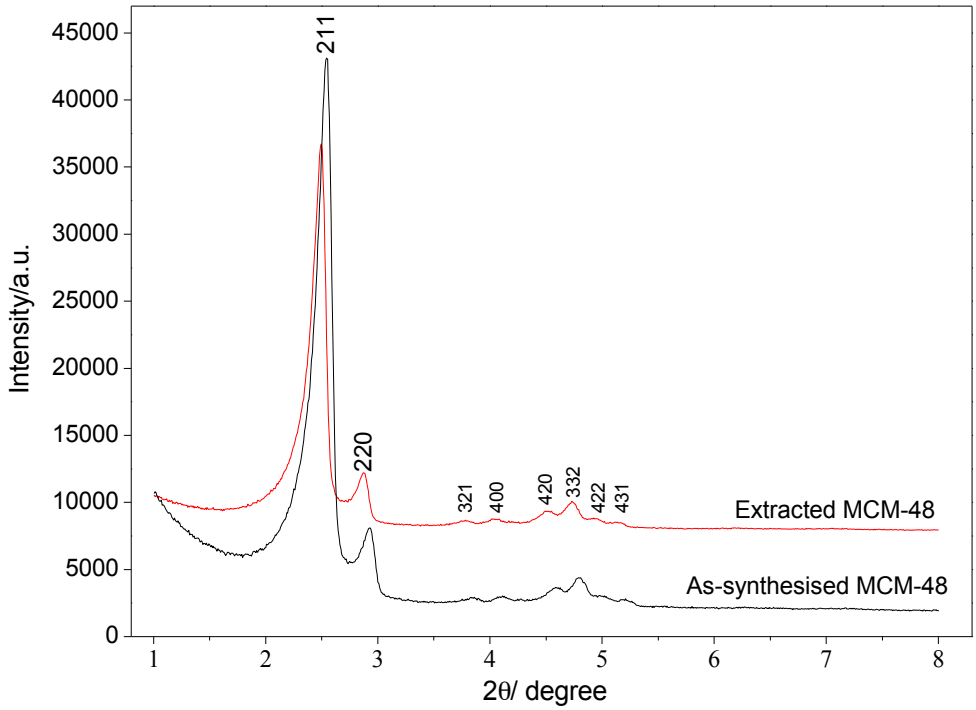

Figure 3.12 Powder X-ray diffraction pattern of MCM-48

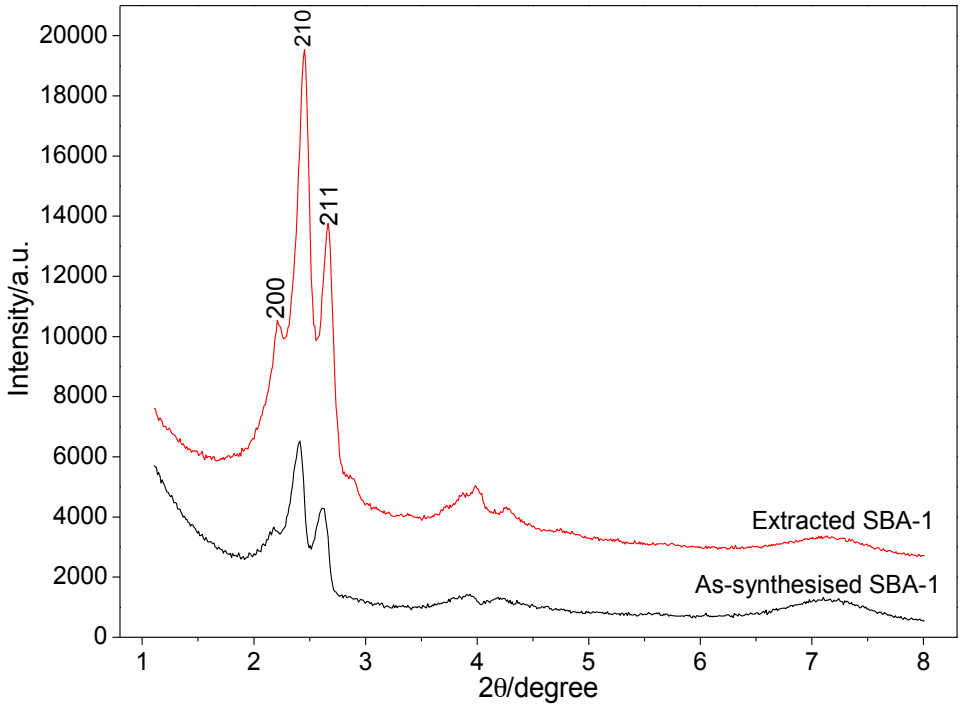

Figure 3.13 Powder X-ray diffraction pattern of SBA-1

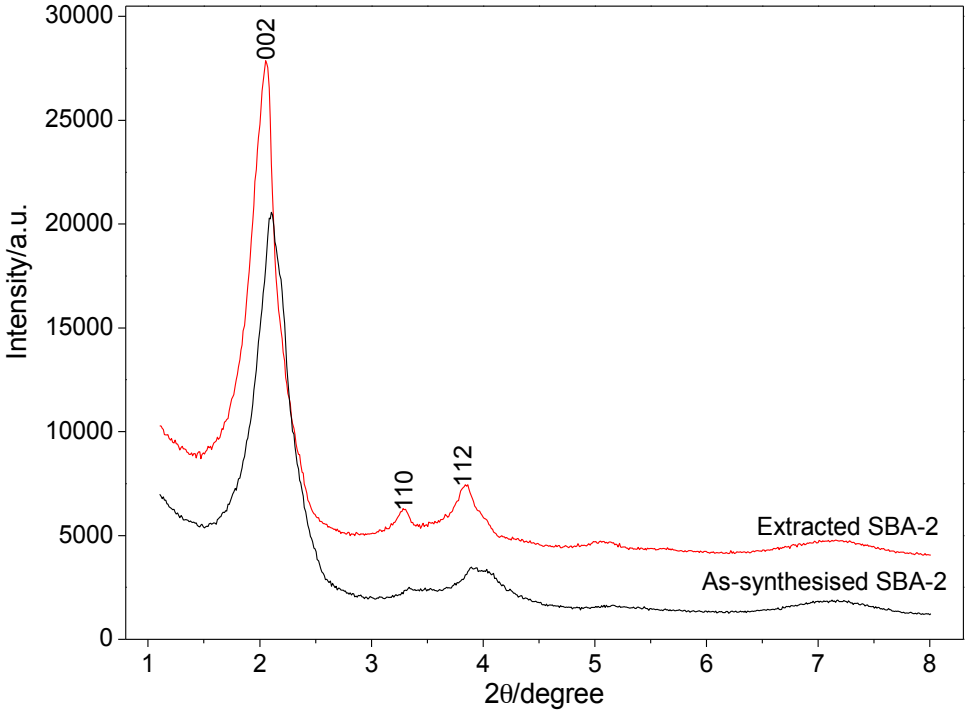

Figure 3.14 Powder X-ray diffraction pattern of SBA-2

3.3.3 Characterisation of mesoporous silicas by nitrogen adsorption-desorption

The measurements of gas (such as nitrogen) adsorption at the gas/solid interface provides essential information of the nature and behaviour of solid surfaces. They are widely used for the determination of surface area and pore size distribution of the solid materials such as catalysts, adsorbents, and pigments[2].

Nitrogen adsorption-desorption isotherms of the synthesised mesoporous silicas have been measured with a Quantachrome Autosorb1 instrument. The adsorption-desorption isotherm and pore size distribution of MCM-41, MCM-48, SBA-1, and SBA-2 are shown in Figure 3.15, Figure 3.16, Figure 3.17, and Figure 3.18, respectively. They all exhibit the type IV adsorption isotherm, which is the characteristic feature of mesoporous materials.

MCM-41 (Figure 3.15) shows a sharp increase of nitrogen uptake at $P/P_0 \approx 0.3$. This step is caused by the capillary condensation in mesopores. The initial part of this isotherm is attributed to the formation of monolayer-multilayer adsorption, where the monolayer coverage is complete and the multilayer adsorption begins at $P/P_0 \approx 0.1$. The unusual desorption steps at $P/P_0 \approx 0.7$ for MCM-41(Figure 3.15) and at $P/P_0 \approx 0.6$ for SBA-2 (Figure 3.18) are observed; this is suggested to be caused by some defect holes in the structure [156].

The adsorption isotherm of MCM-48 (Figure 3.16) shows the capillary condensation of nitrogen inside the pore at the relative pressure $P/P_0 \approx 0.3$. The well-defined step in the adsorption isotherm reveals a narrow and uniform pore size distribution, which is seen for the MCM-48 sample. SBA-1 (Figure 3.17) shows the monolayer- multilayer adsorption and capillary condensation at lower relative pressure (i.e. the monolayer coverage is completed and the multilayer starts at $P/P_0 \approx 0.05$ and capillary condensation occurs at $P/P_0 \approx 0.2$) which

could be attributed to the smaller pore as evidenced by the pore size and pore volume data[157, 158].

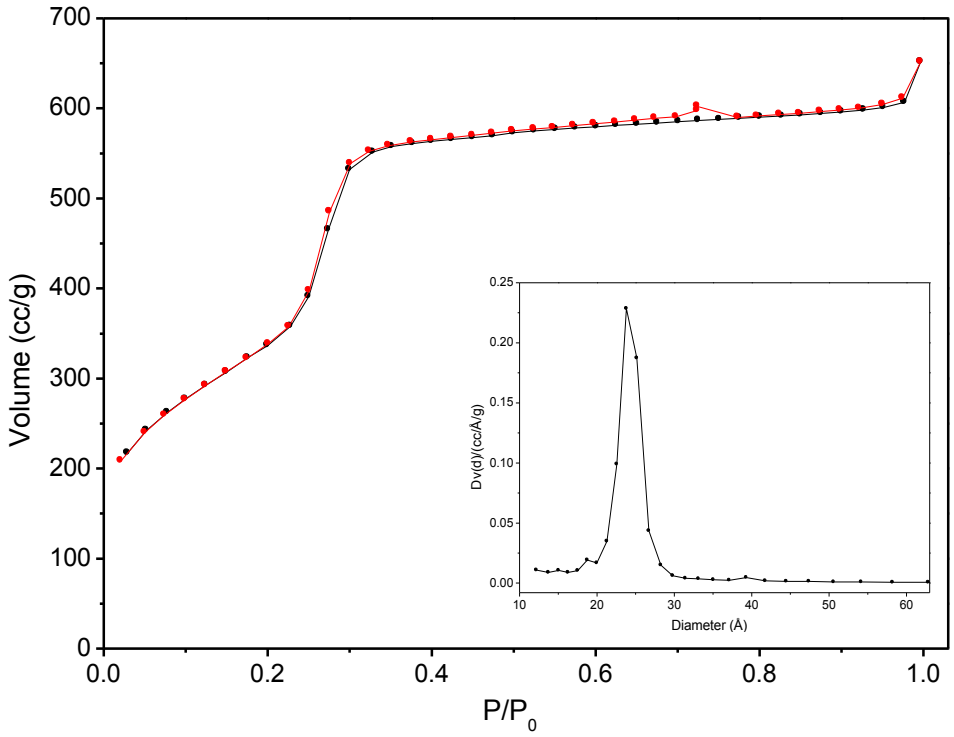

Figure 3.15 Nitrogen adsorption-desorption isotherm and pore size distribution of MCM-41

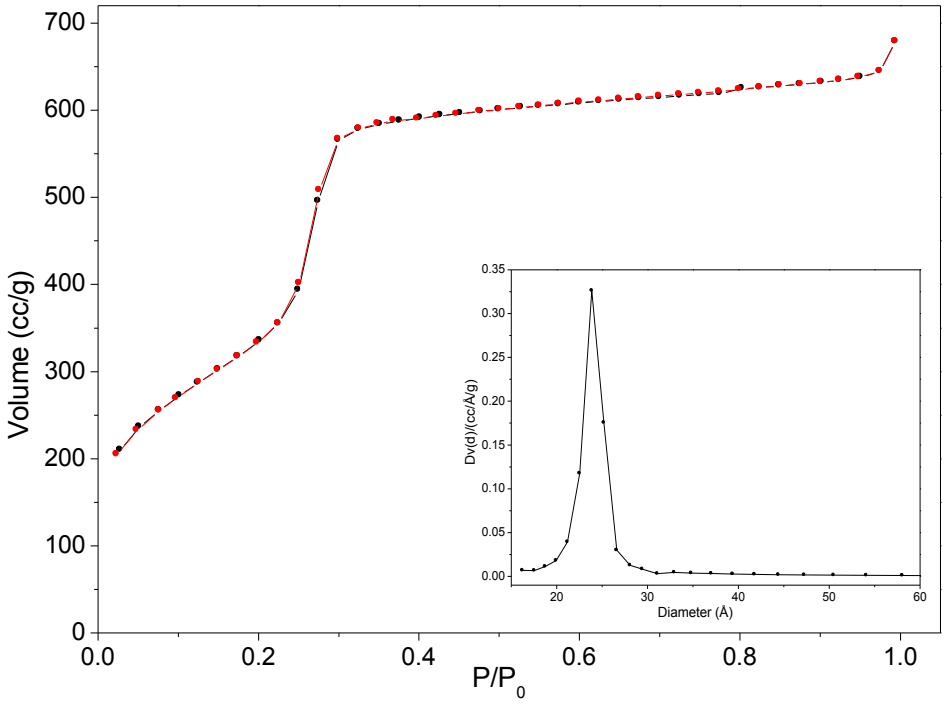

Figure 3.16 Nitrogen adsorption-desorption isotherm and pore size distribution of MCM-48

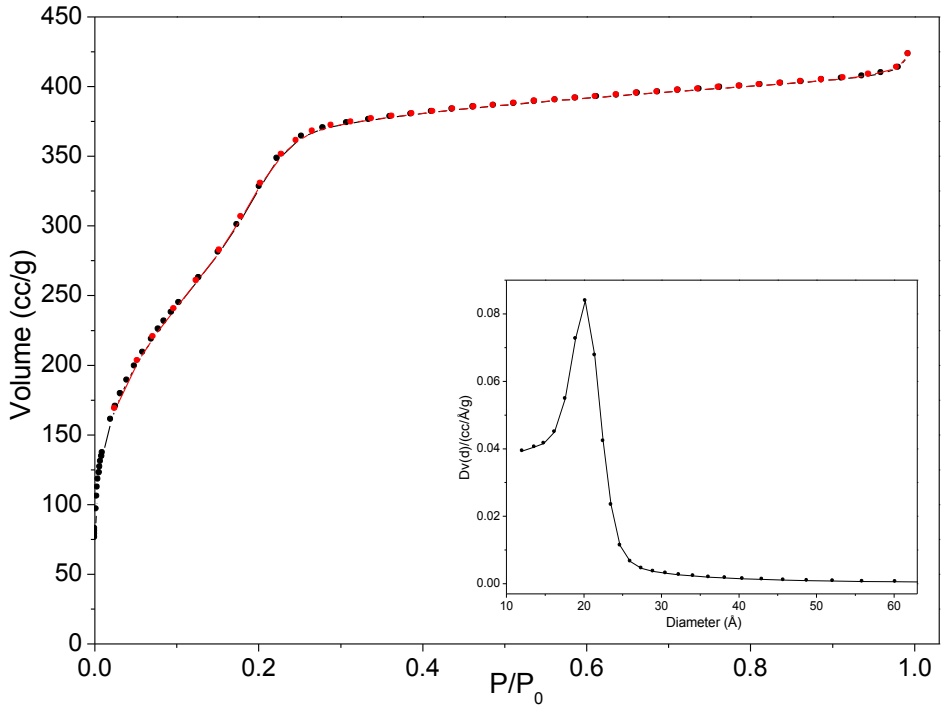

Figure 3.17 Nitrogen adsorption-desorption isotherm and pore size distribution of SBA-1

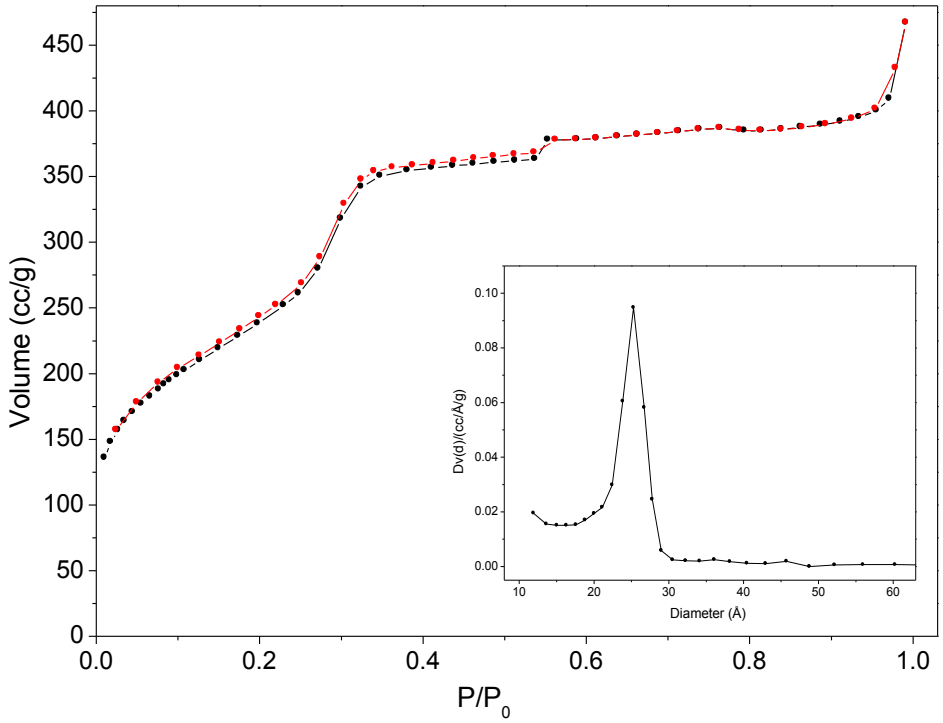

Figure 3.18 Nitrogen adsorption-desorption isotherm and pore size distribution of SBA-2

Surface area, pore diameter, and pore volume of the synthesised mesoporous silicas are presented in Table 3.3. MCM-41 and MCM-48 show larger surface area compared to SBA-1 and SBA-2; from this it could be concluded that MCM-41 and MCM-48 materials have the smaller particles.

Table 3.3 BET Surface area, pore diameter, and pore volume of the synthesised mesoporous silicas

Material	S_{BET} (m^2g^{-1})	Pore diameter* (nm)	Pore volume* (cm^3g^{-1})
MCM-41	1254	2.4	1.12
MCM-48	1229	2.4	1.20
SBA-1	995	2.3	1.02
SBA-2	884	2.5	1.10

*Calculated from the adsorption branch

3.4 CONCLUSION

Ordered mesoporous silicas MCM-41, MCM-48, SBA-1, and SBA-2 have been successfully synthesised using TEOS as silica source with synthesis conditions and structure directing agent varied depending on the final desired structure; CTAB for MCM-41 and MCM-48, CTEAB for SBA-1, and gemini surfactant $C_{16\text{-}3\text{-}1}$ for SBA-2. The resulting materials possess the expected characteristics as confirmed by their powder X-ray diffraction patterns and nitrogen adsorption-desorption isotherms. In all materials, high surface areas and narrow pore size distributions were observed.

CHAPTER 4 AMINO MODIFIED MESOPOROUS SILICAS

4.1 INTRODUCTION

4.1.1 Modification of ordered mesoporous silicas

In Chapter 3, we have discussed the synthesis, structure and properties of ordered mesoporous silicas. This chapter will focus on the modification of these materials with amino groups which are basic organic functional groups that can be used as catalysts in carbon-carbon bond forming reaction such as the Knoevenagel condensation [74, 159-161]. The effect of different mesoporous supports on the catalytic activity and reusability will also be investigated and discussed.

Due to their structures, the ordered mesoporous materials not only possess a high surface area and a uniform pore size but they also provide three different sites for the reaction: internal pore surface, surface near the pore window, and the external surface. Since the surface of these materials exhibit only silanol groups, therefore, in order to obtain the most effective use in specific applications, the silica surface needs to be modified by attachment of other functional groups. Alternatively, various types of functional groups can be incorporated into the silica walls.

The incorporation of heteroatoms such as trivalents cations (Al^{3+}, B^{3+}, Ga^{3+}, Fe^{3+}) permits the materials to be used in acid catalysed reactions[162], while other cations (Ti^{4+}, V^{4+}, Sn^{4+}, Zr^{4+}) allow use in other reactions e.g. redox catalysis[162]. Moreover, the incorporation of organometallic and organic functional groups and their applications had also been reported. Organic groups, for example, vinyl groups[163], organic chromophores[164], alkyl halides [165], thiol groups[166], etc, have all been reported to be attached to mesoporous silica. Organic

functional groups modified mesoporous silica can be used in many applications e.g. catalysis, adsorption, separation, and sensors[3, 69]. Synthesis methods for functionalisation of mesoporous silicas can be broadly categorised into two different routes: direct synthesis (also called co-condensation or one-pot synthesis) and post synthesis grafting methods.

4.1.1.1 Direct synthesis

In direct synthesis, the functional groups can be directly incorporated into the framework; they might be a pendant group on the surface or located as the bridges between silicon atoms within the mesoporous framework[3]. For this synthesis method, the silica precursor is polymerised in the presence of a functional organosilane, which is the standard reagent, used for surface modification of ordered mesoporous silicas. In this way, the homogeneous incorporation of the functional groups is possible. However, calcinations at high temperature cannot be applied for the removal of the structure directing agents in the case of direct synthesis, because it would destroy the organic functionality at the same time as the template is removed. Therefore, acid extraction is used in order to remove the structure directing agent. One drawback for direct synthesis is that the presence of the additional functional silanes may disturb the formation of long-range ordered mesoporous materials and results in a decrease in structural order with increasing organic function. For this reason the maximum concentration of functional groups on the surface is limited (about 0.6%) [165].

4.1.1.2 Post grafting method

The post-grafting method modifies the wall surfaces of the pre-synthesised mesoporous materials, leading to an increase of pore wall thickness and also an increase of the functional group concentration on the surface[167]. By using post-grafting methods, functional groups have been covalently attached to the surface of the pre-made mesoporous materials, but

homogenous distribution of the functional groups on the silica surface is not often achieved and there is the possibility for pore blocking to occur.

4.1.2 Modification of mesoporous silicas by the amino group

The mesoporous silicas have been modified with various functional groups in order to adjust the surface functionality to be used in different applications. One of the most common functional groups to be incorporated into mesoporous materials is the basic amino group. This amino group can act as the active site for base catalysed reactions. With the advantage of mesoporous silicas possessing high surface area, a high concentration of active basic sites can be achieved in the amino-modified mesoporous silicas. 3-aminopropyltrimethoxy silane has been commonly used as the source of amino group to modify the mesoporous silicas surface.

Amino-modified MCM-41 was reported to be an efficient and reusable heterogeneous catalyst for the Knoevenagel condensation reaction[160, 168], and has also been used as a adsorbent for toxic species such as chromate and arsenate via the ionic interaction between ammonium ion and oxyanions (CrO_4^{2-}, $HAsO_4^{2-}$)[169]. Not only has MCM-41 been used as the support material but amino-modified MCM-48 and SBA-1 have also been prepared and their used as adsorbent and catalyst had also been reported[170].

This chapter will focus on the modification of mesoporous silicas with different pore structures; which are 2-dimensional hexagonal MCM-41, 3-dimensional cubic MCM-48, 3-dimensional cage-like cubic SBA-1, and cage-like hexagonal SBA-2 with amino groups via post-grafting methods. Catalytic activity of the modified materials will be tested by using the Knoevenagel condensation as the probe reaction. The effect of pore structure of the support materials to the catalytic activity and reusability will also be investigated. In addition, as the

Knoevenagel condensation is a base catalysed reaction, the further surface modification to capture the remaining silanol is also carried out and will be discussed later in Chapter 6.

4.2 EXPERIMENTAL

4.2.1 Post-synthesis grafting of mesoporous silicas with 3-aminopropyltrimethoxy silane

1.0 g of mesoporous silica (MCM-41, MCM-48, SBA-1, or SBA-2) was suspended in 30 ml anhydrous toluene (99.8%, Sigma Aldrich), and 0.5 g 3-aminopropyltrimethoxysilane (97%, Avocado) was added. The reaction mixture was then refluxed for 24 hours. The resulting amino-modified mesoporous silica (denoted as NH_2-mesoporous silica) was filtered out and washed with toluene followed by drying at room temperature for 24 hours. The schematic diagram of amino-modified mesoporous silica is shown in Figure 4.1.

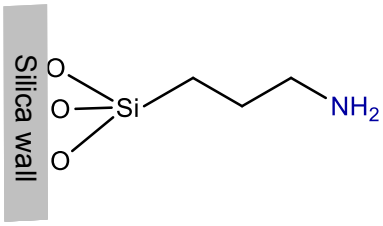

Figure 4.1 Amino-modified mesoporous silica

4.2.2 Catalytic activity testing

Knoevenagel condensation was carried out in the round bottomed flask under nitrogen atmosphere at 70 °C. 0.10 g of catalyst, 5.00 ml dry toluene as a solvent, 0.1 mmol

ethylcyanoacetate (98%, Sigma Aldrich), and 0.1 mmol benzaldehyde (99%, Sigma Aldrich) were mixed and the reaction was performed for 1 hour. The catalyst and reaction mixture were separated by filtration. The reaction mixture was analysed by gas chromatography, while the catalyst was washed with water and dried at 60 °C for 24 hours followed by drying at 150 °C under vacuum for 3 hours.

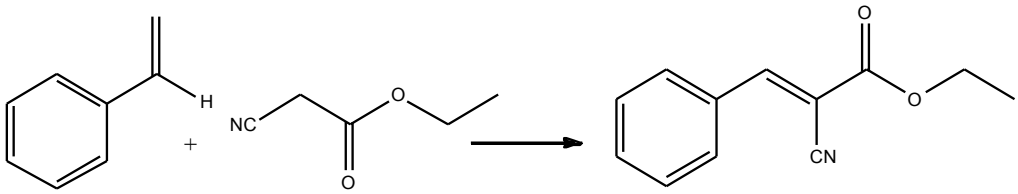

Figure 4.2 Knoevenagel condensation reaction of benzaldehyde and ethylcyanoacetate

4.2.3 The reusability of amino-modified mesoporous silica

The recovered NH_2-mesoporous silica catalysts were reused until they became inactive. The procedure of catalyst reuse is similar to the normal catalytic testing run. When each reaction has finished, the catalyst was washed with water and dried at 60 °C for 24 hours, followed by drying under vacuum. The used catalysts were dried at 150 °C under vacuum for 3 hours before being re-used.

4.3 RESULTS AND DISCUSSION

4.3.1 Characterisation of amino-modified mesoporous silicas

4.3.1.1 Characterisation of amino-mesoporous silicas by powder X-ray diffraction

Powder X-ray diffraction patterns of amino modified mesoporous silicas were recorded on a Bruker D8 instrument with the reflection geometry from 1° to 8°, step size 0.01°. All the amino-modified mesoporous silicas exhibit the characteristic X-ray diffraction pattern of the support materials as shown in Figure 4.3, Figure 4.4, Figure 4.5, and Figure 4.6. For comparison, the X-ray diffraction patterns of the modified and their corresponding pure siliceous materials are shown in the same figure. The diffraction peaks of the modified siliceous materials slightly shift to the higher 2θ angle; this suggests that the incorporation of amino group leads to the reduction of unit cell parameter caused by the surface modification. The compared unit cell parameter, a, of pure and amino-modified mesoporous silicas are shown in Table 4.1

However, the smaller peaks at higher angles appear to be of lower intensity for the modified materials. Since these peaks relate to the long range order mesostructure, this could be suggested that the incorporation of the amino group leads to less structural order of these materials[171-173], or in other words, the structure of amino-modified mesoporous silicas are less ordered than that of the pure mesoporous silicas materials.

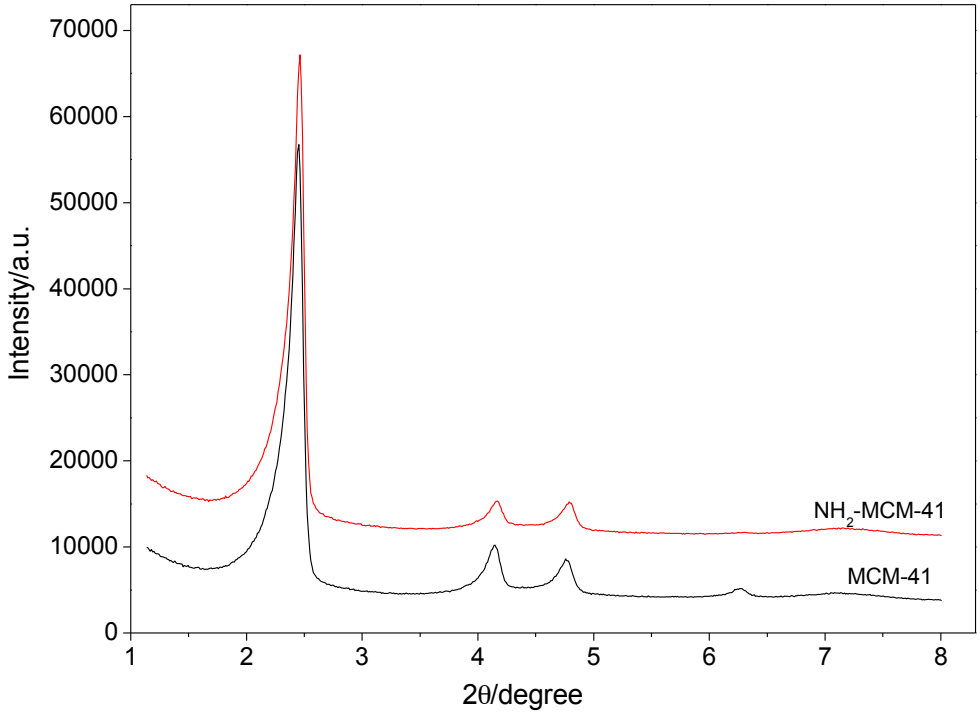

Figure 4.3 Powder X-ray diffraction pattern of NH_2-MCM-41

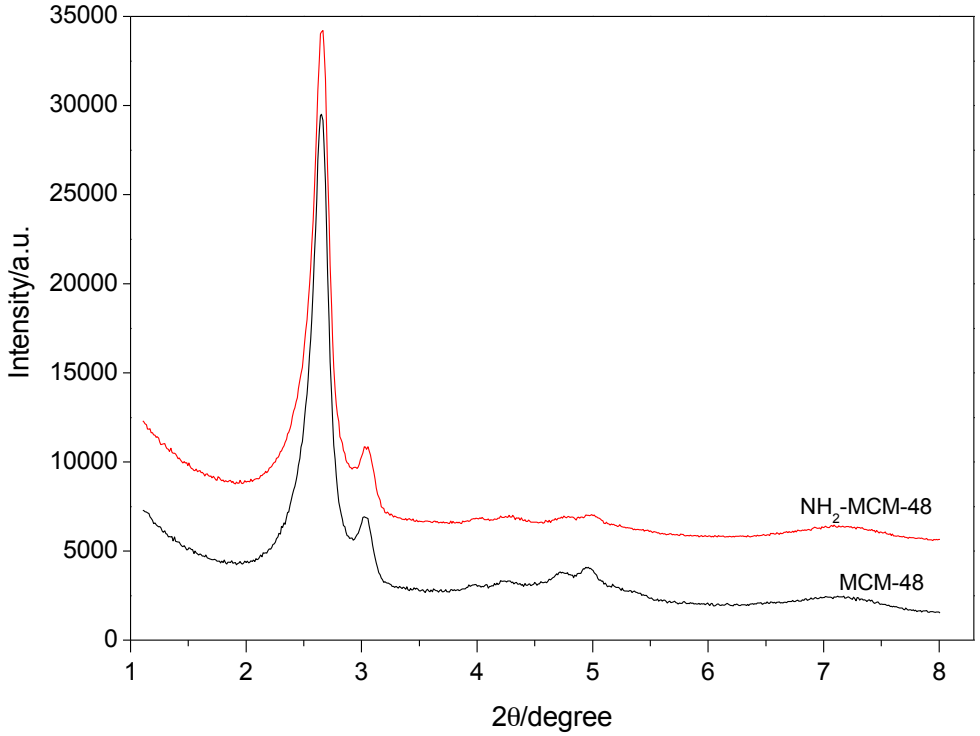

Figure 4.4 Powder X-ray diffraction pattern of NH_2-MCM-48

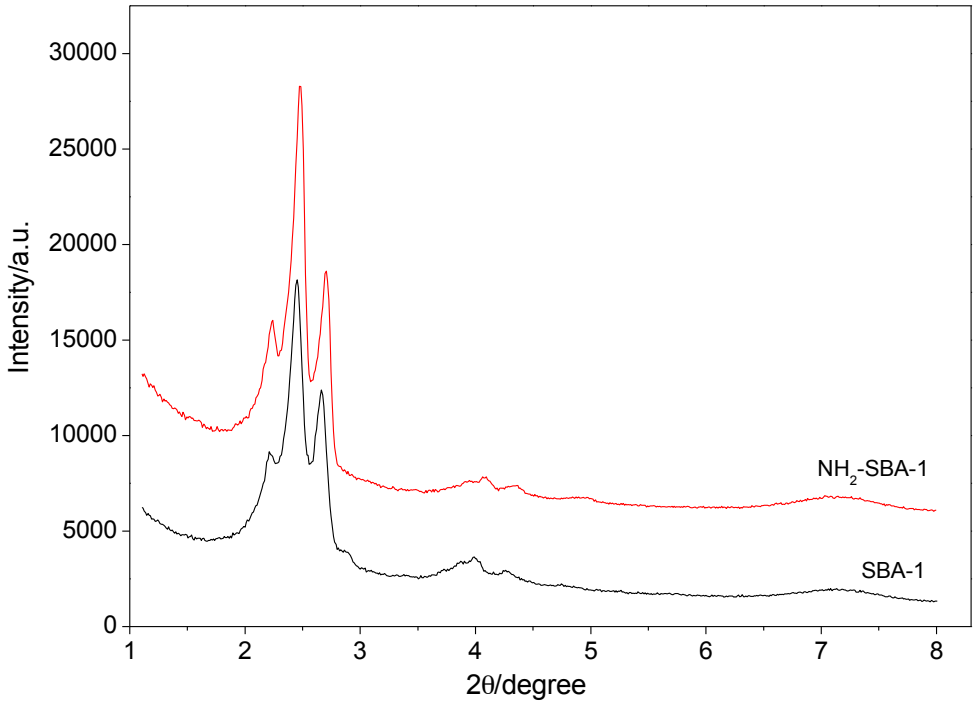

Figure 4.5 Powder X-ray diffraction pattern of NH_2-SBA-1

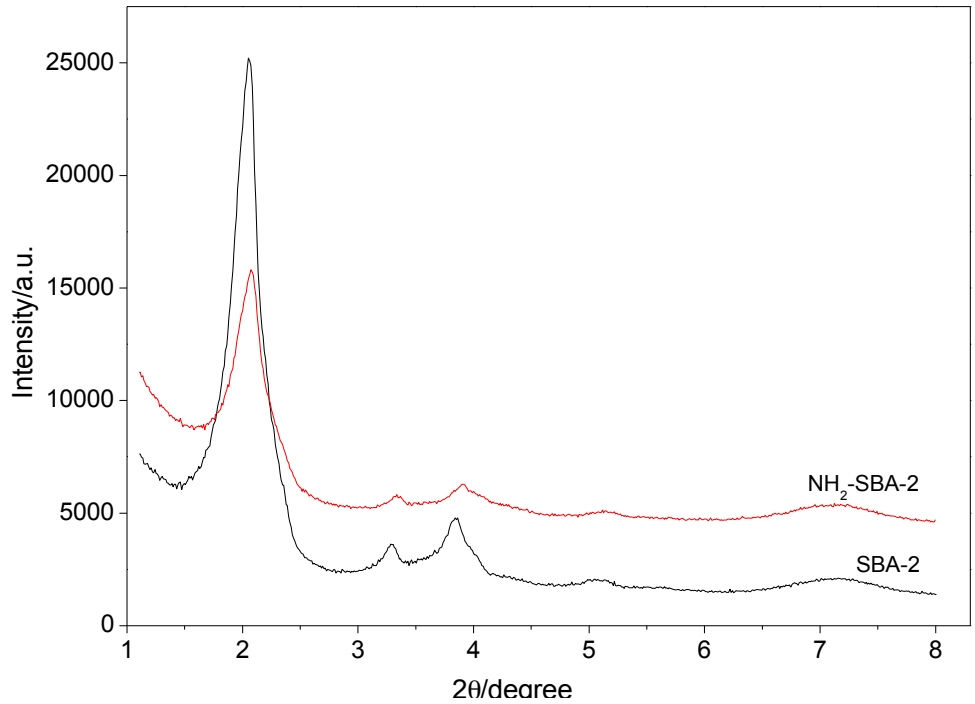

Figure 4.6 Powder X-ray diffraction pattern of NH_2-SBA-2

Table 4.1 Unit cell parameter, a, for amino-modified mesoporous silica

Mesoporous Silicas	Unit cell parameter, a, (Å)	
	Unmodified mesoporous materials	Amino-modified material
MCM-41	36.7	36.5
MCM-48	82.1	81.6
SBA-1	80.5	79.7
SBA-2	46.8	46.0

4.3.1.2 Characterisation of amino-modified mesoporous silica by Elemental Analysis

The appearance of amino groups is revealed by the percentage of nitrogen, as no nitrogen was found in the pure siliceous materials structure, so it can be assumed that all the nitrogen found is from the functional groups attached. Elemental analysis results of the modified materials are shown in Table 4.2.

Table 4.2 Elemental analysis results for amino-modified mesoporous silica

Catalyst	Carbon (mmol/g)	Nitrogen (mmol/g)
NH_2-MCM-41	4.79	1.77
NH_2-MCM-48	5.95	1.92
NH_2-SBA-1	5.50	1.83
NH_2-SBA-2	4.60	1.17

As mentioned in the experimental section, all the mesoporous supports were modified by the same amount of amino functional group (concentration of ca. 2.79 mmol/g). However, the elemental analysis results show that the amounts incorporated are actually different. This suggests that different supports materials can accommodate a different quantity of the functional group; MCM-48 and SBA-1 appear to be the more favourable structures for the incorporation of a higher concentration of amino groups due to their multi-dimensional pore systems.

4.3.1.3 Characterisation of amino-modified mesoporous silica by nitrogen adsorption-desorption

The adsorption isotherm of amino-modified mesoporous silicas NH_2-MCM-41 and NH_2-MCM-48 are shown in Figure 4.7 and Figure 4.8. The well-defined adsorption steps were not observed. The unusual adsorption-desorption hysteresis step was found for NH_2-MCM-48 these have been reported by Eddaoudi et al.[174], Walton et al.[175], and Wang et al.[176] but no comment was made in these papers on this step. Lin et al [156] suggested that the unusual hysteresis process is associated with the pore-blocking effect around the embedded voids in the framework structure.

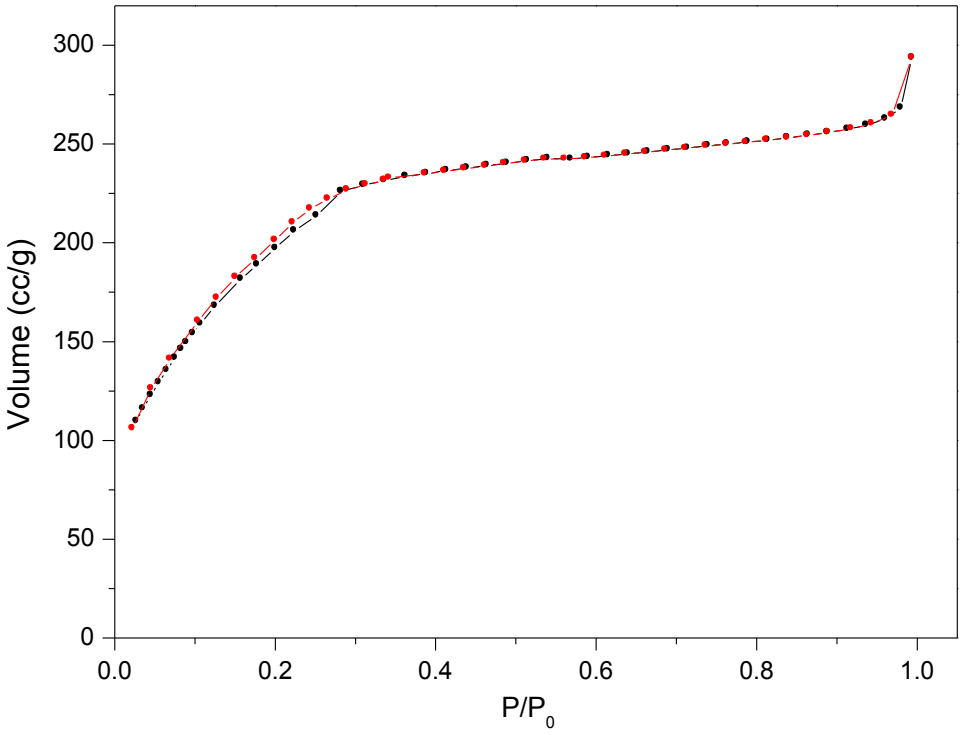

Figure 4.7 Nitrogen adsorption-desorption isotherm of NH_2-MCM-41

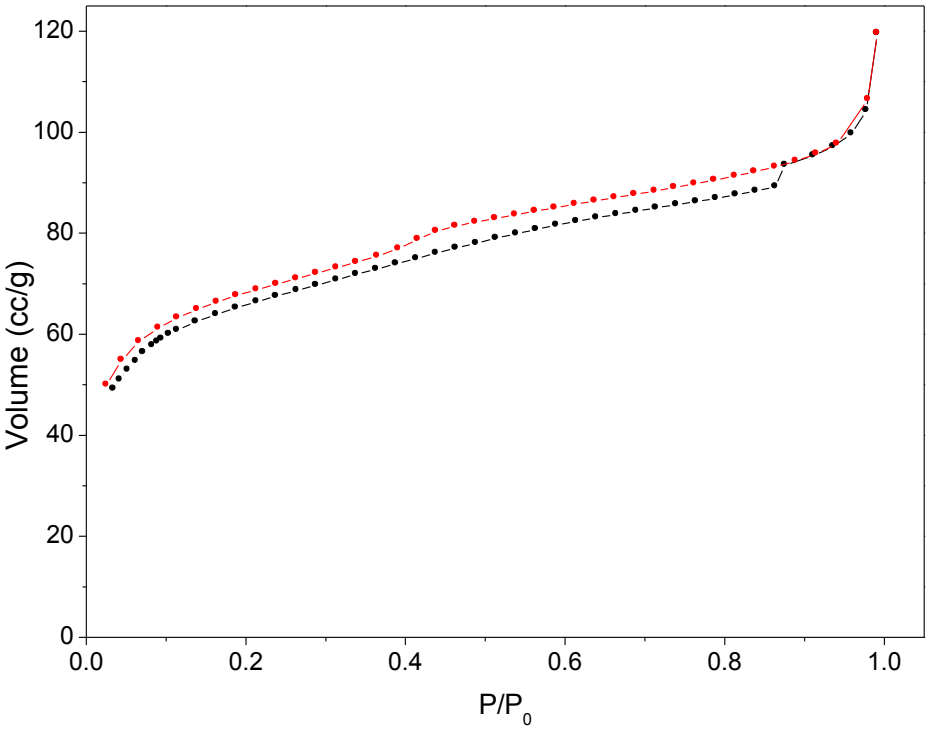

Figure 4.8 Nitrogen adsorption-desorption isotherm of NH_2-MCM-48

Table 4.3 Surface area, pore size and pore volume of amino-modified mesoporous materials

Materials	S_{BET} (m^2g^{-1})	Pore Diameter* (nm)	Pore Volume* (cm^3g^{-1})
NH_2-MCM-41	753	2.1	0.74
NH_2-MCM-48	235	3.1	0.33
NH_2-SBA-1	186	3.2	0.26
NH_2-SBA-2	122	2.5	0.22

*Calculated from the adsorption branch

Table 4.3 presents the surface area, pore volume, and pore diameter of amino-modified mesoporous silicas. Surface area was calculated by the BET method in the range of P/P_0=0.05-0.3. Pore volume and pore diameter were estimated by the BJH method from the adsorption isotherm. The surface area of NH_2-MCM-41 is highest among these 4 catalysts and also possesses the largest pore volume. The modified mesoporous samples show lower surface area and lower pore volume than their parent materials; this could be attributed to the occupation of some space inside the mesopores by the amino groups [177], as also suggested by the lower amount of N_2 adsorbed. For NH_2-MCM-48, the significant decrease in surface area is observed, this may caused by the high percentage of amino group loaded[178-181]. The cage-like structures, NH_2-SBA-1 and NH_2-SBA-2, are found to be more affected by the surface modification with amino group due to more possibility of the pore blockage at the pore window thus resulting in the lowering of surface area and pore volume [177, 182-184].

4.3.2 Activity of the synthesised catalysts

4.3.2.1 Catalytic activity of amino-modified mesoporous silica in the Knoevenagel condensation reaction

The Knoevenagel condensation can be described as the nucleophilic addition of an active hydrogen to a carbonyl group from ketone or aldehyde followed by a dehydration reaction. In this study, the Knoevenagel condensation between benzaldehyde and ethylcyanoacetate, shown in Figure 4.9, was the probe reaction for catalytic activity testing of the prepared amino-modified mesoporous silicas.

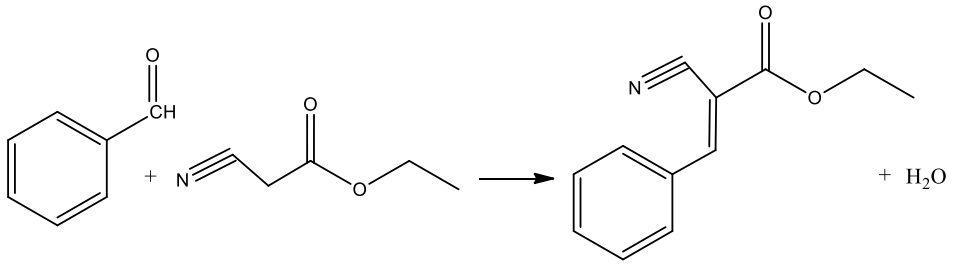

Figure 4.9 Knoevenagel condensation of benzaldehyde and ethylcyanoacetate

Conversions of the Knoevenagel condensation reaction to the expected product, ethyl 2-cyano-3-phenylacrylate at different reaction time for each catalyst and at 1 hour (i.e. when the reaction completed) are shown in Figure 4.10 and Table 4.4.

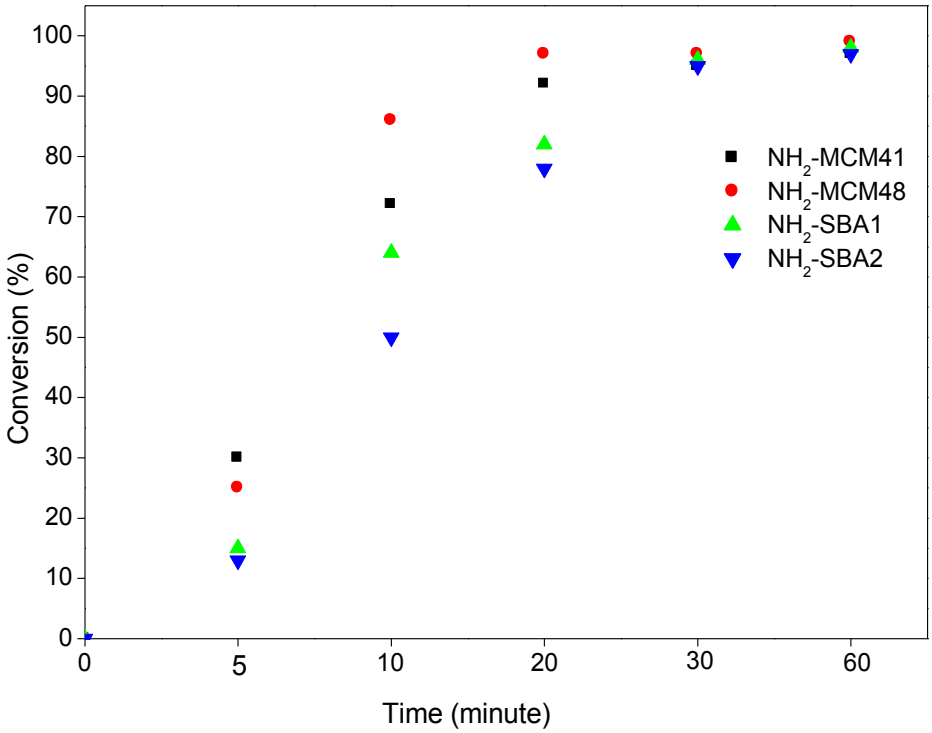

Figure 4.10 Conversion of Knoevenagel condensation reaction using NH_2-mesoporous silica as catalyst at different time

Table 4.4 Conversion of Knoevenagel condensation reaction using NH_2-mesoporous silica as catalyst at 1 hour

Catalyst	Conversion (%) *
NH_2-MCM-41	97.6 ± 1.5
NH_2-MCM-48	99.1 ± 0.8
NH_2-SBA-1	98.2 ± 0.8
NH_2-SBA-2	96.7 ± 1.2

*The conversions shown are from three repeated reactions, reported in (average value ± S.D.)

It is observed that all the amino-modified mesoporous silicas are active in the Knoevenagel condensation reaction of benzaldehyde and ethylcayanoacetae. NH_2-SBA-1 and

NH_2-SBA-2 show lower rate of reaction, however their activities are still high enough to achieve high conversion at after 30 minutes, this could be the benefit of having multi-dimensional pore structures in SBA-1 and SBA-2. There is no significant difference in the reaction conversions between different mesoporous supports at the reaction equilibrium and they are not affected by the small differences in concentration of amino group loaded (Table 4.2); conversion over the NH_2-SBA-2 catalyst reaches the same value as NH_2-MCM-41, and NH_2-SBA-1 despite having the lowest surface functionalisation.

Other factors that must be considered as possibly having an effect on the conversion achieved are the surface area and pore volume, as higher surface area supported catalysts are more capable for providing better functional group distribution. However, the results show that NH_2-MCM-41 which has highest surface area and pore volume shows slower reaction than that of NH_2-MCM-48 whose surface area and pore volume are smaller, this is again could be attributed to the advantage of possessing multi-dimensional pore structure in MCM-48. In addition, the slow reaction that observed from NH_2-SBA-1 and NH_2-SBA-2 catalysts could possibly be caused by the blockage at the pore entrances of the cage-like supports, SBA-1 and SBA-2[182-184].

This is of the same tendency with Kubota et al [160], who proposed that the cage-like mesoporous supported catalyst, NH_2-SBA-1, exhibits slower reaction in the Knoevenagel condensation of benzaldehyde and ethylcyanoacetate (the same reaction as studied here) compared to NH_2-MCM-41; NH_2-MCM-41 shows 81% while NH_2-SBA-1 shows 43% conversion at 30 minutes and reaction with NH_2-MCM-41 reaches equilibrium at 1 hour while 6 hours for NH_2-SBA-1. But it is noted that the amino group loaded in that work is lower than this study (1.3-1.4 mmol/g).

4.3.2.2 Catalyst recycling

All the amino-modified mesoporous silicas show very high conversion in the Knoevenagel condensation reaction, but one of the advantages of using heterogeneous catalysts is their easy recyclability; therefore the reusability of catalysts was examined. Different solvents such as toluene, THF, and water were used in order to wash the catalysts prior to drying and reuse, but it was found after extensive trials that the optimum solvent for catalyst washing is water. The conversions obtained upon catalyst reused are shown in Figure 4.11. For most of catalyst, the activity remained high until the third use.

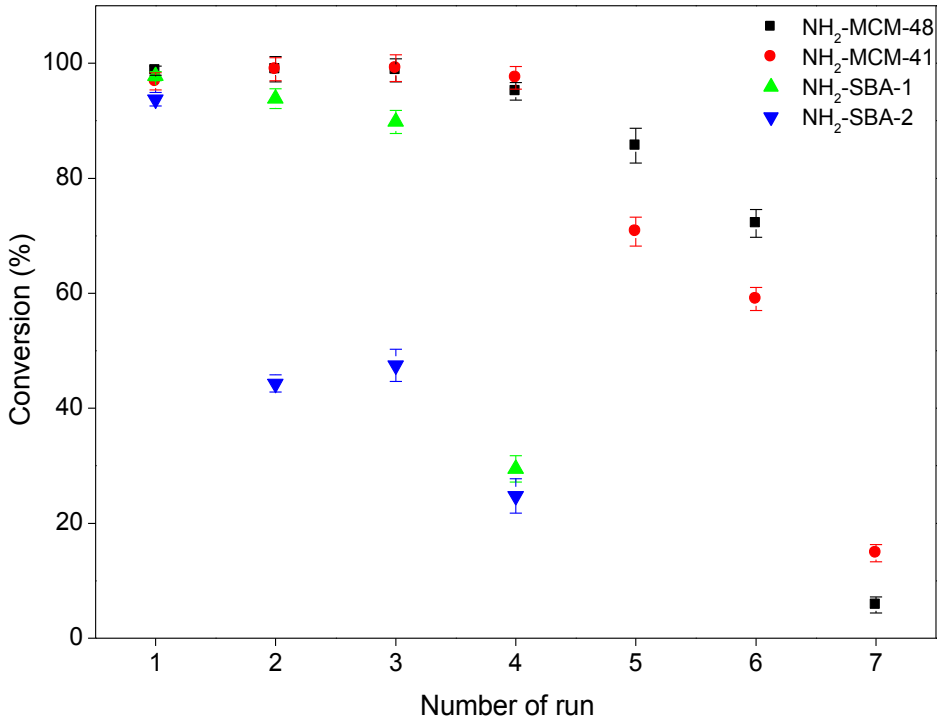

Figure 4.11 Reusability of the amino-modified mesoporous silica catalysts

As discussed in 4.3.2.1, conversion achieved in the Knoevenagel condensation reaction at the equilibrium was not affected by slightly different amounts of amino groups incorporated or the structure of the support materials, all catalysts exhibiting high conversion (>95%). However, in terms of recycling, the structure of the support material plays an

important role. The amino-modified MCM-48 shows the best reusability, and can be used 5 times without any significant loss in conversion. This is suggested to be attributed to the 3-dimensional cubic structure of MCM-48 allowing better diffusion of reactants through the pores (i.e. more possibility for reaction to take place at the active sites inside the pore) than the 2-dimensional hexagonal MCM-41 or the cage-like mesoporous silicas SBA-1 and SBA-2, whose pore entrances are smaller than their pore diameter (pore entrances of cage-like SBA-1 and SBA-2 are of ca. 0.4-1.5 nm [184-186]). Therefore in these latter cases, pore blocking is more likely to occur upon use and may cause the reduction in catalyst activity.

4.3.2.3 Reaction mechanism

The reaction mechanism of the Knoevenagel condensation using the amino-modified ordered mesoporous materials has been proposed[168]. The proposed mechanism of Knoevanegel condensation reaction catalysed by primary amine is that primary amine grafted on the silica wall surface activates the carbonyl group of the aldehyde via the formation of an imine intermediate. The imine intermediate formed enhances the base strength and this increased the condensation activity. Figure 4.12 shows schematically proposed reaction mechanism using the NH_2-mesoporous silica as the catalyst; and suggests that only one amine site is involved in each catalytic cycle.

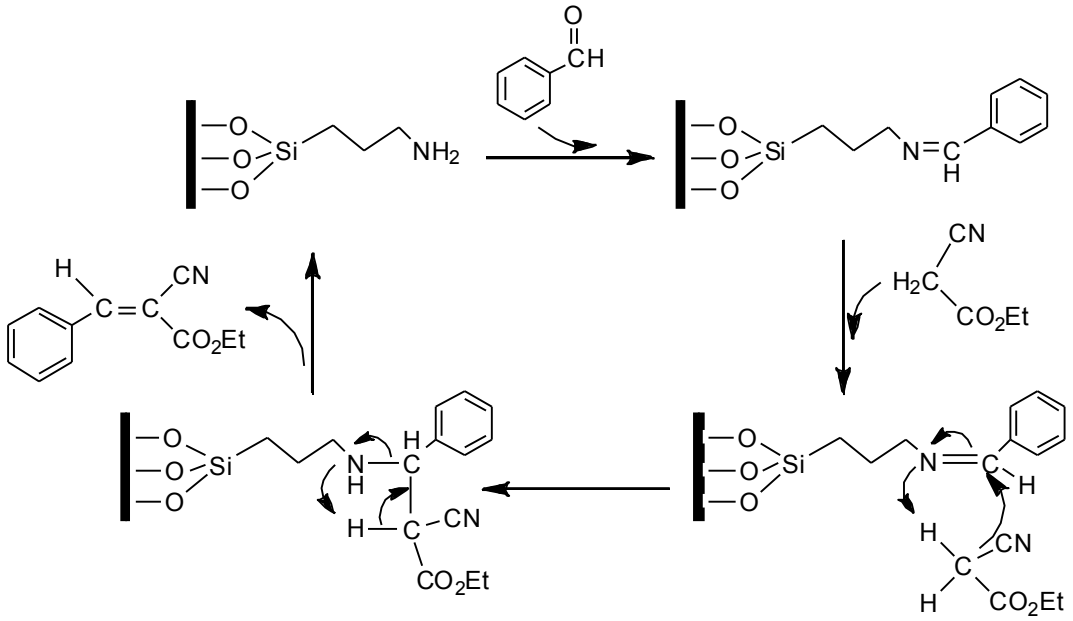

Figure 4.12 Proposed mechanism of the Knoevenagel condensation reaction using NH_2-mesoporous silica as the catalyst

4.4 CONCLUSION

The synthesised mesoporous silicas MCM-41, MCM-48, SBA-1, and SBA-2 have been modified with amino groups and used as the catalyst in the base-catalysed Knoevenagel condensation reaction. All modified materials exhibit the characteristic of mesoporous supports as presented by XRD patterns, however the incorporation of amino groups leads to the lower surface area and pore volume compared to the parent materials due to the fact that spaces in the mesopores are occupied by the functional groups.

Catalytic property of the modified materials was tested and it was found that all catalysts showed high conversion on the first run (>95%), despite the different pore structure and different functional group concentration on the surface. The catalyst reusability was also investigated and it was found that NH_2-MCM-41 and NH_2-MCM-48 showed better reusability than NH_2-SBA-1 and NH_2-SBA-2 possibly due to the greater possibility of pore blockage in the cage-like structure of SBA-1 and SBA-2.

CHAPTER 5 ASYMMETRIC NICKEL-SALEN COMPLEX MODIFIED MESOPOROUS SILICAS

5.1 INTRODUCTION

5.1.1 Importance of nickel-catalysed carbon-carbon bond forming reaction

Metal-catalysed carbon-carbon bond forming reactions are an important reaction in the synthesis of pharmaceutical and fine chemical compounds. One of the first cross coupling reaction catalysed by a transition metal was the nickel catalysed reaction of sp^3 and sp^2-hybridised carbons with a Grignard reagent reported by Kumada and Corriu[187, 188].

The Kumada-Corriu reaction did not gain much attention from researchers compared to other carbon-carbon coupling reactions, such as the Suzuki and Heck reactions, due to the difficulties in working with Grignard reagents, which are very sensitive to moisture and oxygen, and also because not many functional groups were available in the Grignard reagent range.

However, the Kumada-Corriu reaction is of more interest than previous because of the desire to use cheaper alkyl and aryl chlorides commercially. It is also more favourable to undergo the nickel catalysed carbon-carbon coupling with these reagents under the Kumada-Corriu reaction than under Suzuki and Heck conditions. In addition, Kumada-Corriu reactions have been found to be practical economically because this reaction can be performed at room temperature. Therefore, no external energy is needed and these reactions have been used on a commercial scale for the synthesis of fine chemicals.

The majority of the Kumada-Corriu reactions catalysed by nickel have been carried out with homogenous catalysts. Examples of nickel catalysts used in this reaction are nickel complexed to bis(pyridyl)-silane ligands[189], phosphine sulfide ligands[190], imidazole derived ligands[191], and the most popular ligand complexed with nickel to be used as catalyst in this reaction is the phosphine ligand [192-197].

5.1.2 Heterogeneous nickel-catalysed carbon-carbon bond forming reaction

Despite the high activity that is sometimes obtained from homogenous catalysis, the difficulties involved with catalyst recovery and reuse of the catalysts are drawbacks of their use, especially when this done on an industrial scale. Therefore, the heterogenisation of nickel species by attaching to solid supports is the way to solve this problem. There are several kinds of solid supports that can be used for this purpose, e.g. zeolites, amorphous silica, macroporous resin, and mesoporous materials.

The immobilisations of some nickel species to solid support materials to be used as catalysts for Kumada-Corriu reaction have previously been studied. Lipshutz et al [198] reported the immobilisation of $NiCl_2(PPh_3)_2$ on charcoal and this Ni(II) was then reduced to the active Ni(0) and used as the catalyst for both Kumada-Corriu and amination reactions. It was found that the catalytic activity depended critically on the method of nickel reduction. The anchoring of nickel onto macroporous polymer supports and also silica materials via covalent grafting were studied by Styring et al[199-202]. In these studies, nickel in the form of a nickel-salen coordination complex was used; high conversion was observed and the catalysts could also be reused five times without significant loss in conversion. The mesoporous silica, SBA-15, has also been used as the solid support for anchoring nickel. The SBA-15 surface was pre-modified with diamine and pyridine, prior to grafting with $Ni(acac)_2$, before these

were used in the Kumada-Corriu reaction of 4-bromoanosole and phenylmagnesium chloride; these catalysts could be reused three times without significant loss in final yield[203].

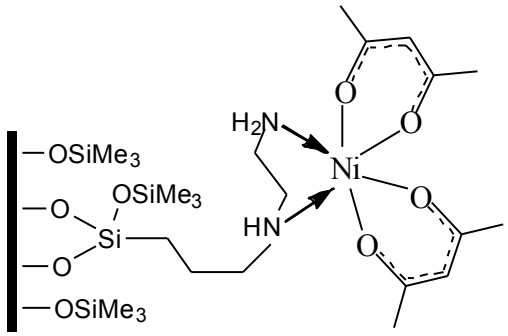

Figure 5.1 Ni(acac)$_2$-diamine anchored SBA-1[203]

In this study, we will perform the nickel-catalysed Kumada-Corriu reaction by using a nickel-salen type complex immobilised on mesoporous silicas as the catalyst.

5.1.3 Nickel salen-type ligand compound

Salens are a type of Schiff base ligand derived from salicyldehyde and amines. They are one of the oldest classes of ligands in coordination chemistry, and have been widely used to coordinate with both transition and main group metals because of their flexible and simple structure, straightforward synthesis, and also kinetically non-labile ligand template[204, 205]. Transition metals complexed with salen-type ligands were widely applied as oxidation catalysts in the synthesis of fine chemical and exhibited high activity under homogenous and heterogeneous conditions[206]. However, not many nickel-salen complexes have been studied as catalysts compared to their analogues; Mn, Co, or Cr. Although only a few studies of nickel-salen complex have been reported, the outstanding catalytic activities in olefin epoxidation and phenol oxidation were observed[207].

Nickel-salen complexes immobilised on solid supports as heterogeneous catalysts have also been reported. They have been immobilised on a range of different solid supports such as layered double hydroxides (LDH)[208], macroporous polymers[199], and also silica materials[202]. In this study, an asymmetrical salen-type ligand has been synthesised which will enable preparation of catalysts with a single point of attachment to the surface of the mesoporous materials. By designing the catalyst in this way the objective was to ensure mobility of the complex when tethered in the channels, to aid with accessibility of reagents to the active sites.

5.2 EXPERIMENTAL

5.2.1 Synthesis of [9-(2,4-dihydroxypheny)-5,8-diaza-4-methyl-non-2,3,8-trienato](2-) nickel(II); Nickel complex (1)

The method for the synthesis of asymmetric nickel-salen complex was modified from Styring et al[199]. Ethanol was used as the solvent during synthesis instead of dichloromethane, and as the desired product was not obtained by recrystallisation from methanol, acetonitrile was used instead.

1.0 g (10 mmol) of 2,4-pentanedione (99%, Sigma Aldrich) was dissolved in 10.0 ml ethanol. 0.6 g (10 mmol) ethylenediamine (99%, Sigma Aldrich) in 10.0 ml ethanol was added dropwise to 2,4-pentanedione solution while being stirred and stirring continued for 10 minutes. 1.38 g (10 mmol) 2,4-dihydroxybenzaldehyde (98%, Avocado) in 10.0 ml ethanol was added to the reaction mixture and stirring continued for another 10 minutes. 2.48 g (10 mmol) nickel acetate tetrahydrate (99%, Acros Organics) was added to the reaction mixture before refluxing for 1 hour. The crude red solid was filtered off and dried at room temperature. The crude product was recrystallised in acetonitrile (laboratory reagent grade, Fisher Scientific) to obtain the final product. The resulting product was assigned as compound (1).

Yield: 14.6%

^{1}H NMR (DMSO-d_6, 300 MHz, TMS): δ_H 9.70 (s, 1H, Ar-OH), 7.50 (s, 1H, N=C(Ar)-H), 7.00 (d, 1H, Ar-H), 6.00 (d, 1H, Ar-H), 5.90 (d, 1H, Ar-H), 4.95 (s, 1H, CH=), 3.25 (t, 2H, N-CH_2), 2.95 (t, 2H, N-CH_2), 1.90 (s, 3H, CH_3), 1.75 (s, 3H, CH_3)

Elemental analysis: calculated for $C_{14}H_{16}N_2O_3Ni$: C 52.71, H 5.02, N 8.78; found C 52.85, H 4.94, N 8.65

MS (m/z): 319

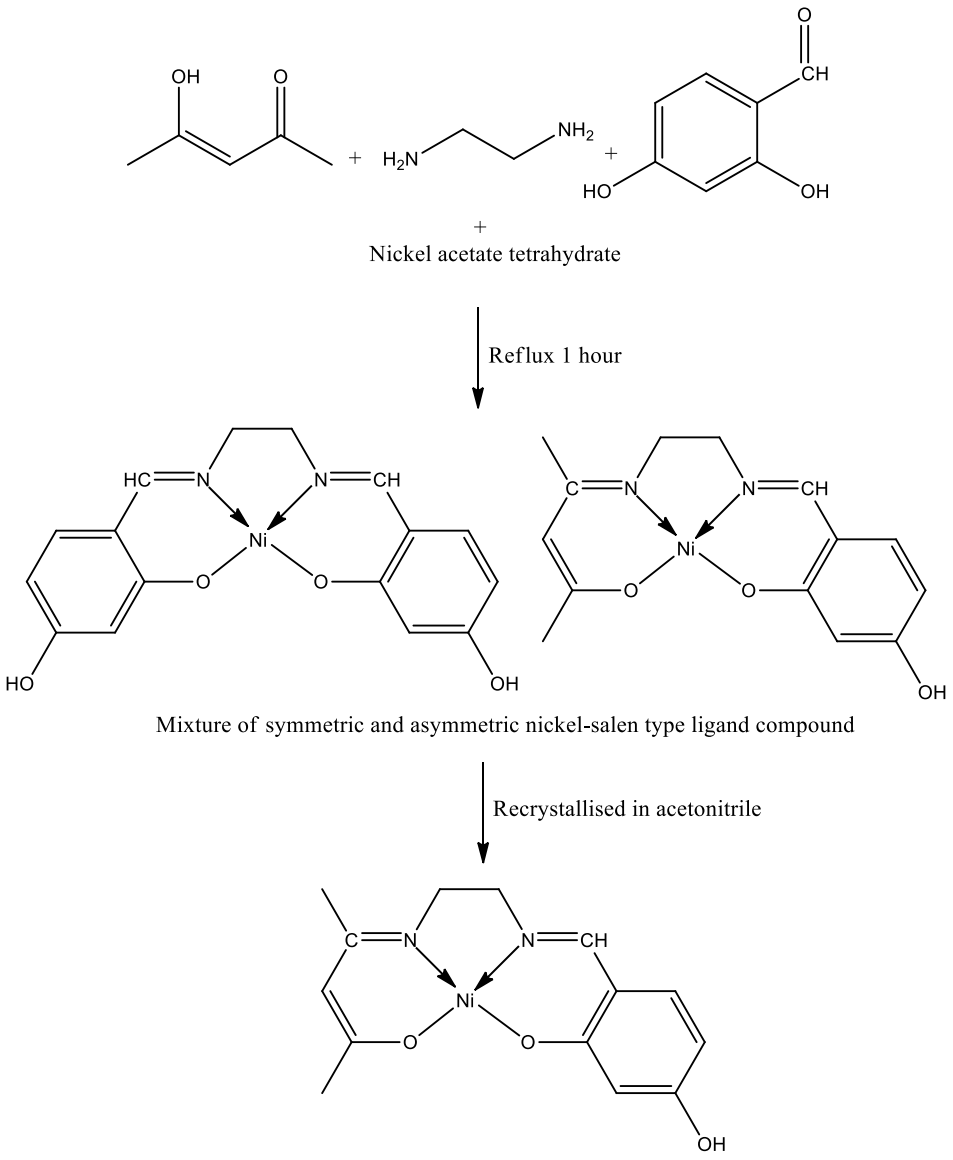

Figure 5.2 Synthesis scheme for [9-(2,4-dihydroxypheny)-5,8-diaza-4-methyl-non-2,3,8-trienato](2-) nickel(II)

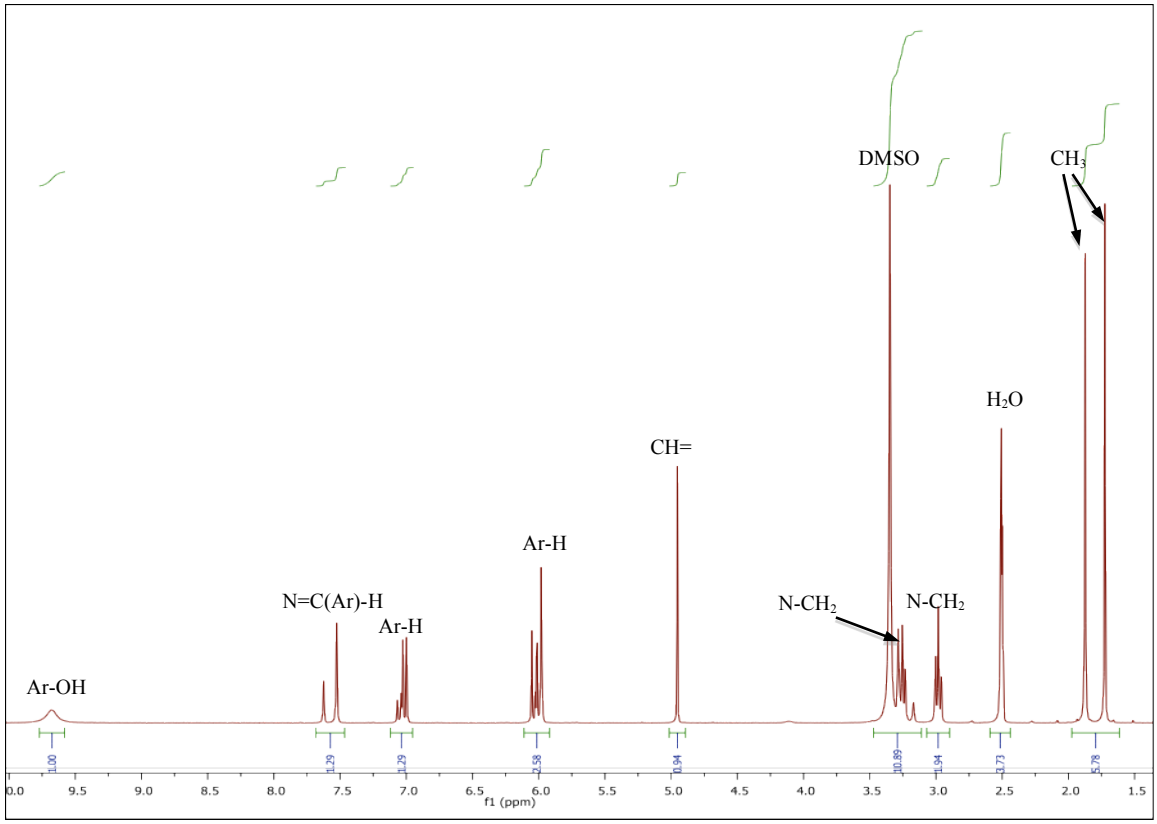

Figure 5.3 NMR spectrum for compound (1)

5.2.2 Modification of mesoporous silica by asymmetric nickel-salen complex

The synthesised mesoporous silicas were modified using the asymmetric nickel-salen complex (compound 1) to be used as the heterogeneous catalyst in the Kumada-Corriu reaction. As the surface of mesoporous silica possesses only silanol groups, a silane coupling agent to link between silica surface and nickel complex was required. The silanol surface of mesoporous silica was first modified with 3-chloropropyltrimethoxysilane to obtain the chloropropyl functionalised mesoporous silica, and this was subsequently reacted with the pendant hydroxyl group from the asymmetric nickel-salen complex.

1.0 g of mesoporous silica (MCM-41, MCM-48, SBA-1, or SBA-2) was dispersed in dry toluene, before 0.1 g 3-chloropropyltrimethoxysilane (98%, Avocado) was added while

being stirred. 30 mg of the asymmetric nickel-salen complex, (1), was dissolved in 5.0 ml THF and 5.0 ml DMF and was then added dropwise to 20 mg sodium hydride (60% dispersion in mineral oil, Sigma Aldrich), and stirred for 10 minutes. The nickel containing solution was added to the suspension of mesoporous silica and 3-chloropropyl trimethoxysilane prior to reflux for 24 hours. The resulting solid was filtered, washed with toluene and dried at room temperature. A schematic diagram of the modification of mesoporous silica by the asymmetric nickel-salen complex is shown in Figure 5.4.

The resulting mesoporous silicas modified by the asymmetric nickel-salen complex materials are assigned as (1)-MCM-41, (1)-MCM-48, (1)-SBA-1, and (1)-SBA-2. The dried modified mesoporous silicas were characterised by X-ray diffraction, X-ray fluorescence, and nitrogen adsorption-desorption.

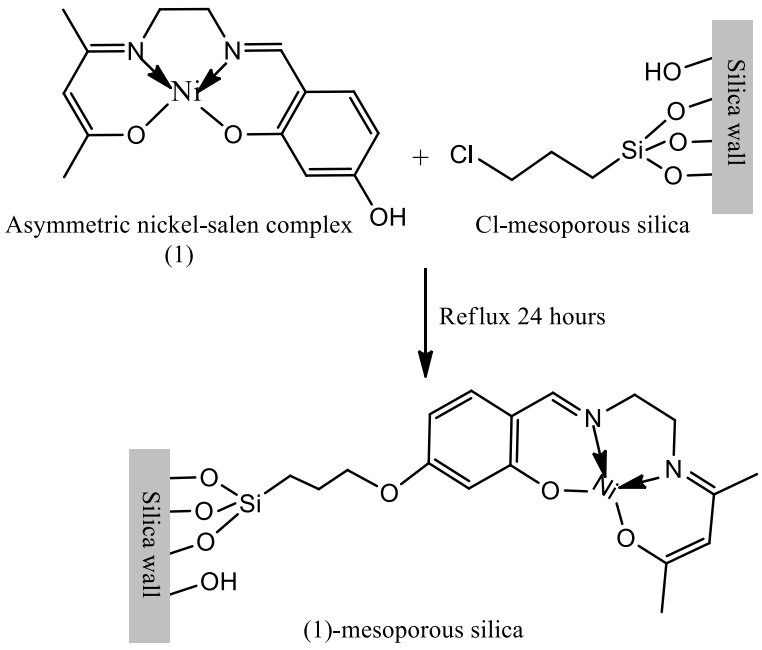

Figure 5.4 Modification of mesoporous silica with the asymmetric nickel-salen complex

5.2.3 Catalytic testing using Kumada-Corriu reaction

This reaction is a carbon-carbon bond forming reaction that can be carried out at room temperature so an external energy source is not required. 4-bromoanisole and phenyl magnesium bromide were used as the reactants for the Kumada-Corriu reaction[199]. The catalytic activity testing of (1)-mesoporous silicas are as follows: 0.1 g catalyst was added to a reaction tube purged with nitrogen. 2.0 ml THF was added and followed by the addition of 0.18 g (0.1 mmol) 4-bromoanisole (99%, Aigma Aldrich), before 2.0 ml (0.2 mmol) of phenyl magnesium bromid (1 M in THF, Acros Organics) was added to initiate the reaction. The reaction was completed in 5 minutes due to the reactivity of phenyl magnesium bromide. The reaction mixture was filtered off from the catalyst and was analysed by gas chromatography while the catalyst was washed with THF and then dried prior to recycling.

5.3 RESULTS AND DISCUSSION

5.3.1 Characterisation of (1)-mesoporous silicas

5.3.1.1 Characterisation of (1)-mesoporous silicas by powder X-ray diffraction

Powder X-ray diffraction patterns of nickel modified mesoporous silicas were recorded on a Bruker D8 instrument with the reflection geometry from 1° to 8°, step size 0.01°. Figure 5.4, Figure 5.5, Figure 5.6, and Figure 5.7 are the X-ray diffraction patterns of the (1)-MCM-41, (1)-MCM-48, (1)-SBA-1, and (1)-SBA-2, respectively.

The XRD patterns of all the nickel-modified mesoporous silicas show the presence of the mesoporous host used. In each pattern, the peaks at 2θ = 2°-3° are clearly observable, but the peaks at higher angle (2θ = 4°-6°) are not as strong and clear as in the parent mesoporous materials, which indicates that the modified materials possess a slightly lower order of mesostructure than that of pure siliceous materials[171-173]. In addition, the intensity of the XRD patterns decreased when nickel complexes are incorporated, this could be attributed to changing of the wall thickness or reduction of the scattering contrast between the silicate wall and the functional group, resulting in the lowering of the local order of the structure.

All the XRD patterns of the modified materials show a small peak shift to higher angle, indicating a slight reduction in d-spacing. This reduction in d-spacing could be explained by the contraction of the unit cell caused by the surface modification with the asymmetric nickel-salen complexes. Comparison of the unit cell parameter of (1)-MCM-41, (1)-MCM-48, (1)-SBA-1, and (1)-SBA-2 with the value of its pure siliceous materials are shown in Table 5.1.

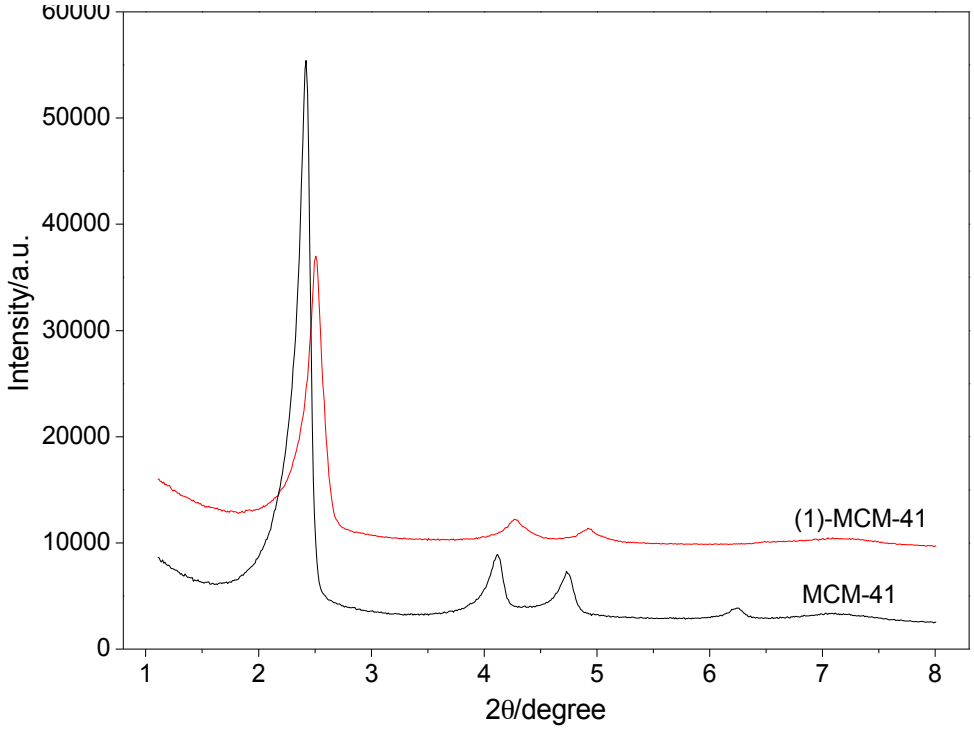

Figure 5.5 Powder x-ray diffraction patterns of MCM-41 and (1)-MCM-41

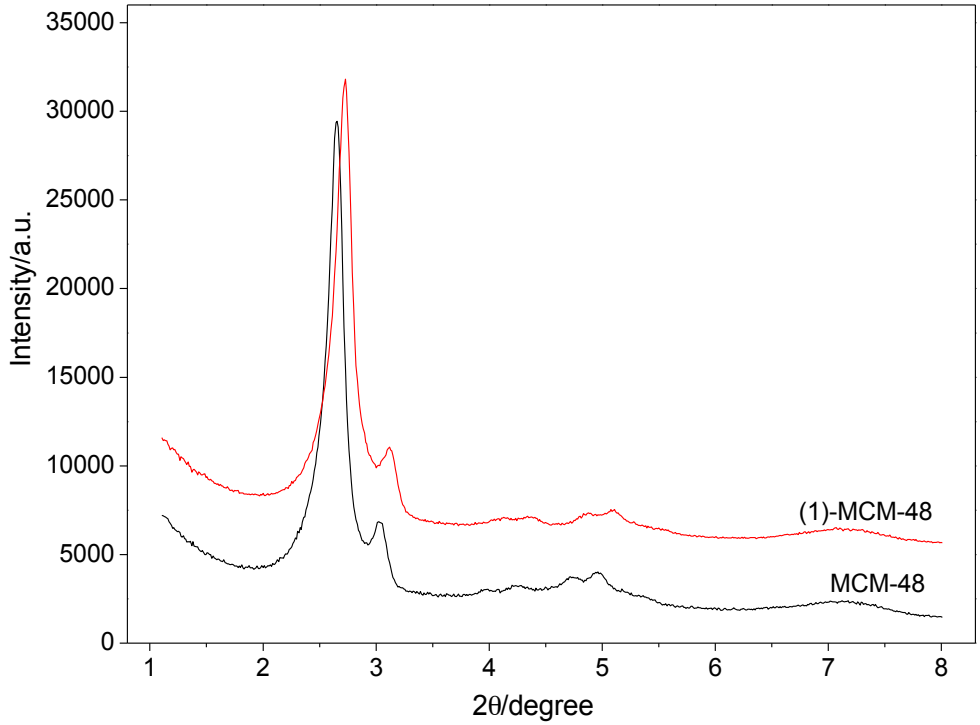

Figure 5.6 Powder x-ray diffraction patterns of MCM-48 and (1)-MCM-48

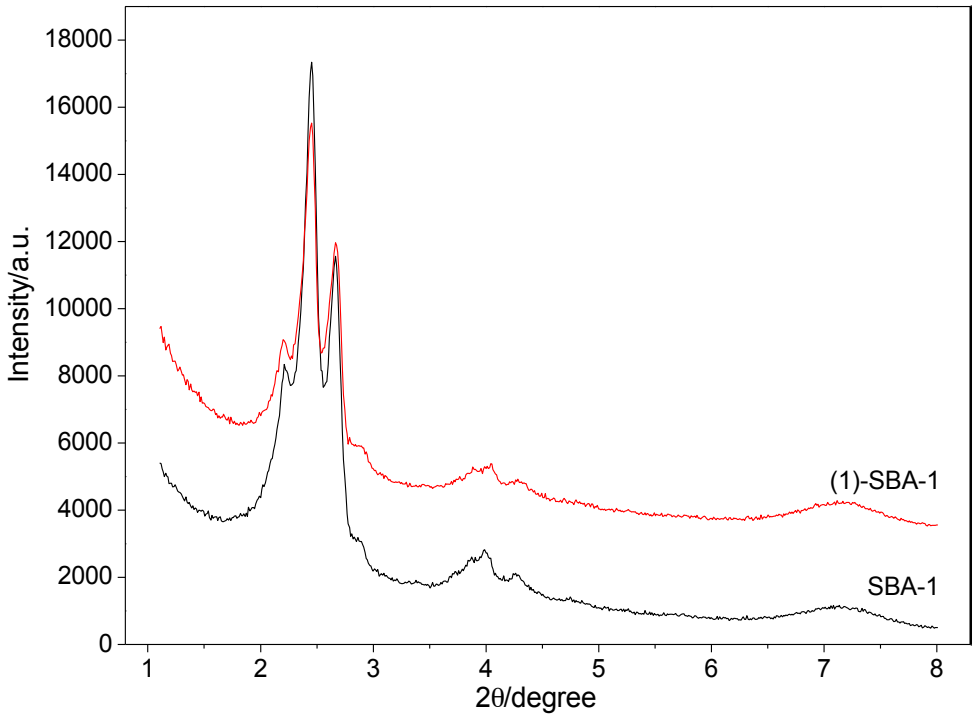

Figure 5.7 Powder x-ray diffraction patterns of SBA-1 and (1)-SBA-1

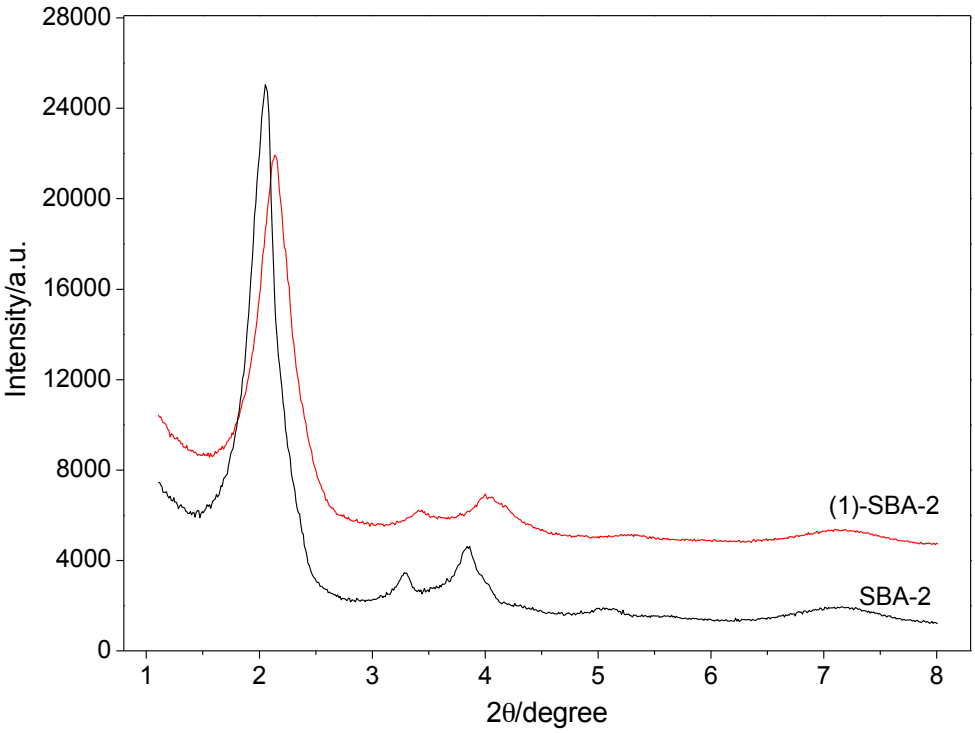

Figure 5.8 Powder x-ray diffraction patterns of SBA-2 and (1)-SBA-2

Table 5.1 Unit cell parameter of (1)-mesoporous silicas and their corresponding pure materials

Material	Unit cell parameter (Å)	
	Unmodified mesoporous materials	(1)-mesoporous silica
MCM-41	37.0	35.6
MCM-48	82.2	79.8
SBA-1	80.6	80.4
SBA-2	46.7	45.4

5.3.1.2 Characterisation of the (1)-mesoporous silicas by X-ray fluorescence (XRF)

During the surface modification process, there is the possibility that the isolated nickel complex molecules could be encapsulated but not covalently bound within the mesoporous support structures. Therefore, after the modification process, the modified materials were washed 3 times with 50 ml THF, and the final washing solution was collected and analysed by atomic absorption spectroscopy (AAS). For all the collected solutions no nickel was detected showing that all nickel complexes present in the structure were covalently bonded to the siliceous mesoporous surface and there were no isolated nickel complexes left in the structure.

The amount of nickel present after reaction in the mesoporous silicas was examined by X-ray fluorescence techniques using solid powder samples. The nickel content in the mesoporous silicas is presented in Table 5.2.

Table 5.2 Nickel content in (1)-mesoporous silicas determined by XRF

Catalyst	Ni (mmol/g)
(1)-MCM-41	0.11
(1)-MCM-48	0.12
(1)-SBA-1	0.08
(1)-SBA-2	0.06

Cubic *Ia3d* MCM-48 shows the highest nickel content, which could be attributed to the 3-dimensional cubic structure allowing better pore accessibility than the 2-dimensional hexagonal structure of the *P6mm*, MCM-41. On the other hand, the cage-like mesoporous silicas, SBA-1 and SBA-2, contain lower percentages of nickel, which can also be explained by the structure of the support materials. In these cage-like structures the pore entrances are smaller than the pore diameter, and can cause poorer diffusion of reagent molecules into the pore, which results in a lower functional group concentration on the internal surface.

5.3.1.3 Characterisation of (1)-mesoporous silicas by Elemental Analysis

The incorporation of nickel-salen complex, (1), to mesoporous silica was also confirmed by the appearance of carbon and nitrogen as these two elements are part of the salen ligand. Table 5.3 shows elemental analysis results for (1)-mesoporous silicas. It was observed from Table 5.3 that the amount of carbon and nitrogen content found for (1)-MCM-48 > (1)-MCM-41 > (1)-SBA-1 > (1)-SBA-2, which is of the same tendency as found for the amount of nickel as the complex composes of nickel and salen ligand. However, the amount

of carbon is higher than it would be compared to nitrogen and nickel, as it is also part of tether molecule.

Table 5.3 Elemental analysis results for (1)-mesoporous silicas

Catalyst	Carbon (mmol/g)	Nitrogen (mmol/g)
(1)-MCM-41	3.84	0.30
(1)-MCM-48	4.12	0.38
(1)-SBA-1	3.04	0.23
(1)-SBA-2	2.98	0.18

5.3.1.4 Characterisation of (1)-mesoporous silicas by nitrogen adsorption-desorption

Surface areas and pore size distribution of the (1)-mesoporous silicas were determined by nitrogen physisorption. Type IV adsorption isotherms, characteristic of mesoporous solids, are observed. The well defined steps in the adsorption-desorption isotherm and the sharp increase in nitrogen uptake at $P/P_0 \approx 0.18$-0.30, correlating to capillary condensation within mesopores are seen for (1)-mesoporous silica samples. This indicates that the mesopores are uniform in size, as also presented by the pore size distribution. The unusual adsorption-desorption steps are observed for (1)-SBA-1 and (1)-SBA-2, as discussed earlier in Chapter 4 these are suggested to be caused by some structural defect associated with the pore-blocking effect around the embedded voids in modified mesoporous structure[156], and also lead to the broader pore size distribution (Figure 5.11 and Figure 5.12).

Surface area, pore diameter, and pore volume of the (1)-mesoporous silicas are presented in Table 5.4. Surface area was calculated by the BET method in the range of P/P_0 = 0.05-0.3. Pore volume and pore diameter were estimated by the BJH method from the adsorption branch.

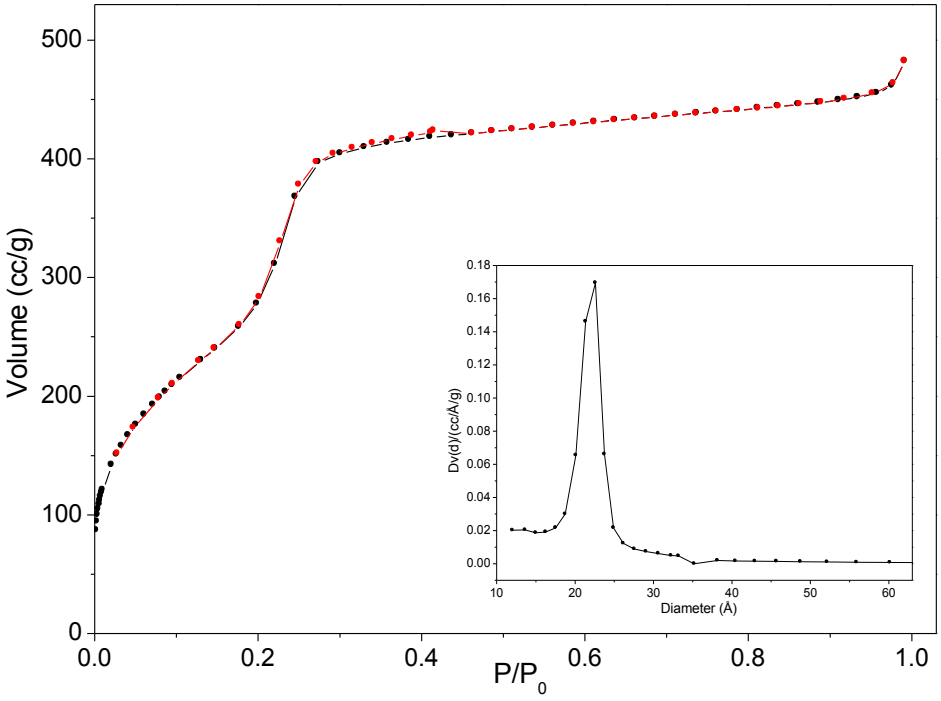

Figure 5.9 Nitrogen adsorption-desorption isotherm and pore size distribution of (1)-MCM-41

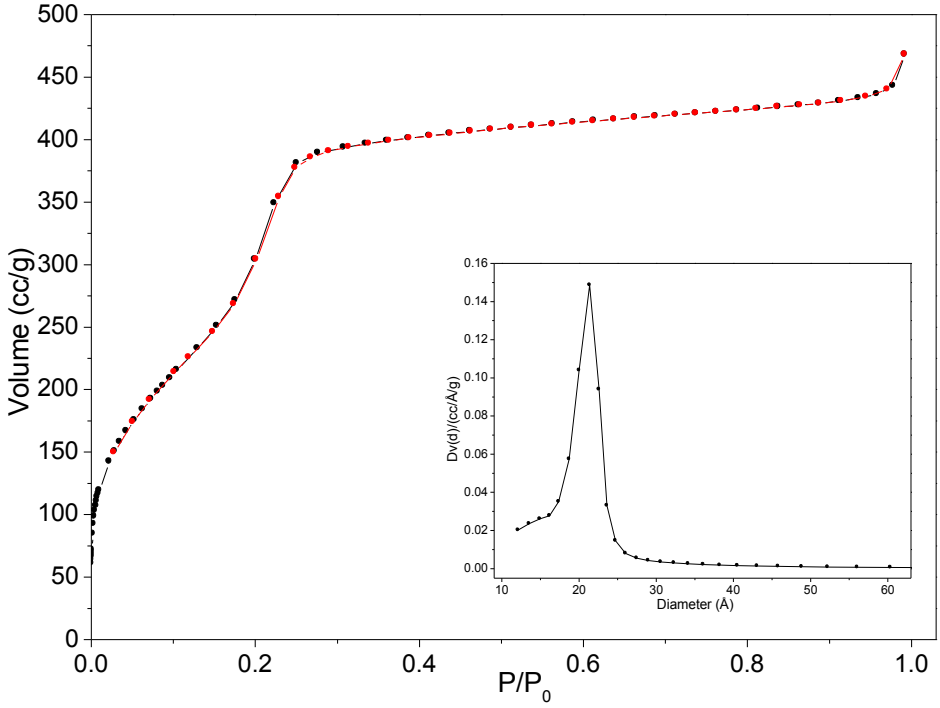

Figure 5.10 Nitrogen adsorption-desorption isotherm and pore size distribution of (1)-MCM-48

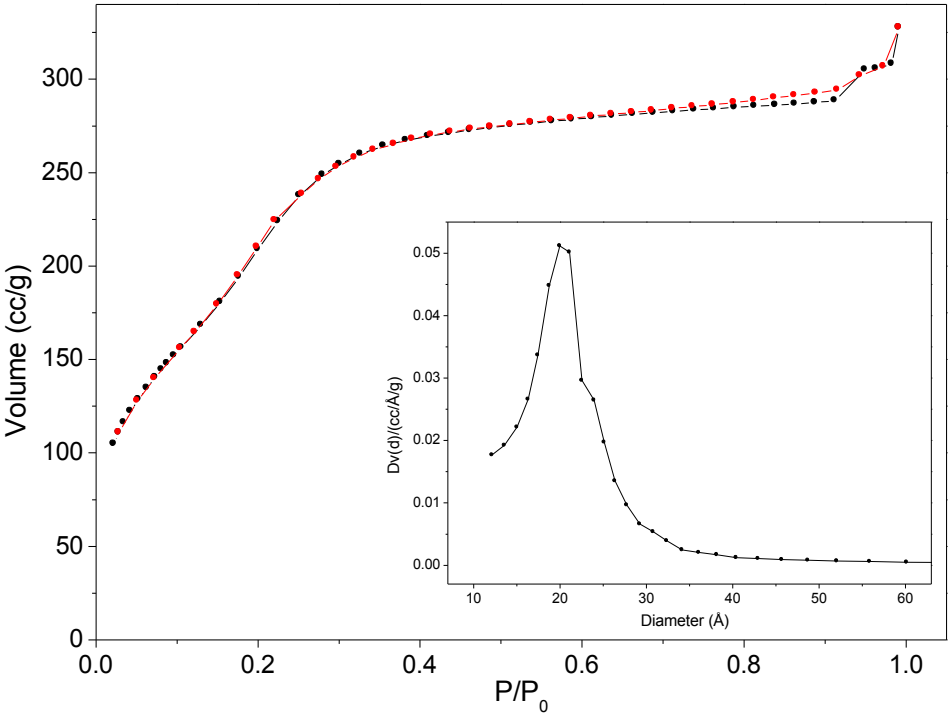

Figure 5.11 Nitrogen adsorption-desorption isotherm and pore size distrubution of (1)-SBA-1

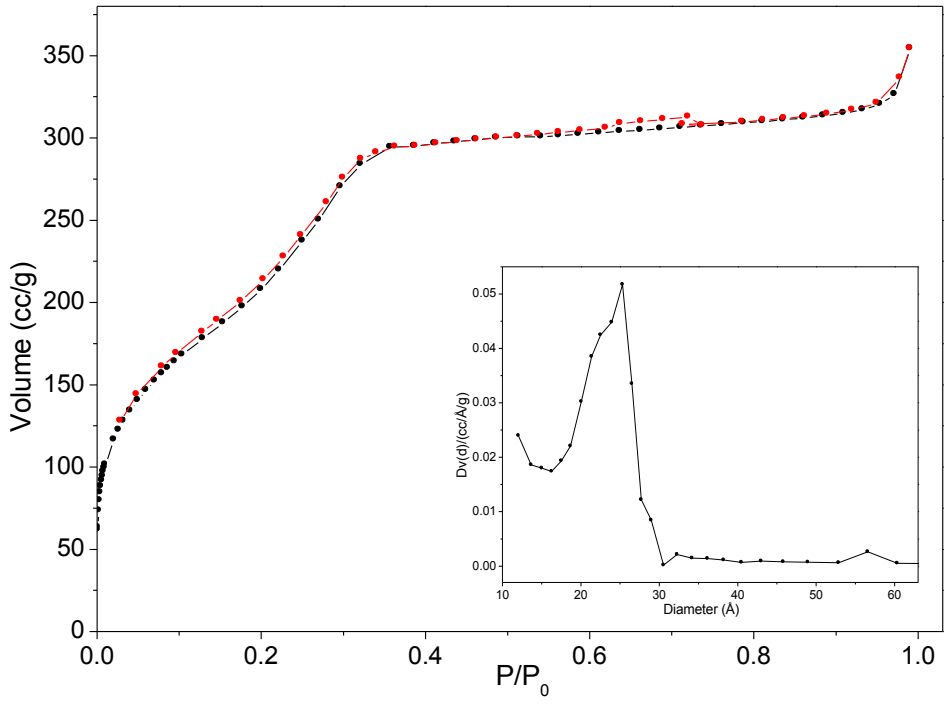

Figure 5.12 Nitrogen adsorption-desorption isotherm and pore size distribution of (1)-SBA-2

Table 5.4 Surface area, pore diameter and pore volume of (1)-mesoporous silicas

Catalyst	S_{BET} (m^2g^{-1})	Pore diameter* (nm)	Pore volume* (cm^3g^{-1})
(1)-MCM-41	1013	2.2	1.10
(1)-MCM-48	915	2.1	1.09
(1)-SBA-1	740	2.0	1.02
(1)-SBA-2	765	2.7	0.82

* Calculated from the adsorption branch

As seen in Table 5.4, (1)-MCM-41 shows the highest surface area and pore volume, however all the (1)-mesoporous silicas exhibit lower surface area and pore volume compared to their corresponding pure siliceous materials as also evidenced by the lower adsorption capacity. As the nickel complexes are a bulky functional group, incorporation into the inner pore surface of mesoporous silica is likely to be harder than for the amino group, as suggested by higher amount of N_2 adsorbed[209]. And when compared to NH_2-mesoporous silicas, the (1)-mesoporous silicas possess a larger surface area and pore diameter.

5.3.2 Catalytic testing

5.3.2.1 Catalytic testing of (1)-mesoporous silicas

All the asymmetric nickel-salen complex modified mesoporous silicas were used as catalyst in the Kumada-Corriu reaction between 4-bromoanisole and phenyl magnesium bromide. This reaction was carried out under a nitrogen atmosphere at room temperature. The reaction scheme of this reaction is presented in Figure 5.13.

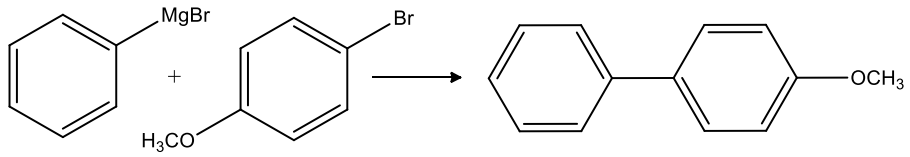

Figure 5.13 Kumada-Corriu reaction between benzaldehyde and phenylmagnesium bromide

The reaction mixtures from the Kumada-Corriu reaction were analysed by gas chromatography, with the product of reaction being 4-methoxy biphenyl and the self-coupling of phenylmagnesium bromide being a competitor reaction to the desired reaction resulting in formation of biphenyl as the side-product. The reaction mechanism had previously been proposed and will be discussed later in section 5.3.4.

In order to optimise the reaction conditions, different approaches including the continuous flow of reactants through a packed catalysts column using a syringe pump to control flow rate had been tried. However, it was found that the conversion observed was relatively low compared to the batch system and the main product was biphenyl, this could be attributed to the self coupling of phenylmagnesium bromide occurring before passing through the catalyst. In addition, the reaction time and ratio between 4-bromoanisole and phenylmagnesium bromide were also varied. The conversion from fresh (1)-MCM-41 was

found to be increased from 42% to 75% when the ratio between 4-bromoanisole: phenylmagnesium bromide increased from 1:1 to 1:2. However the conversion was decreased when the ratio increased to 1:3 as more self coupling of phenylmagnesium bromide occurred. On investigating the effect of reaction time, it was found that a long reaction time was not necessary as the maximum conversion (75%) was obtained after about 5 minutes and did not increase any further when the reaction time was longer due to the reactivity of phenylmagnesium bromide. Moreover the same trend was found when increasing the amount of catalyst; there was no significant improvement in conversion when the amount of catalyst increased from 0.1 g to 0.3 g. Therefore, the optimised reaction conditions that we derived using the asymmetric nickel-salen complex modified mesoporous silica as catalyst in the Kumada-Corriu reaction is to use a batch system under a nitrogen atmosphere, with a ratio between 4-bromoanisole: phenylmagnesium bromide of 1:2, a reaction time of 5 minutes, and using 0.1 g catalyst.

Table 5.5 Conversion of Kumada-Corriu reaction

Catalyst	Conversion (%)*
(1)-MCM-41	74.9 ± 3 .2
(1)-MCM-48	62.1 ± 2.6
(1)-SBA-1	69.8 ± 3.1
(1)-SBA-2	64.3 ± 2.4
Nickel complex (homogenous reaction)	62.6 ± 2.2

*The conversions shown are from three repeated reactions, reported in (average value ± S.D.)

Table 5.5 represents the conversion to expected product, 4-methoxybiphenyl, for the Kumada-Corriu reaction using fresh (1)-mesoporous silicas as the catalyst. No reaction was observed in the absence of catalyst or in the presence of unfunctionalised mesoporous silica. (1)-MCM-41 shows the highest conversion. The 3-dimensional cubic *Ia3d* MCM-48, would have been thought most likely to provide the best accessibility of reactants to the active sites at the inner pore and the X-ray fluorescence result also shows that the highest amount of nickel complex was found in MCM-48. However, as shown in Table 5.5 (1)-MCM-48 shows the lower conversion which may be explained by (1)-MCM-48 possessing a lower surface area and smaller pore volume than (1)-MCM-41. As observed in NH_2-mesoporous silicas catalysts in Chapter 4 and the report from previous study with different mesoporous supported catalyst[160], the catalysts with higher surface area and larger pore volume tend to exhibit the higher conversion which could be attributed to better functional group distribution is likely to be obtained with a larger surface area.

In the case of the cage-like mesoporous silicas, SBA-1 and SBA-2, the conversions obtained from (1)-SBA-1 is higher than (1)-SBA-2. The results from (1)-SBA-1 and (1)-SBA-2 could also be the effect of having a larger surface area and better functional group distribution on the surface of the support material in a similar manner to what was as observed in (1)-MCM-41 and (1)-MCM-48.

It is generally accepted that a reduction in activity has been observed when the molecular catalysts have been immobilised on a solid support[210-213]. However in this study, conversion found from homogeneous catalyst is lower than that of the heterogeneous, (1)-mesoporous silicas catalysts under the same reaction condition, this indicating the cooperative effect of the support[214, 215]. This is important as it is much easier to separate the

heterogeneous catalysts after reaction, and therefore there is greater scope of their use and recycling.

In addition, the conversions obtained from the Kumada-Corriu reaction using (1)-mesoporous silicas are also comparable to conversion from the nickel-salen complex immobilised macroporous polymer resins as catalyst (71-73% conversion) reported by Styring et al[199]. However their catalyst presents 0.883 wt% nickel and the reaction[199] was carried out for 24 hours with the ratio between 4-bromoanisole: phenylmagnesium bromide of 1:1.

5.3.2.2 Catalyst reusability

At the completion of each reaction, catalysts were separated from the reaction mixture by filtration. Reaction mixtures were analysed by gas chromatography while the catalysts were washed with THF and dried at room temperature, followed by drying under vacuum at 80 °C for 5 hours prior to reuse. The procedure for catalytic activity testing of the used catalysts was the same as used for the fresh catalyst. After each reaction run, catalysts were filtered out from the mixture and prepared for another use as described.

Figure 5.14 represents the conversion for the Kumada-Corriu reaction against number of run using the (1)-mesoporous silicas as catalyst. All catalysts show lower conversion when reused. However, upon recycling, (1)-MCM-48 presents the highest conversion with slower reduction in conversion compared to other catalysts and became almost inactive on the fourth use. Although fresh (1)-MCM-41 shows the highest conversion as discussed in 5.3.3.1, on recycling its conversion reduced faster than (1)-MCM-48. This could be attributed to the 3-dimensional structure of MCM-48 as catalyst supported facilitating better pore accessibility for the reactants on subsequent runs due to less problems caused by pore blocking.

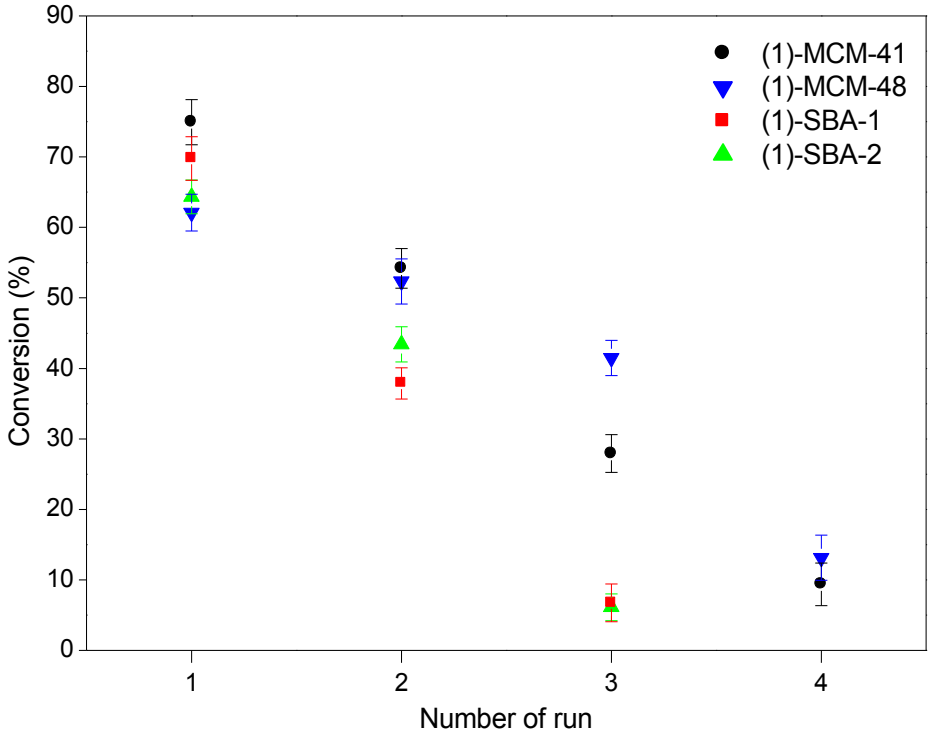

Figure 5.14 Conversion of Kumada-Corriu reaction upon recycling

The cage-like mesoporous silicas as hosts, SBA-1 and SBA-2, show poorer ability in retaining activity upon recycling, as the activity is almost completely lost on the third used. The drastic reduction in activity of (1)-SBA-1 and (1)-SBA-2 could be attributed to the properties of the cage-like support materials, as pore entrances of these materials are smaller than their pore diameter, therefore any pore blockage caused by the reactant molecules are more likely to happen due to their size selective structure[182-184], as also observed for NH_2-mesoporous silica catalysts.

5.3.3 Post-reaction solution study

During the catalytic reaction it is possible that some of the loss of activity could be due to nickel being leached from the support, causing deactivation. Therefore when each catalytic

reaction finished, the reaction mixtures were also analysed by atomic absorption (AAS) for the presence of any nickel. Nickel leaching results are shown in Table 5.6.

Table 5.6 Nickel leached from Kumada-Corriu reaction using nickel complex-modified mesoporous silicas catalyst

Number of run	Nickel leached (%)			
	(1)-MCM-41	(1)-MCM-48	(1)-SBA-1	(1)-SBA-2
1	4.09	2.01	0.92	1.06
2	1.38	0.70	1.44	0.79
3	0.94	1.06	0.90	1.31
4	1.23	0.51		

As seen in Table 5.6, it was found in the first run that the highest amount of nickel leaching was from (1)-MCM-41. However, from this study; the nickel leaching results are suggested to be unrelated to the structure of the support materials, as there is no particular trend observed in the amount of nickel leached from the different catalyst. In addition, upon recycling, the nickel leached from the catalyst is not related to the order of run. It was previously reported that the leaching of nickel is dependent on the presence of Grignard reagent, either by causing the ligand degradation or reduction of Ni(II) to Ni(0)[216].

In order to fully understand the catalyst deactivation, it is important to assess how much nickel remains in the catalyst on each recycle used (if all nickel were leached, thus would leave no nickel on the catalyst support!). Therefore the amount of nickel remaining in the used catalysts was estimated. The leached nickel from the first run was subtracted from the initial nickel content (from XRF) and this was done for each run. It was found that the nickel

content in the used catalyst was lower than that of the fresh catalysts and decreased upon further use. However there is still nickel in the deactivated catalyst, the estimated amount of nickel in the inactive used catalyst is shown in Table 5.6. Therefore it could be concluded that the catalyst deactivation was not only caused by the leaching, but pore blockage also played an important role as has been previously discussed.

Table 5.7 Amount of the remained nickel in the inactive catalyst

Catalyst	Initial nickel content (mmol)[(a)]	Remaining nickel in deactivated catalyst (mmol)
(1)-MCM-41	$10.74x10^{-3}$	$9.95x10^{-3}$ [(b)]
(1)-MCM-48	$12.33x10^{-3}$	$11.82x10^{-3}$ [(b)]
(1)-SBA-1	$8.46x10^{-3}$	$8.19x10^{-3}$ [(c)]
(1)-SBA-2	$6.357x10^{-3}$	$6.16x10^{-3}$ [(c)]

[(a)] The amount of initial nickel in catalyst was calculated on the basis of SiO_2 as the silica wall with the assumption of one tether molecule (chloropropyl trimethoxy silane) for each nickel complex molecule

[(b)] Nickel remained in catalysts after the fourth run

[(c)] Nickel remained in catalyst after the third run

5.3.4 Reaction mechanism

The Kumada-Corriu coupling reaction involves the oxidative addition of an organobromide to a transition metal catalyst, which then reacts with a Grignard reagent to give a coupled product by reductive elimination. In the Kumada-Corriu reaction between 4-bromoanisole and phenylmagnesium bromide, biphenyl was observed as the side product. So, there is the possibility of having two competing reaction cycles. Styring et al[199] have proposed the mechanism of this reaction as shown in Figure 5.15.

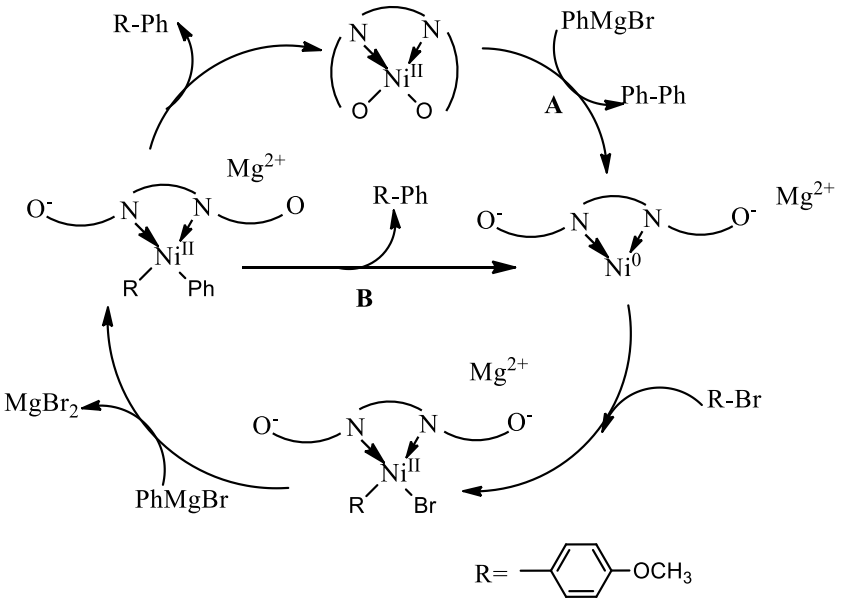

Figure 5.15 Proposed catalytic cycle of Kumada-Corriu reaction[199]

The nickel atom in the complex is bound to the ligand by the attraction between Ni^{2+} to the anionic oxygen and also the neutral nitrogen. From Figure 5.15, route A consists of the reduction of nickel from Ni^{2+} to Ni(0) with the sacrifice of Grignard reagent; the homocoupled product is produced in this step. This is the catalyst pre-activation step and is important as Ni^{2+} is not active towards oxidative addition of the organobromide. However, the

yield of homocoupled product is not proportional to the main cross-coupling product. Therefore, another possibility is that the reaction goes via an alternative route (route B) once the catalyst activation has taken place.

5.4 CONCLUSION

Asymmetric nickel-salen complexes have been successfully synthesised and immobilised within the mesoporous silicas MCM-41, MCM-48, SBA-1, and SBA-2 to be used as catalysts in carbon-carbon bond forming reactions. The modified mesoporous silicas show the characteristics of the parent materials and surface area still remains high. All catalysts show high conversion in Kumada-Corriu reaction in short time (5 minutes) and also can be reused for three times. However the reusability of (1)-MCM-41 and (1)-MCM-48 are better than (1)-SBA-1 and (1)-SBA-2 due to the greater possibility of pore blockage caused in cage-like mesoporous silicas.

CHAPTER 6 FURTHER METHYLATION ON MODIFIED MESOPOROUS SILICAS

6.1 INTRODUCTION

The modification of mesoporous silica by amino groups and asymmetric nickel-salen complexes has been achieved in Chapter 4 and Chapter 5. In addition, catalytic activity and reusability of the synthesised catalysts was tested and it was found that the conversion achieved was dependent on the structure of the support materials and reduced upon recycling of the catalyst.

The silanol groups present on mesoporous silica result in a hydrophilic hydroxylated surface and these groups can react with proton donor and proton acceptor molecules via hydrogen bonding, and these provide the attaching point between the mesoporous silicas and the functional groups. In general, the population of surface silanol groups varies depending on the preparation method. Zhao and Lu [217] reported that the density of total silanol group on the template-extracted MCM-41 surface, including free, hydrogen-bonded, and geminal silanols is *ca*. 3.0 per nm^2. However, only the free and geminal groups are eligible to react with the functional group molecules.

In the surface modification process with both the amino-functionalised silanes and the asymmetric nickel-salen complexes, not all free and geminal silanol are reacted, resulting in silanol groups remaining on the modified-mesoporous silicas surface. It was previously reported that the silanol groups on the surface of modified mesoporous silicas could affect the catalyst activity in base-catalysed reactions because hydrogen bonds between silanol group

and the basic site can be formed as shown in Figure 6.1, resulting in a decrease of base catalyst activity[218].

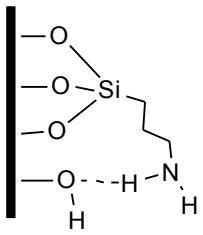

Figure 6.1 Hydrogen bond between basic site and silanol group on mesoporous silica sufrace

Moreover, in some metal substituted mesoporous silica catalysed reactions, such as the Ti-MCM-41 catalysed epoxidation reaction, the catalyst activity decreased due to Ti leaching in aqueous solution caused by the hydrophilicity of silanol surface in titania-silica mixed oxide[219].

The hydrophobisation of the silica surface can be achieved by substitution of the remaining silanols with a hydrophobic reagent or organosilane such as hexamethyldisilazane (HMDS) or trimethylchlorosilane (TMCS) through covalent bonding[220]. In this work, TMCS was used. Figure 6.2 represents the surface modification of NH_2-mesoporous silica with the TMCS; the remaining silanol groups on surface are capped by trimethylsilyl groups. Nevertheless, Sutra et al[221] have studied the elimination of the surface silanol of MCM-41 by capping with HMDS and found that not all the silanol groups were capped, evidenced by ^{29}Si and ^{13}C MAS NMR. It was reported that the methylation process leaves -NH_2 surface of amino modified-mesoporous silica untouched, the resulting surface is hydrophobic and stable[222].

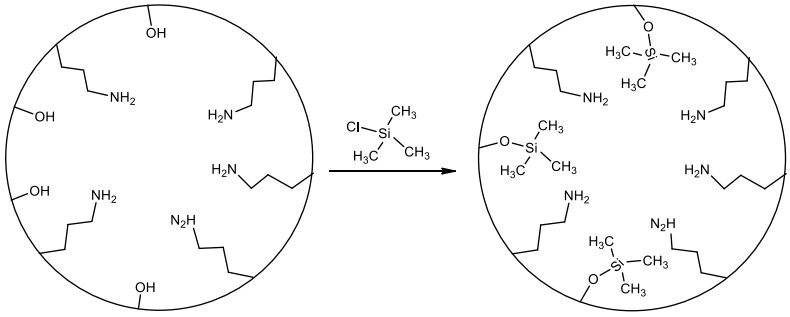

Figure 6.2 Surface modification of NH_2-mesoporous silica with TMCS

Furthermore, the advantages of surface hydrophobicity are not only found in catalysis but also in other applications such as the mesoporous silica film used in low dielectric constant sensors and semiconductors[223]. The hydrophobic surface is the important factor for keeping low dielectric constant, good thermal stability, and also mechanical strength.

Further surface modification of the prepared NH_2-mesoporous silicas and (1)-mesoporous silicas have been carried out in order to observe the effect these silanol groups in the Knoevenagel condensation and Kumada-Corriu reaction using these modified-mesoporous silica catalyst.

6.2 EXPERIMENTAL

6.2.1 Methylated amino-mesoporous silicas

The pure mesoporous silica and amino-modified mesoporous silicas were synthesised as described in Chapter 3 and Chapter 4. 1.0 g of dried amino-modified MCM-41, MCM-48, SBA-1, and SBA-2 were suspended in 30.0 ml dry toluene, followed by the addition of 0.05 g of the methyl source, trimethylchlorosilane. The reaction mixture was refluxed for 24 hours. When the refluxing has finished, the modified materials were filtered and washed with

toluene. The resulting methylated-amino modified mesoporous materials, denoted as Me-NH_2-mesoporous silica, were dried at 60 °C for 20 hours.

6.2.2 Methylated (1)-mesoporous silicas

The further modification of asymmetric nickel-salen complex, (1), modified mesoporous silicas has been carried out by using the (1)-modified MCM-41, MCM-48, SBA-1, and SBA-2, as synthesised in Chapter 5. 1.0 g of (1)-mesoporous silica was dispersed in 30.0 ml dry toluene, then trimethylchlorosilane was added. The reaction mixture was brought to reflux for 24 hours. After that, the product was filtered and washed with toluene. Finally, the methylated-nickel complex-modified mesoporous materials were dried at 60 °C for 20 hours. The resulting materials are assigned as Me-(1)-mesoporous silica.

6.3 RESULTS AND DISCUSSION

6.3.1 Me-NH_2-mesoporous silicas

6.3.1.1 Characterisation of Me-NH_2-mesoporous silicas by powder X-ray diffraction (XRD)

Powder X-ray diffraction is an effective technique for the structure characterisation of the synthesised materials, as mentioned in Chapter 3, Chapter 4, and Chapter 5. All the resulting materials had been characterised by powder X-ray diffraction to confirm the structure and to determine a unit cell parameter.

The X-ray diffraction patterns of Me-NH_2-MCM-41, Me-NH_2-MCM-48, Me-NH_2-SBA-1, and Me-NH_2-SBA-2 are presented in Figure 6.3, Figure 6.4, Figure 6.5, and Figure 6.6, respectively. The XRD patterns of Me-NH_2-mesoporous silicas show that all the

modified materials retain the structure of the siliceous supports. However, a slight peak shift to higher 2θ angle is observed correlating to a slightly smaller d-spacing, attributed to the incorporation of amino and methyl group to the structure. The unit cell parameters of the pure and modified materials are shown in Table 6.1. The Me-NH_2-mesoporous silicas exhibit smaller unit cell parameter than non-methylated; this could be attributed to the further structure contraction during the methylation process.

Moreover, as seen in Chapter 4 from the amino-modified mesoporous silicas, the small peaks at the higher angle, 2θ of 4-6 degree, are weaker than those in the XRD patterns of the pure siliceous materials caused by the incorporation of the amino group. The further surface modification of amino-modified mesoporous silicas by the methyl groups results in the further weakening of those small peaks. Therefore, it could be concluded that the mesostructure ordering of methylated-amino-modified mesoporous silicas is lower than that of the amino-modified mesoporous silicas indicated by the decrease in intensity of these peaks. However, even though the structures are less ordered, they still retain the characteristics of the silica mesoporous supports.

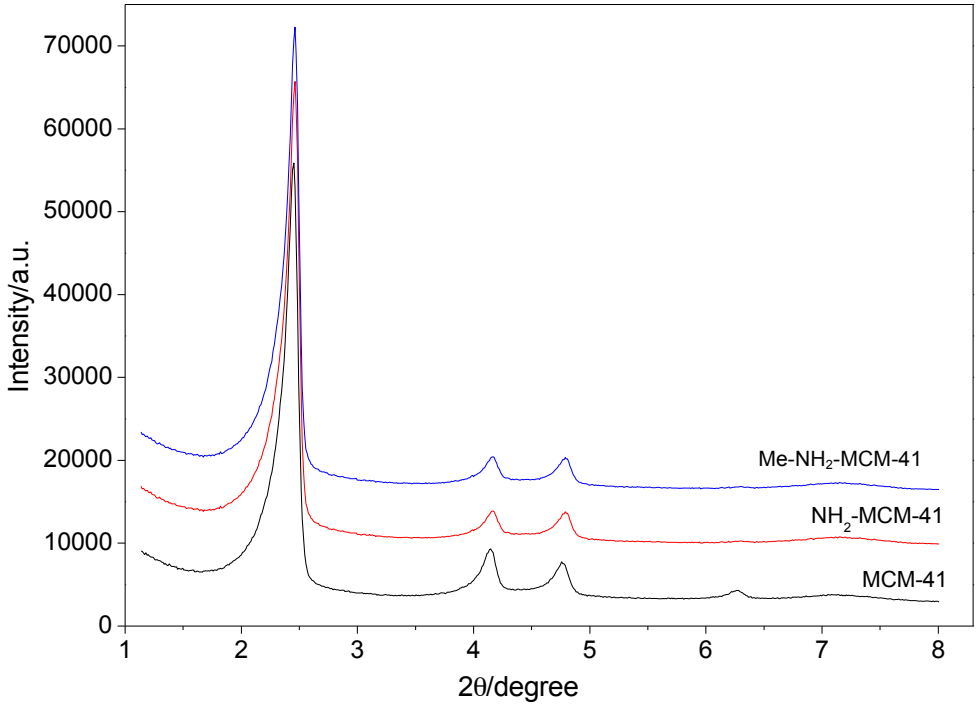

Figure 6.3 Powder X-ray diffraction pattern of Me-NH_2-MCM-41

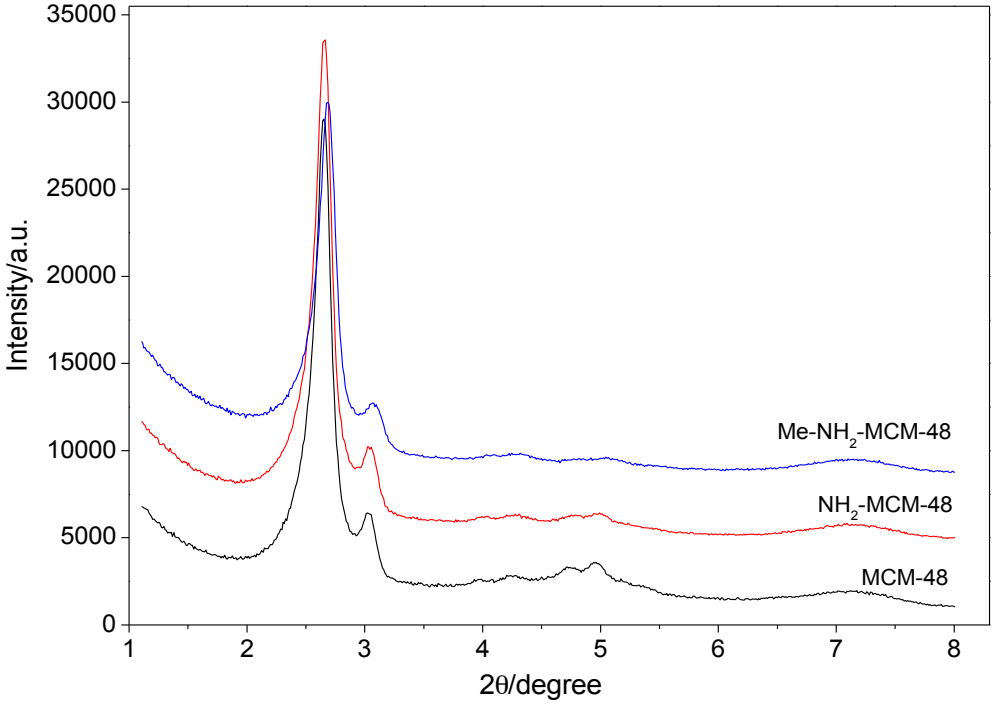

Figure 6.4 Powder X-ray diffraction pattern of Me-NH_2-MCM-48

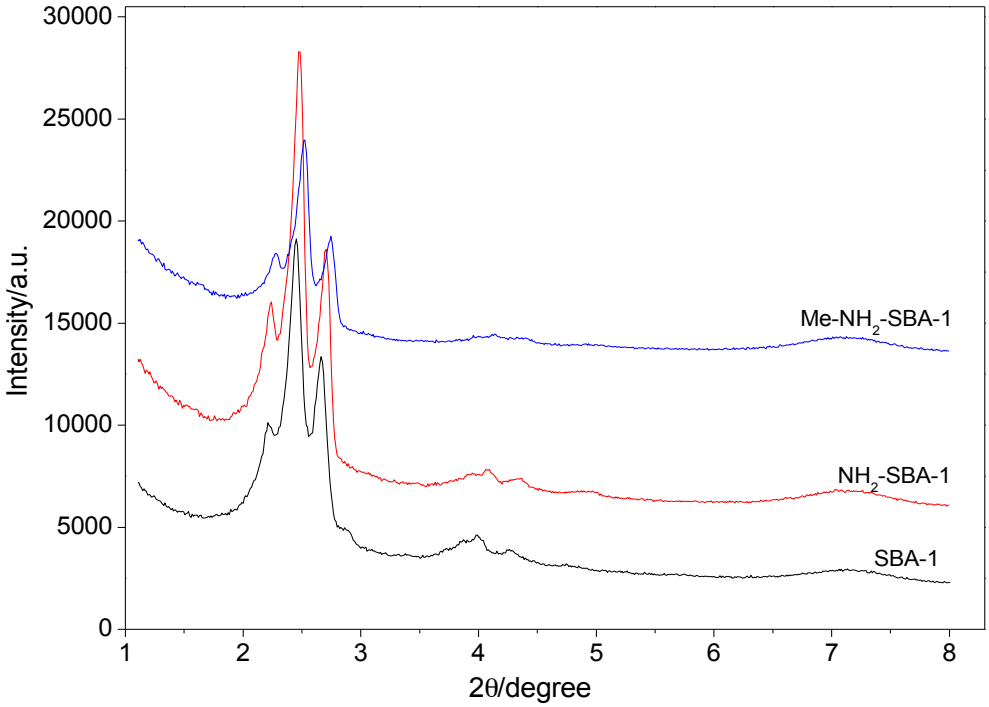

Figure 6.5 Powder X-ray diffraction pattern of Me-NH_2-SBA-1

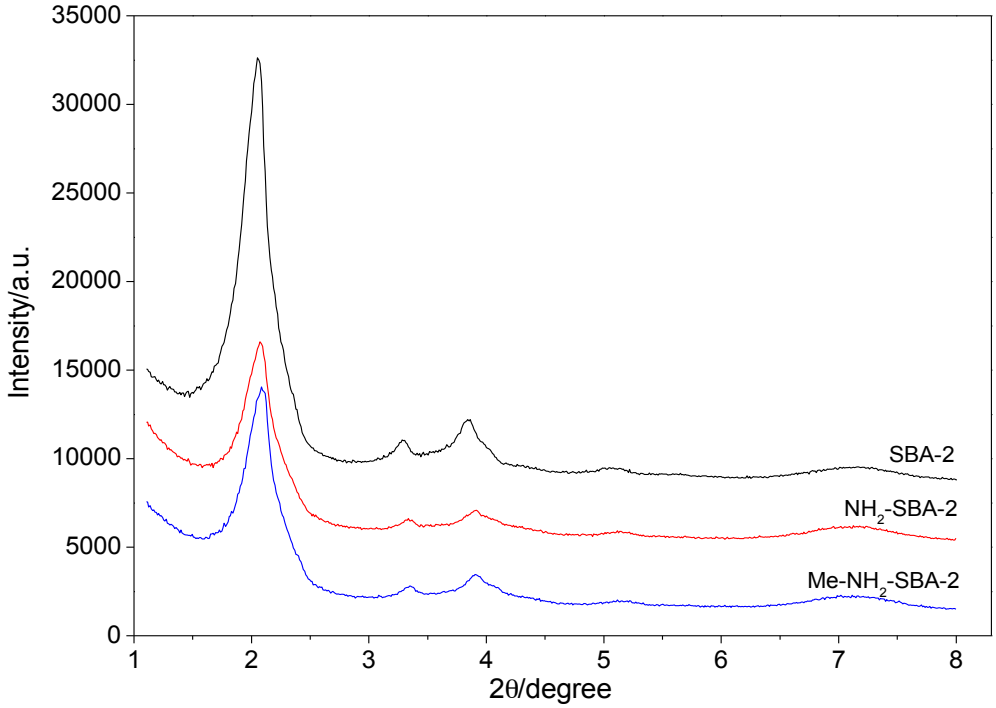

Figure 6.6 Powder X-ray diffraction pattern of Me-NH_2-SBA-2

Table 6.1 Unit cell parameter of pure mesoporous silica, NH_2-mesoporous silica, and Me-NH_2-mesoporous silica

Materials	Unit cell parameter, a, (Å)		
	Pure mesoporous silica	NH_2-mesoporous silica	Me-NH_2-mesoporous silica
MCM-41	36.7	36.5	36.4
MCM-48	82.1	81.6	80.5
SBA-1	80.5	79.7	78.1
SBA-2	46.8	46.0	45.7

6.3.1.2 Characterisation of Me-NH_2-mesoporous silicas by nitrogen adsorption-desorption

The adsorption-desorption isotherms and pore size distributions of Me-NH_2-MCM-41 and Me-NH_2-MCM-48 are shown in Figure 6.7 and Figure 6.8. The unusual adsorption-desorption steps are observed, these are suggested to be caused by some structural defect in the mesostructure[156], as discussed earlier. In addition, the amount of adsorbed N_2 of the Me-NH_2-mesoporous silicas are decreased, which is expected due to the introduced functional groups occupying part of the pore volume.

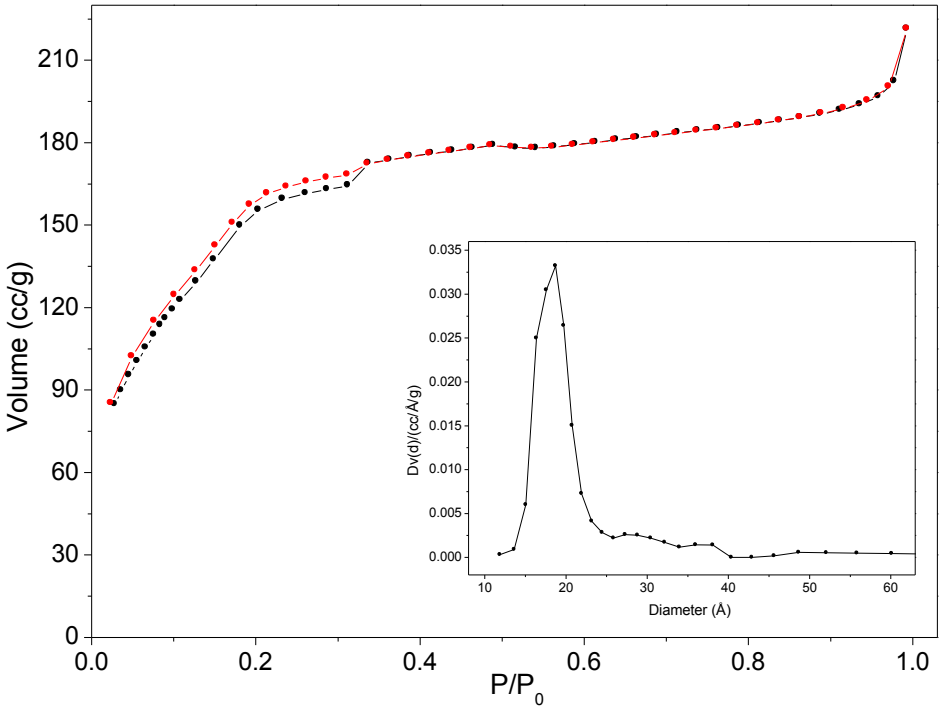

Figure 6.7 Nitrogen adsorption-desorption isotherm and pore size distribution of Me-NH_2-MCM-41

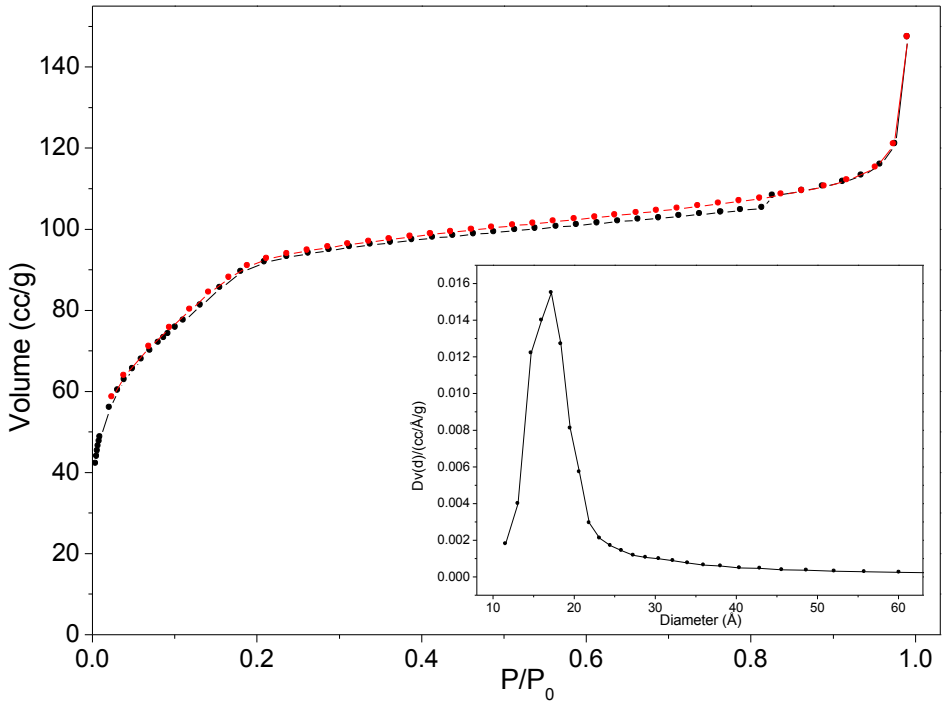

Figure 6.8 Nitrogen adsorption-desorption isotherm and pore size distribution of Me-NH_2-MCM-48

Surface area, pore diameter, and pore volume of the Me-NH_2-mesoporous silicas are presented in Table 6.2. Me-NH_2-MCM-41 shows the highest surface area, pore diameter, and also highest pore volume. Surface area, pore diameter, and pore volume of all the Me-NH_2-mesoporous silicas are lower than that of the corresponding NH_2-mesoporous silicas. This can be explained by the incorporation of methyl groups meaning space inside the mesopores is now occupied by the functional groups results in the lower surface area, pore diameter, and pore volume. In addition, pore diameter of these materials are found to be lower than 2 nm, which is not in the mesoporous range (pore diameter of mesoporous material is in the range of 2-50 nm). This is frequently found for the modified-mesoporous silicas whose pore size of parent materials are close to the border of mesoporous and microporous range[170, 224-227] and the BET method for surface area determination is still applicable as the straight line BET plot in the range of $P/P_0 \approx 0.05$-0.3 is obtained.

Table 6.2 Surface area, pore size and pore volume of the Me-NH_2-mesoporous silicas

Materials	S_{BET} (m^2g^{-1})	Pore diameter * (nm)	Pore volume* (cm^3g^{-1})
Me-NH_2-MCM-41	587 (753)**	1.9 (2.1)	0.56 (0.74)
Me-NH_2-MCM-48	215 (235)	1.7 (3.1)	0.30 (0.33)
Me-NH_2-SBA-1	108 (186)	1.7 (3.2)	0.23 (0.26)
Me-NH_2-SBA-2	115 (122)	1.5 (2.5)	0.20 (0.22)

*Calculated from the adsorption branch
** Values in the parentheses are from their corresponding NH_2-mesoporous silica

6.3.1.3 Characterisation of Me-NH_2-mesoporous silicas by Elemental Analysis

Me-NH_2-mesoporous silicas were also characterised by Elemental Analysis to confirm the methylation, and the results are shown in Table 6.3. Carbon content found in Me-NH-2 mesoporous silicas is higher than that of the corresponding non-methylated materials. As was previously found in the amino-modified mesoporous silicas, the different mesoporous supports are able to accommodate different amounts of functional groups. The 3-dimensional cubic structure *Ia3d* MCM-48 and *Pm3n* SBA-1 were found to contain a higher amount of functional group, indicated by the higher carbon and nitrogen content, than the 2-dimensional hexagonal *P6mm* MCM-41 and the cage-like hexagonal SBA-2, as had been found in NH_2-mesoporous silicas.

Table 6.3 Elemental analysis results for Me-NH_2-mesoporous silicas

Catalyst	Carbon (mmol/g)	Nitrogen (mmol/g)	Methyl (mmol/g)*
Me-NH_2-MCM-41	5.68	1.56	0.29
Me-NH_2-MCM-48	6.56	1.65	0.20
Me-NH_2-SBA-1	5.99	1.58	0.16
Me-NH_2-SBA-2	5.08	1.19	0.16

*Calculated from the increase in carbon content

6.3.1.4 Catalytic testing of Me-NH_2-mesoporous silicas

The methylated-amino-modified mesoporous silicas were used as catalyst in Knoevenagel condensation between benzaldehyde and ethylcyanoacetate as carried out with amino-modified mesoporous silicas, and the results are presented in Table 6.4. For MCM-41 and MCM-48 supported catalysts, the conversion appears to be higher than 97%, while SBA-1 and SBA-2 supported catalysts show significantly lower conversion.

Table 6.4 Catalytic activity of the Methylated-amino-modified mesoporous silicas

Catalyst	Conversion (%)*
Me-NH_2-MCM-41	97.4 ± 0.8 (97.6 ± 1.5)**
Me-NH_2-MCM-48	98.7 ± 0.6 (99.1 ± 0.8)
Me-NH_2-SBA-1	33.1 ± 1.1 (98.2 ± 0.8)
Me-NH_2-SBA-2	7.4 ± 1.7 (96.7 ± 1.2)

*The conversions shown are from three repeated reactions, reported in (average value ± S.D.)
** Values in the parentheses are from the reaction catalysed by NH_2-mesoporous silica

The incorporation of methyl groups to cap the remaining silanols was carried out in order to obtain a hydrophobic surface and was expected to benefit the base-catalysed reaction as they are active towards the base site catalyst; therefore, the capturing of silanol groups provides the elimination of hydrogen bonding interactions between the base site and silanol groups. However, as shown in Table 6.4, Me-NH_2-SBA-1 and Me-NH_2-SBA-2 show significantly reduced conversion for the Knoevenagel condensation compared to NH_2-SBA-1 and NH_2-SBA-2.

This could be attributed to the structural effect of catalyst supports. The cage-like mesoporous silicas SBA-1 and SBA-2 are more affected by the further surface modification by methyl groups. Pore blockages are more likely to occur with the cage-like structure according to their pore entrances size (pore entrances are of ca. 0.4-1.5 nm [184-186]). Pore blockage may cause the difficulties with reactants diffusing through the catalyst supports results in the decrease in catalyst activity. This lack of access to the catalytically active sites correlates with the lower surface areas and pore volumes seen for these catalysts. Therefore, in the case of cage-like mesoporous silicas as support for a base catalyst used for Knoevenagel condensation reaction, the accessibility of the pores appears to have more affect on the conversion observed than the surface hydrophilicity.

6.3.1.5 Catalyst recycling

The recyclability of methylated-amino-modified mesoporous silicas has also been investigated via the Knoevenagel condensation reaction. The used catalysts were washed with water and dried at 60 °C for 20 hours followed by drying under vacuum at 80 °C for 5 hours prior to further use. Figure 6.9 shows the conversion of Knoevenagel condensation reaction using Me-NH_2-mesoporous silicas against recycling (for comparison, conversion upon

recycling for NH2-mesoporous silica is shown in Figure 6.10). The cage-like mesoporous silicas support materials, SBA-1 and SBA-2 show a very low conversion compared to non-methylated catalyst and conversion decreased upon recycling, which suggested to be the effect of pore blockage. This blockage can possibly be cauåsed by not only the methyl groups but also the by the reactants and product from the reaction over repeated use, and this pore blockage may cause difficulties in the catalyst washing process of the used catalyst as well.

These problems of pore blockage appear not to have as much effect in hexagonal MCM-41 and cubic MCM-48 supports, as they can also be used for 4 times without any loss in conversion which is comparable to the NH_2-MCM-41 and NH_2-MCM-48. On further use of catalysts after the fourth cycle different conversion trends are seen. The MCM-41 supported catalyst shows lower conversion than MCM-48, which can be explained by the 3D structure of MCM-48 allowing better diffusion upon repeated use.

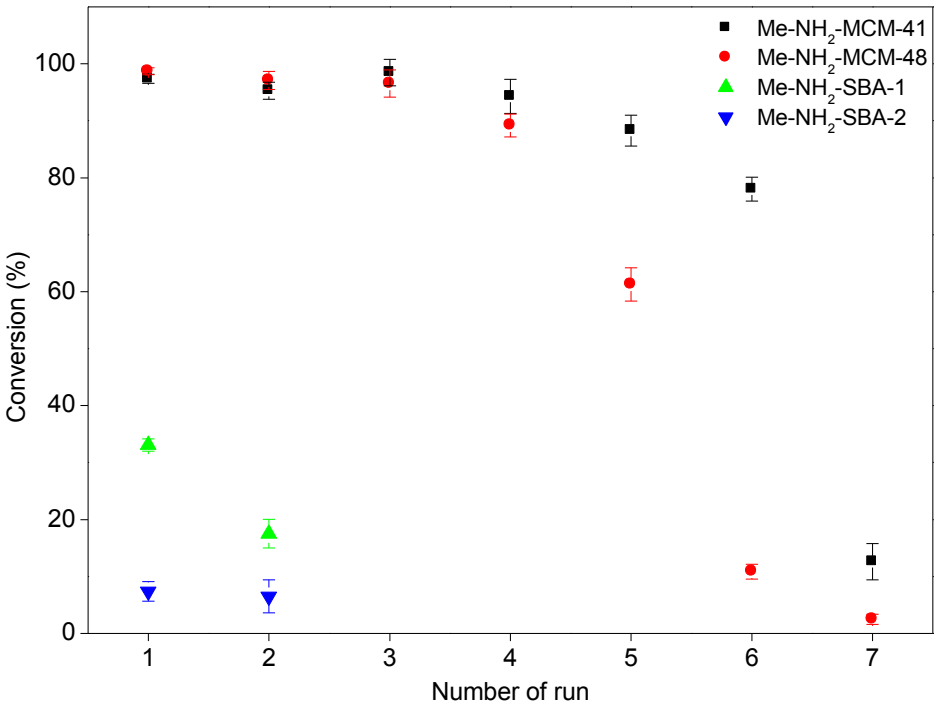

Figure 6.9 Catalyst recycling for Me-NH2-mesoporous silica

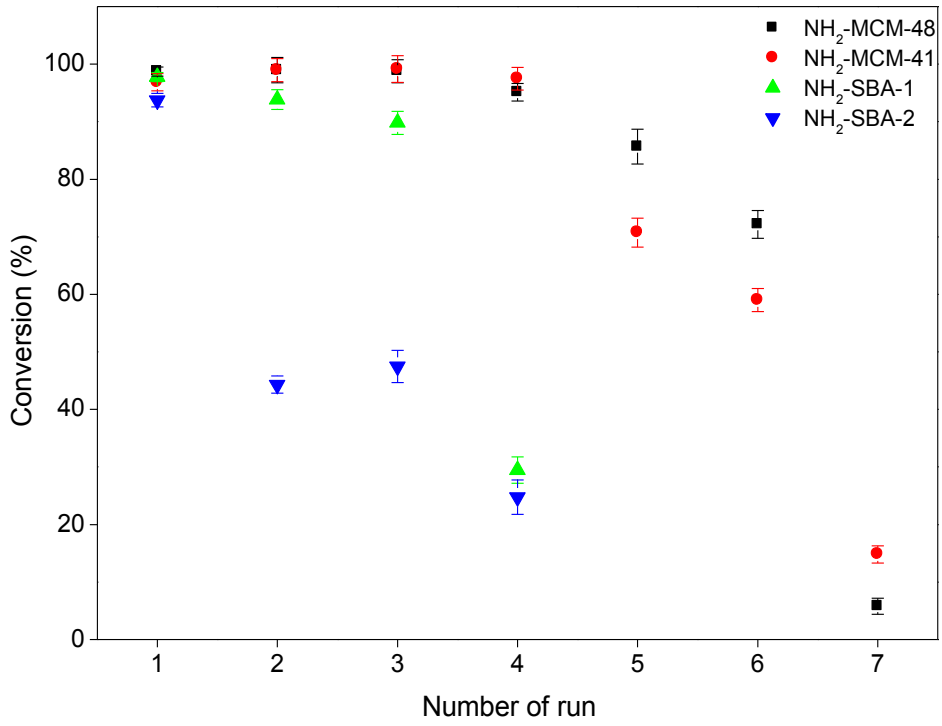

Figure 6.10 Catalyst recycling for NH_2-mesoporous silica

6.3.2 Me-(1)-mesoporous silicas

The (1)-mesoporous silicas were also modified with methyl groups to capture silanol groups on the surface. The resulting materials were characterised and the catalytic activity was tested.

6.3.2.1 Characterisation of Me-(1)-mesoporous silicas by powder X-ray diffraction (XRD)

The X-ray diffraction pattern of the methylated (1)-MCM-41, MCM-48, SBA-1, and SBA-2 are shown in Figure 6.11, Figure 6.12, Figure 6.13, and Figure 6.14, respectively. All the modified mesoporous materials show the expected characteristics of the support materials, however, again slight peak shifting to higher angle is observed. This reveals that the addition of the methyl group causes the structure contraction resulting in the slightly smaller unit cell parameter. Comparison of the unit cell parameter values of the pure siliceous material, (1)-, and Me-(1)-mesoporous silicas is shown in Table 6.5.

In addition, the small peaks at 2θ of 3.5-6 degree appear to be weaker intensity, which is the indication of a less ordered mesostructure of the modified materials compared to the pure siliceous materials.

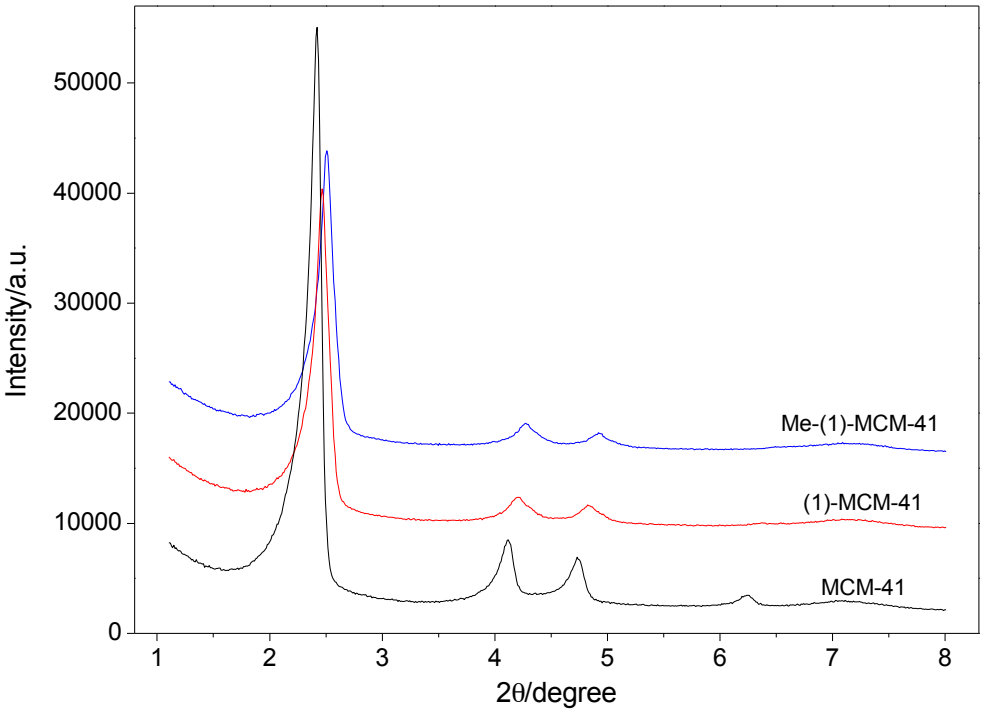

Figure 6.11 Powder X-ray diffraction pattern of Me-(1)-MCM-41

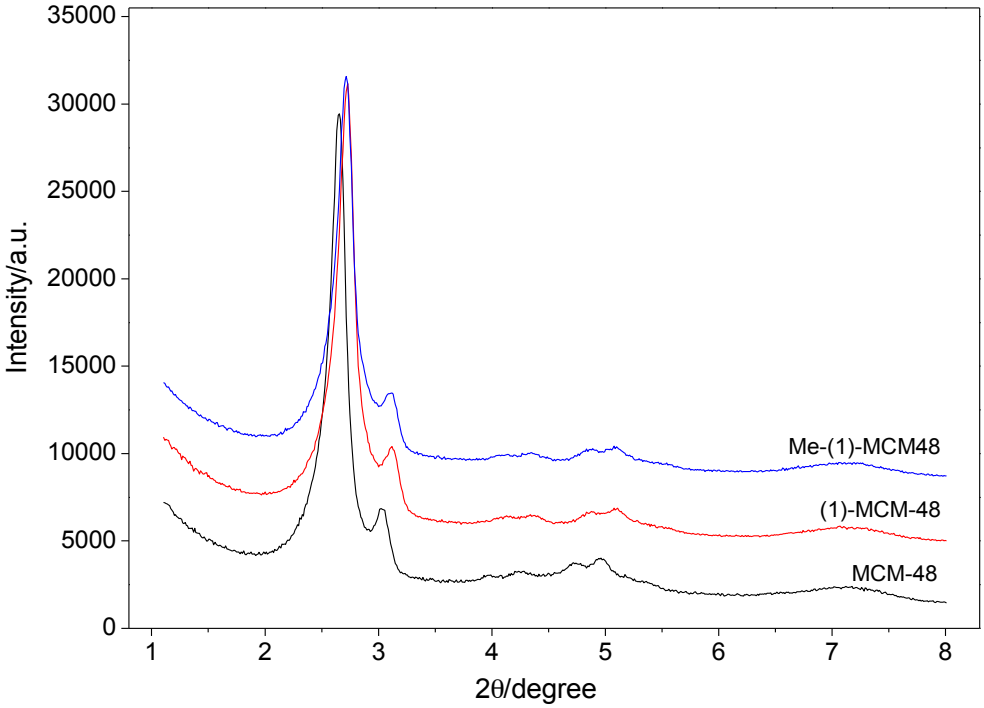

Figure 6.12 Powder X-ray diffraction pattern of Me-(1)-MCM-48

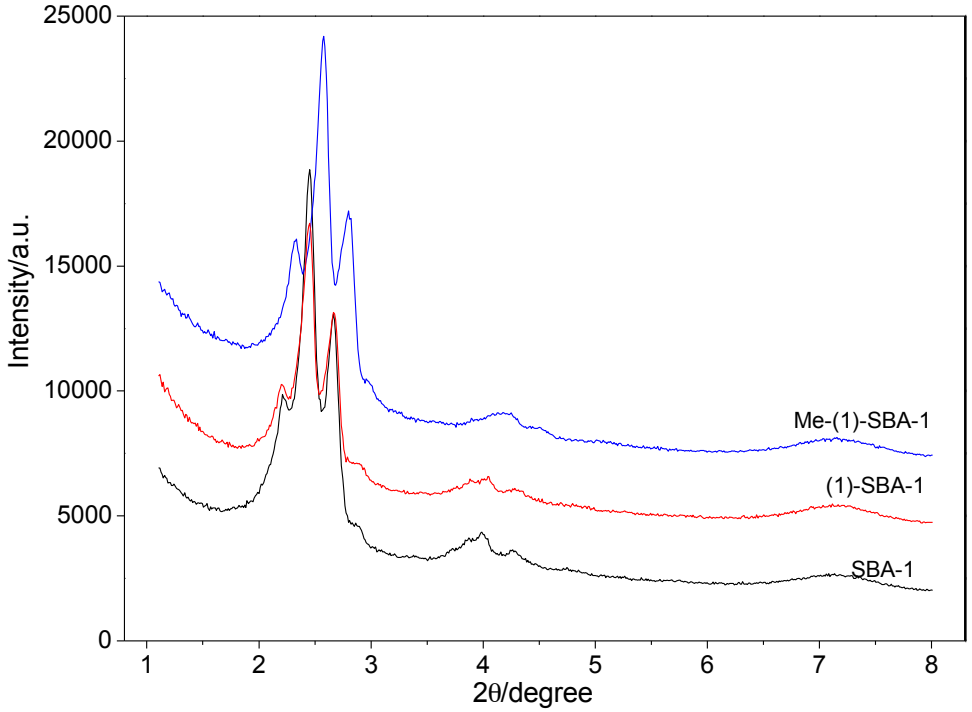

Figure 6.13 Powder X-ray diffraction pattern of Me-(1)-SBA-1

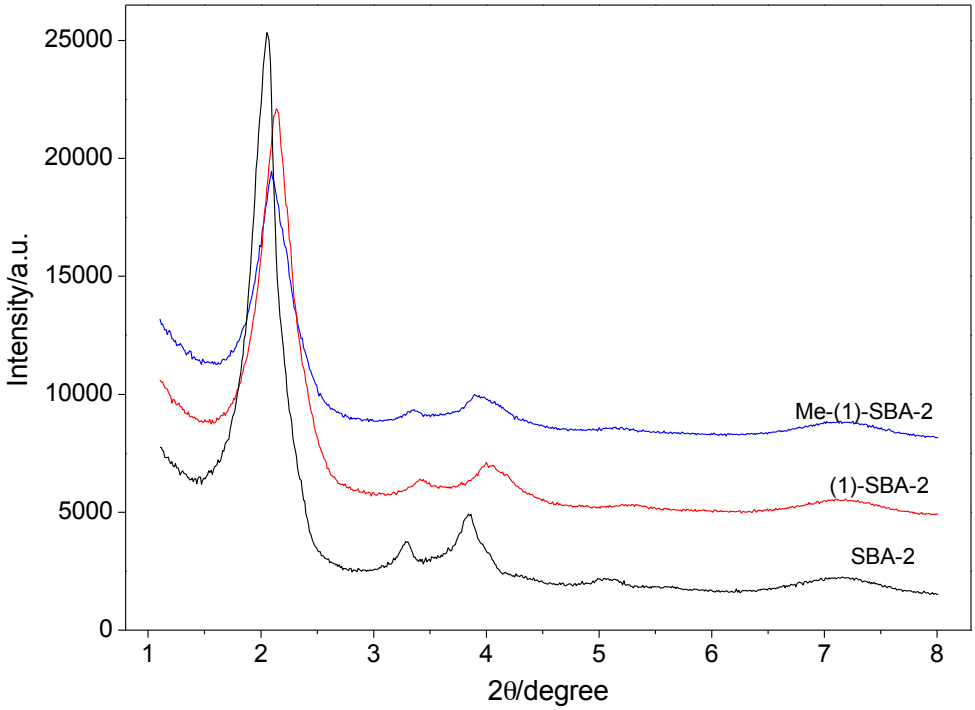

Figure 6.14 Powder X-ray diffraction pattern of Me-(1)-SBA-2

Table 6.5 Unit cell parameter of pure mesoporous silica, (1)-mesoporous silica, and Me-(1)-mesoporous silicas

Materials	Unit cell parameter, a, (Å)		
	Pure mesoporous silica	(1)-mesoporous silica	Me-(1)-mesoporous silica
MCM-41	37.0	35.6	35.4
MCM-48	82.2	79.8	79.4
SBA-1	80.6	80.4	76.8
SBA-2	46.7	45.4	45.3

6.3.2.2 Characterisation of Me-(1)-mesoporous silicas by Elemental Analysis

Me-(1)-mesoporous silicas were analysed by elemental analysis to confirm the methylation process, results are shown in Table 6.6.

Table 6.6 Elemental Analysis results for Me-(1)-mesoporous silicas

Catalyst	Carbon (mmol/g)	Nitrogen (mmol/g)	Methyl (mmol/g)*
Me-(1)-MCM-41	4.47	0.28	0.20
Me-(1)-MCM-48	4.98	0.36	0.29
Me-(1)-SBA-1	3.53	0.23	0.16
Me-(1)-SBA-2	3.38	0.20	0.13

* Calculated from the increase in carbon content

Carbon content in the Me-(1)-mesoporous silica samples are found to be higher than that of the un-methylated counterpart which could be attributed to the incorporation of methyl groups introduces more carbon to the materials.

6.3.2.3 Characterisation of Me-(1)-mesoporous silicas by X-ray fluorescence spectroscopy (XRF)

The nickel content in Me-(1)-mesoporous silicas was determined by XRF and the results are presented in Table 6.7. The Me-(1)-mesoporous silicas show the same nickel content as the corresponding non-methylated materials, which could confirm the covalent bonding between the asymmetric nickel-salen complex and silica surface.

Me-(1)-MCM-48 shows the highest amount of nickel due to the 3-dimensional cubic structure of the supported material which allows better accessibility of the nickel complex,

therefore more possibility for the asymmetric nickel-salen complex to be attached to the inner pore surface, in the same manner as was found in the (1)-mesoporous silicas.

Table 6.7 Nickel content in Me-(1)-mesoporous silica determined by XRF

Catalyst	Ni (mmol/g)*
Me-(1)-MCM-41	0.10
Me-(1)-MCM-48	0.12
Me-(1)-SBA-1	0.07
Me-(1)-SBA-2	0.05

* Calculated based on the assumption of one tether molecule per complex and the total mass of catalyst includes the incorporated methyl from elemental analysis result

6.3.2.4 Characterisation of Me-(1)-mesoporous silicas by nitrogen adsorption-desorption

The nitrogen adsorption-desorption isotherms and pore size distributions of the methylated-asymmetric nickel-salen complex modified mesoporous MCM-41, MCM-48, and SBA-1 are shown in Figure 6.15, Figure 6.16, and Figure 6.17, respectively. The characteristic, type IV adsorption isotherm expected for mesoporous materials is observed, but the steps are not well-defined which lead to the broader pore size distribution, compared to un-methylated samples. The amount of N_2 adsorbed of all samples is decreased due to the occupation of inner pore by the additional methyl groups; this also explains the smaller pore volume. The unusual hysteresis steps that are suggested to be associated with the pore-blocking effect around the embedded voids in the framework structure [156] are also observed.

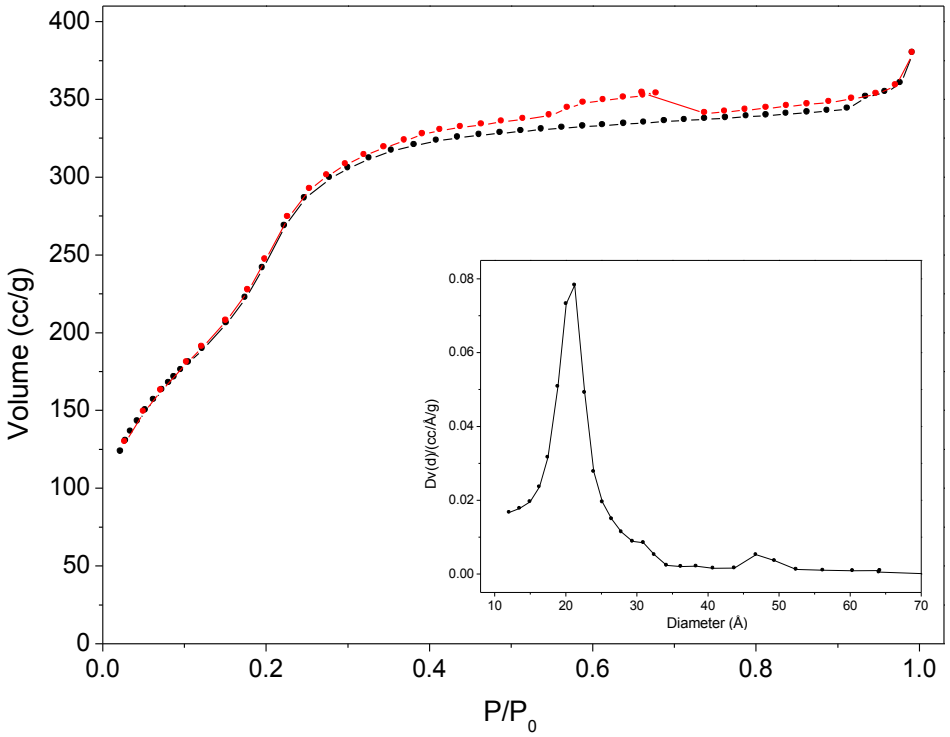

Figure 6.15 Nitrogen adsorption-desorption isotherm and pore size distribution of Me-(1)-MCM-41

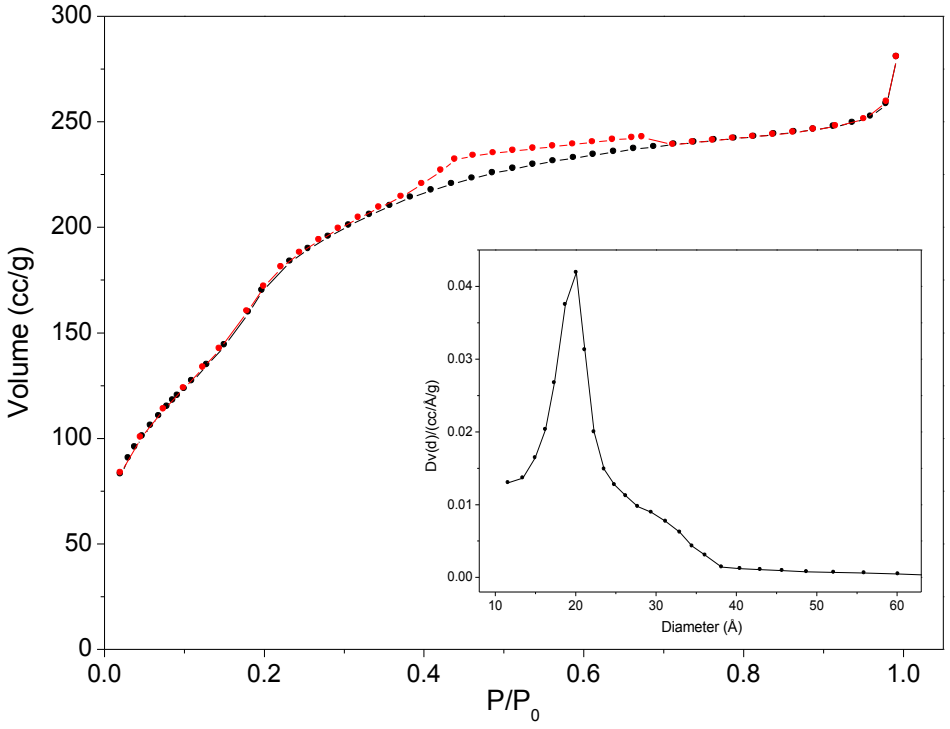

Figure 6.16 Nitrogen adsorption-desorption isotherm and pore size distribution of Me-(1)-MCM-48

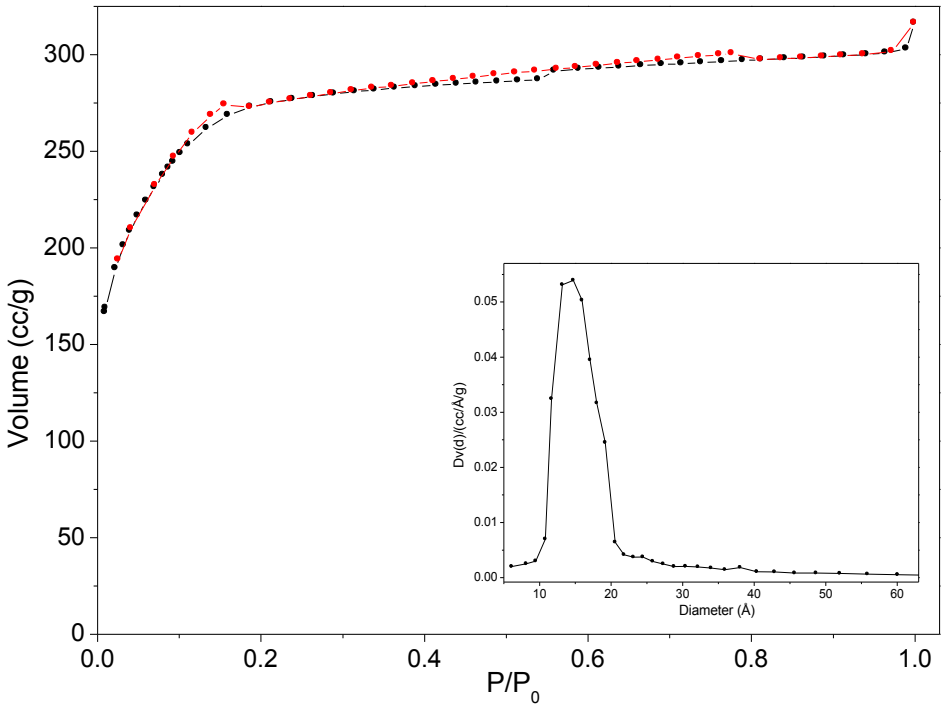

Figure 6.17 Nitrogen adsorption-desorption isotherm and pore size distribution of Me-(1)-SBA-1

Table 6.8 Surface area, pore size, and pore volume of Me-(1)-mesoporous silicas

Catalyst	Surface area (m^2g^{-1})	Pore diameter* (nm)	Pore volume* (cm^3g^{-1})
Me-(1)-MCM-41	816 (1013)**	2.0 (2.2)	0.90 (1.10)
Me-(1)-MCM-48	582 (915)	2.0 (2.1)	0.64 (1.09)
Me-(1)-SBA-1	545 (740)	2.0 (2.0)	0.77 (1.02)
Me-(1)-SBA-2	422 (765)	2.5 (2.7)	0.54 (0.82)

*Calculated from the adsorption branch
**Values in the parentheses are from their corresponding non-methylated counterpart

Table 6.8 presents the surface area, pore diameter, and pore volume of methylated-asymmetric nickel-salen complex modified mesoporous silica samples. It has been found that the surface area, pore size, and pore volume of the Me-(1)- mesoporous silicas are lower than

that of the (1)-mesoporous silicas, as also suggested by the lower amount of N_2 adsorbed. This could be attributed to the incorporated methyl groups occupying some more space in the mesopores.

6.3.2.5 Catalytic testing

The catalytic activity of the methylated-(1)-mesoporous silicas was tested in the Kumada-Corriu reaction of phenylmagnesium bromide and 4-bromoanisole following the same reaction conditions as for (1)-mesoporous silica catalysts. As the Grignard reagent is active toward silanol groups therefore the presence of methyl groups to capture these silanol groups is believed to benefit the Kumada-Corriu reaction. From the conversions shown in Table 6.9, only when MCM-48 is used as the support material does show the higher conversion compared to its corresponding non-methylated catalyst, this could be due to the 3D cubic structures allowing better reactants accessibility to the active sites inside the pores even with the presence of methyl groups, whilst the lower conversion observed for (1)-MCM-41 could be due to methyl groups causing difficulties for the reactants to access the 2D hexagonal structure hence the active sites inside the pore could not be reached[228-230]. As we found in methylated-amino-modified mesoporous silicas, the methyl groups can possibly cause blockage at the pore entrance of cage-like mesoporous silicas SBA-1 and SBA-2, resulting in lower activity.

Table 6.9 Conversion of Kumada-Corriu reaction using Me-(1)-mesoporous silicas

Catalyst	Conversion (%)*
Me-(1)-MCM-41	61.7 ± 2.7 (74.9 ± 3.2)**
Me-(1)-MCM-48	74.4 ± 2.9 (62.1 ± 2.6)
Me-(1)-SAB-1	55.4 ± 3.2 (69.8 ± 3.1)
Me-(1)-SBA-2	62.6 ± 2.6 (62.6 ± 2.2)

*The conversions shown are from three repeated reactions, reported in (average value ± S.D.)
** Values in the parentheses are from the reaction catalysed by NH_2-mesoporous silica

6.3.2.6 Catalyst recycling

Methylated-(1)-mesoporous silica catalysts were reused and the catalytic activity of the reused catalysts was investigated. Figure 6.18 shows the conversions for the reused Me-(1)-mesoporous silica catalysts (for comparison, the conversion upon recycling for (1)-mesoporous silica is shown in Figure 6.19). For SBA-1 and SBA-2 supported catalysts, there was a dramatic decrease in conversion upon reuse, while better conversions upon recycling were observed from the MCM-48 and MCM-41 supported catalysts compared to their corresponding non-methylated-(1)-modified mesoporous silicas catalysts. Me-(1)-MCM-41 and MCM-48 can be used for 7 times before dropping to about 10% conversion compared to 4 times for the non-methylated catalysts.

Since a Grignard reagent is used in the Kumada-Corriu reaction, this reaction is highly sensitive to silanol groups. Therefore, the further surface modification to capture surface silanol groups improves the activity of the catalyst in terms of recycling. The catalyst withstands more reaction cycles before losing activity compared to the non-methylated catalysts.

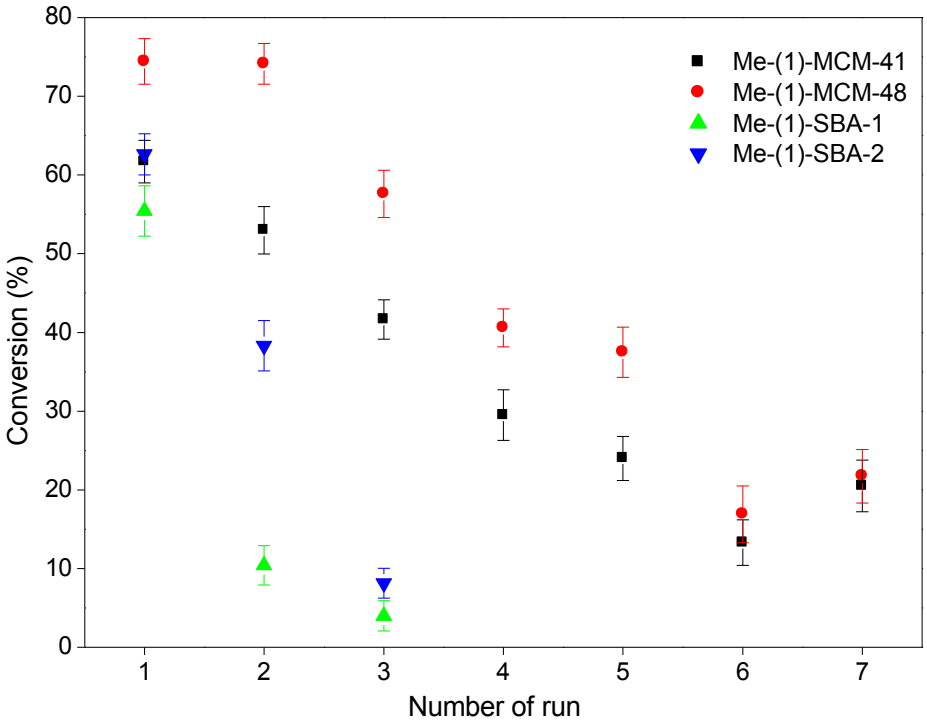

Figure 6.18 Conversion upon recycling for Me-(1)-mesoporous silica catalysts

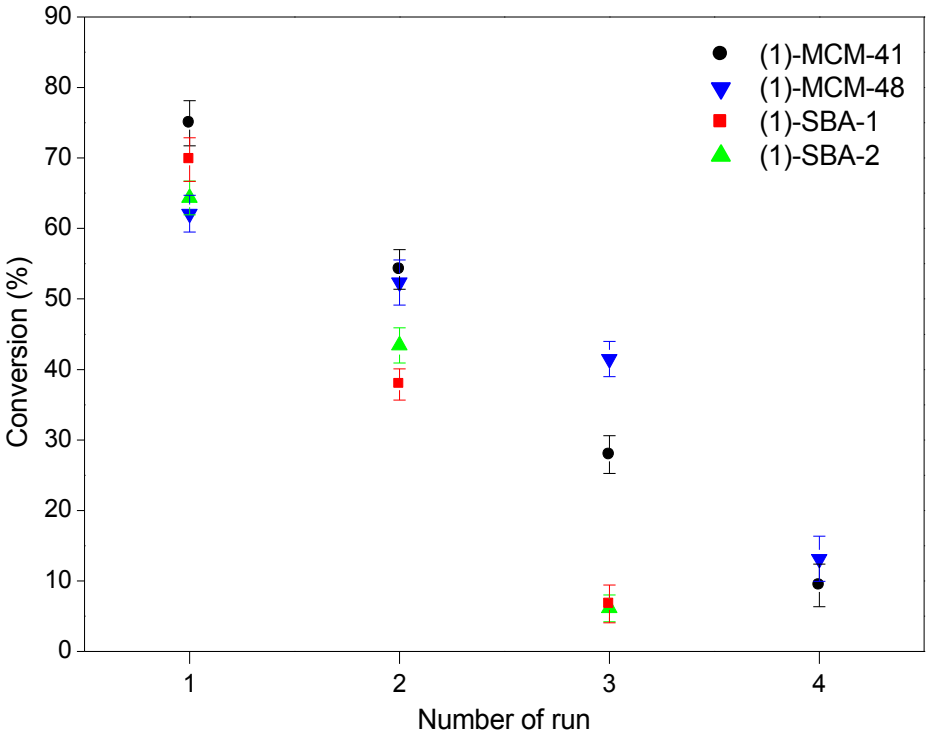

Figure 6.19 Conversion upon recycling for (1)-mesoporous silica catalysts

6.3.2.7 Post reaction solution study

As discussed in Chapter 5, leaching of nickel from the catalyst during reaction appears to be un-related to structure of support materials and does not show any relationship between number of runs and the amount of leached nickel.

Nickel leaching study results of Me-(1)-mesoporous silicas are shown in Table 6.10. The highest amount of leached nickel from the catalyst is found in the first run. However, upon recycling, it has also been found from these methylated-catalysts that the amount of nickel leaching is not related to the order of run. In addition, no particular trend of the leached nickel was observed with different mesoporous supports, as reported with (1)-mesoporous silicas. The remaining nickel in deactivated catalysts are presented in Table 6.11, it is suggested that the deactivation caused by pore blockage also plays an important role as there are still nickel species in the catalyst.

Table 6.10 Nickel leached from Kumada-Corriu reaction using Me-(1)-mesoporous silicas

Number of run	Nickel leached (%)			
	Me-(1)-MCM-41	Me-(1)-MCM-48	Me-(1)-SBA-1	Me-(1)-SBA-2
1	2.45	2.40	3.47	1.80
2	1.24	0.71	0.74	1.63
3	1.51	0.95	1.12	1.25
4	0.84	0.39		
5	0.62	0.30		
6	0.81	0.60		
7	0.71	0.36		

Table 6.11 Remaining nickel in the deactivated catalysts for Me-(1)-mesoporous silicas

Catalyst	Initial nickel content (mmol)[(a)]	Remaining nickel in deactivated catalyst (mmol)
Me-(1)-MCM-41	10.01×10^{-3}	9.37×10^{-3} [(b)]
Me-(1)-MCM-48	12.20×10^{-3}	11.51×10^{-3} [(b)]
Me-(1)-SBA-1	6.88×10^{-3}	6.52×10^{-3} [(c)]
Me-(1)-SBA-2	5.26×10^{-3}	5.01×10^{-3} [(c)]

[(a)] The amount of initial nickel in catalyst was calculated on the basis of SiO_2 as the silica wall with the assumption of one tether molecule (chloropropyl trimethoxy silane) for each nickel complex molecule and included the incorporated methyl

[(b)] Nickel remained in catalysts after the seventh run

[(c)] Nickel remained in catalyst after the third run

6.4 CONCLUSION

Further surface modification of amino and asymmetric nickel-salen complex modified mesoporous silicas with methylsilyl groups has been carried out in order to capture the remaining silanol groups on the mesoporous materials surface; this is expected to improve the catalytic activity of the base catalysed, Knoevenagel condensation, reaction and the Kumada-Corriu reaction in which a Grignard reagent is involved. It was found that the Me-NH_2-mesoporous silicas and Me-(1)-mesoporous silicas possess the expected characteristics although unit cell parameter, surface area, and pore volume are smaller than that of the corresponding un-methylated samples due to the contraction during the methylation process and also the occupation of methyl groups on the inner pore surface.

The catalytic activity and recyclability of the obtained materials were tested via Knoevenagel condensation for Me-NH_2-mesoporous silicas and Kumada-Corriu reaction for Me-(1)-mesoporous silicas. The activity and recyclability of the methylated amino and asymmetric nickel-salen complex with the cage-like mesoporous supports, SBA-1 and SBA-2, are poorer than that of the corresponding un-methylated catalysts due to higher likelihood of pore blockage at the pore entrances that may cause difficulties in reactant diffusion. Me-NH_2-MCM-41 also shows poorer recyclability compared to NH_2-MCM-41 whereas this is not observed in Me-NH_2-MCM-48 and NH_2-MCM-48, which is suggested to be caused by 2-dimensional MCM-41 support structures allowing poorer pore accessibility with the presence of methyl groups, whilst this is not dominant for the 3-dimensional MCM-48. In addition, Me-(1)-MCM-41 and Me-(1)-MCM-48 show improvement in recyclability, which suggests that the presence of methyl groups to capture the remaining silanols on the surface play an important role in the Kumada-Corriu reaction upon subsequent runs.

CHAPTER 7 CONCLUSIONS AND FUTURE WORK

7.1 CONCLUSIONS

Mesoporous silicas with different pore structure have been successfully synthesised using TEOS as the silica source. The synthesis conditions and the structure directing agent used were varied depending on the desired structure; CTAB was used in the synthesis of the hexagonal MCM-41 and cubic MCM-48 while the larger head group surfactant, CTEAB, was used for the synthesis of SBA-1 and the Gemini surfactant, $C_{16\text{-}3\text{-}1}$, for SBA-2. The resulting materials show the characteristics of mesoporous materials and also uniform pore size and high surface area.

Taking the advantage of having large pore and high surface area, the synthesised mesoporous silicas were modified in order to be used as catalysts. Firstly, the obtained materials were modified by amino groups via post-grafting methods and were used as base catalysts in the Knoevenagel condensation reaction. All amino-modified mesoporous silicas exhibit high initial conversion (>95%) and no significant difference in conversion was observed for the different silica supports used. However, the structure of supporting materials played an important role in terms of catalyst recycling. The catalysts with a cage-like support, SBA-1 and SBA-2, were found to deactivate faster than the MCM-41 and MCM-48 due to the higher possibility of pore blockage at the narrower pore entrances of the cage-like structure, therefore the reactant diffusion was obstructed.

The obtained mesoporous silicas were also modified with an organometallic complex for use in another reaction. Asymmetric nickel-salen complexes (denoted as (1)) were synthesised and functionalised in a manner suitable for attachment to the mesoporous

supports. The modified materials were utilised as catalysts in the Kumada-Corriu reaction and result in comparable conversion to the homogeneous asymmetric nickel-salen complex catalyst. However, the supported catalysts have an advantage in term of catalyst separation and recycling. (1)-MCM-41 and (1)-MCM-48 can be used for four times while the (1)-SBA-1 and (1)-SBA-2 can be used three time before significant degradation in performance. This is of the same tendency as seen for the amino modified mesoporous silicas that the catalyst with cage-like supporters are more likely to lost their activity due to the pore blockage.

Surface hydrophobicity is another factor that needs to be considered when the amino-modified mesoporous silica is used as a base catalyst in the Knoevenagel condensation reaction and also when (1)-mesoporous silica is used in the Kumada-Corriu reaction, which involves a Grignard reagent. Therefore the further modification of catalysts to capture the remaining surface silanol groups in the modified-mesoporous silicas has been carried out by using chlorotrimethylsilane to obtain the surface functionalised with trimethyl groups instead of silanols. The catalysts with MCM-41 and MCM-48 as support demonstrate better recyclability for both amino and asymmetric nickel-salen complex functions while this was not observed in the cage-like SBA-1 and SBA-2 supports catalyst as the presence of additional trimethylsilyl groups could cause further pore blocking.

7.2 FUTURE WORK DIRECTION

Regarding the immobilisation of nickel-salen complex onto mesoporous silica materials, more research needs to be carried out to improve the catalyst properties e.g. to prevent or minimise catalyst leaching and to improve catalyst stability. In addition testing more of the catalytic reaction which homogeneous nickel-salen complex have been shown to selectively catalyse is warranted e.g. Heck reaction, to include an activity study using kinetic

data. There are many alterations that may be applied to try and improve the catalyst properties. One possible method is to alter the salen ligand systems, 1,4-pentanedione, ethylenediamine, and salicyldehyde have been used in this study but there are various diamines and salicylaldehyde derivatives that can derive different selen ligand[231-235]. Another possible method is to alter the tether molecule during the tethering process, we have used a chloropropyltrimethoxy silane to react with silica surface leaving chloro-mesoporous silica surface to bond with the catalyst complex, bromo- or iodo- ended group which are the better leaving groups might have been tried.

For amino-modified mesoporous silicas, to improve their catalytic activity and stability upon recycling amino functional group with different basicity e.g. secondary amine may be incorporated to improve the activity in base-catalysed reaction due to stronger basicity in secondary amine. As amino groups are active toward some other functional groups e.g. carbonyl therefore the introduction of additional functions to provide the materials with suitable surface properties to allow preferential catalytic activity is possible. In addition, amino-modified mesoporous silicas may be applied in different application other than catalysis e.g. as the adsorbent.

This study concentrates upon a small number of mesoporous silica materials as supports but a wide variety of supporting materials still remains unused, some of which are described in Chapter 1. Many of these supports have different structure and do not share the same chemical make up as MCM-41, MCM-48, SBA-1, and SBA-2 which have been used in this study; therefore it could be assumed that they would have different ways to behave towards the catalyst complexes immobilisation within their framework. There are also different procedures for synthesis of the supporting materials, and even though we focused on one synthesis method for each material in this study, the alternative synthesis methods for

mesoporous silicas such as hydrothermal[236-238] or microwave-assisted[239-243] synthesis might give the different environment for the incorporated functional groups.

Research in this area is still open as there are many functional groups and mesoporous supports to be utilised depending on the desired application. Therefore, different functional groups and modification method can be applied in order to tune the properties of the materials. Modifications of mesoporous silicas offers the wide range of functionalities and are highly robust and flexible as they can be chemically modified to fit the circumstances of almost any desired settings. In addition to catalysis that has been studied in this work, the other applications of modified-mesoporous silicas include adsorption[244-248], separation[249-253], chromatography[254-257], sensor[258-262], drugs delivery[263-268], etc.

REFERENCES

[1] Gate, B. C., *Catalytic Chemistry, John Wiley & Sons, Inc.* , (1991) **1st ed**,

[2] Sing, K. S. W.; Everett, D. H.; Haul, R. A. W.; Moscou, L.; Pierotti, R. A.; Rouquerol, J.; Siemieniewska, T., *Pure and Applied Chemistry*, (1985) **57**, 603.

[3] Taguchi, A.; Schuth, F., *Microporous and Mesoporous Materials*, (2005) **77**, 1.

[4] Chiola, V.; Ritsko, J. E.; Vanderpool, C. D., *US Patent No. 3 556 725*, (1971),

[5] Yanagisawa, T.; Shimizu, T.; Kuroda, K.; Kato, C., *Bulletin of the Chemical Society of Japan*, (1990) **63**, 988.

[6] Inagaki, S.; Fukushima, Y.; Kuroda, K., *Journal of the Chemical Society-Chemical Communications*, (1993), 680.

[7] Inagaki, S.; Koiwai, A.; Suzuki, N.; Fukushima, Y.; Kuroda, K., *Bulletin of the Chemical Society of Japan*, (1996) **69**, 1449.

[8] Kresge, C. T.; Leonowicz, M. E.; Roth, W. J.; Vartuli, J. C.; Beck, J. S., *Nature*, (1992) **359**, 710.

[9] Beck, J. S.; Vartuli, J. C.; Roth, W. J.; Leonowicz, M. E.; Kresge, C. T.; Schmitt, K. D.; Chu, C. T. W.; Olson, D. H.; Sheppard, E. W.; McCullen, S. B.; Higgins, J. B.; Schlenker, J. L., *Journal of the American Chemical Society*, (1992) **114**, 10834.

[10] Vartuli, J. C.; Schmitt, K. D.; Kresge, C. T.; Roth, W. J.; Leonowicz, M. E.; McCullen, S. B.; Hellring, S. D.; Beck, J. S.; Schlenker, J. L.; Olson, D. H.; Sheppard, E. W., *Chemistry of Materials*, (1994) **6**, 2317.

[11] Dubois, M.; Gulikkrzywicki, T.; Cabane, B., *Langmuir*, (1993) **9**, 673.

[12] Ying, J. Y.; Mehnert, C. P.; Wong, M. S., *Angewandte Chemie-International Edition*, (1999) **38**, 56.

[13] Anderson, M. W., *Zeolites*, (1997) **19**, 220.

[14] Tanev, P. T.; Pinnavaia, T. J., *Science*, (1995) **267**, 865.

[15] Tanev, P. T.; Liang, Y.; Pinnavaia, T. J., *Journal of the American Chemical Society*, (1997) **119**, 8616.

[16] Tanev, P. T.; Pinnavaia, T. J., *Science*, (1996) **271**, 1267.

[17] Prouzet, E.; Pinnavaia, T. J., *Angewandte Chemie-International Edition*, (1997) **36**, 516.

[18] Huo, Q. S.; Margolese, D. I.; Stucky, G. D., *Chemistry of Materials*, (1996) **8**, 1147.

[19] Zhou, W. Z.; Hunter, H. M. A.; Wright, P. A.; Ge, Q. F.; Thomas, J. M., *Journal of Physical Chemistry B*, (1998) **102**, 6933.

[20] Schmidt-Winkel, P.; Lukens, W. W.; Zhao, D. Y.; Yang, P. D.; Chmelka, B. F.; Stucky, G. D., *Journal of the American Chemical Society*, (1999) **121**, 254.

[21] Yang, P. D.; Zhao, D. Y.; Margolese, D. I.; Chmelka, B. F.; Stucky, G. D., *Nature*, (1998) **396**, 152.

[22] Yang, P. D.; Zhao, D. Y.; Margolese, D. I.; Chmelka, B. F.; Stucky, G. D., *Chemistry of Materials*, (1999) **11**, 2813.

[23] Soler-Illia, G.; Sanchez, C., *New Journal of Chemistry*, (2000) **24**, 493.

[24] Soler-Illia, G.; Scolan, E.; Louis, A.; Albouy, P. A.; Sanchez, C., *New Journal of Chemistry*, (2001) **25**, 156.

[25] Antonelli, D. M.; Ying, J. Y., *Angewandte Chemie-International Edition in English*, (1995) **34**, 2014.

[26] Putnam, R. L.; Nakagawa, N.; McGrath, K. M.; Yao, N.; Aksay, I. A.; Gruner, S. M.; Navrotsky, A., *Chemistry of Materials*, (1997) **9**, 2690.

[27] Antonelli, D. M.; Nakahira, A.; Ying, J. Y., *Inorganic Chemistry*, (1996) **35**, 3126.

[28] Bagshaw, S. A.; Pinnavaia, T. J., *Angewandte Chemie-International Edition in English*, (1996) **35**, 1102.

[29] Khushalani, D.; Dag, O.; Ozin, G. A.; Kuperman, A., *Journal of Materials Chemistry*, (1999) **9**, 1491.

[30] Cassiers, K.; Linssen, T.; Mathieu, M.; Benjelloun, M.; Schrijnemakers, K.; Van Der Voort, P.; Cool, P.; Vansant, E. F., *Chemistry of Materials*, (2002) **14**, 2317.

[31] Galarneau, A.; Desplantier-Giscard, D.; Di Renzo, F.; Fajula, F., *Catalysis Today*, (2001) **68**, 191.

[32] Igarashi, N.; Koyano, K. A.; Tanaka, Y.; Nakata, S.; Hashimoto, K.; Tatsumi, T., *Microporous and Mesoporous Materials*, (2003) **59**, 43.

[33] Igarashi, N.; Tanaka, Y.; Nakata, S.; Tatsumi, T., *Chemistry Letters*, (1999), 1.

[34] Macquarrie, D. J., *Chemical Communications*, (1996), 1961.

[35] Inagaki, S.; Guan, S.; Fukushima, Y.; Ohsuna, T.; Terasaki, O., *Journal of the American Chemical Society*, (1999) **121**, 9611.

[36] Koyano, K. A.; Tatsumi, T.; Tanaka, Y.; Nakata, S., *Journal of Physical Chemistry B*, (1997) **101**, 9436.

[37] Kloetstra, K. R.; vanLaren, M.; vanBekkum, H., *Journal of the Chemical Society-Faraday Transactions*, (1997) **93**, 1211.

[38] Occelli, M. L.; Biz, S.; Auroux, A.; Ray, G. J., *Microporous and Mesoporous Materials*, (1998) **26**, 193.

[39] Kao, H. M.; Chang, P. C.; Liao, Y. W.; Lee, L. P.; Chien, C. H., *Microporous and Mesoporous Materials*, (2008) **114**, 352.

[40] Kosslick, H.; Landmesser, H.; Fricke, R., *Journal of the Chemical Society-Faraday Transactions*, (1997) **93**, 1849.

[41] Zhao, D. Y.; Nie, C.; Zhou, Y. M.; Xia, S. J.; Huang, L. M.; Li, Q. Z., *Catalysis Today*, (2001) **68**, 11.

[42] Corma, A.; Gonzalez-Alfaro, V.; Orchilles, A. V., *Journal of Catalysis*, (2001) **200**, 34.

[43] Pater, J. P. G.; Jacobs, P. A.; Martens, J. A., *Journal of Catalysis*, (1999) **184**, 262.

[44] Corma, A.; Grande, M. S.; GonzalezAlfaro, V.; Orchilles, A. V., *Journal of Catalysis*, (1996) **159**, 375.

[45] Armengol, E.; Corma, A.; Garcia, H.; Primo, J., *Applied Catalysis a-General*, (1997) **149**, 411.

[46] Armengol, E.; Corma, A.; Garcia, H.; Primo, J., *Applied Catalysis a-General*, (1995) **126**, 391.

[47] Armengol, E.; Cano, M. L.; Corma, A.; Garcia, H.; Navarro, M. T., *Journal of the Chemical Society-Chemical Communications*, (1995), 519.

[48] Zou, J. J.; Xu, Y.; Zhang, X. W.; Wang, L., *Applied Catalysis a-General*, (2012) **421**, 79.

[49] Tang, H.; Ji, M.; Wang, X. K.; He, M.; Cai, T. X., *Chinese Journal of Catalysis*, (2010) **31**, 725.

[50] Iwanami, K.; Seo, H.; Choi, J. C.; Sakakura, T.; Yasuda, H., *Tetrahedron*, (2010) **66**, 1898.

[51] Chen, X. Y.; Jia, M.; Liu, G. Z.; Zhang, X. W.; Wang, L.; Mi, Z. T., *Applied Surface Science*, (2010) **256**, 5856.

[52] Bhange, P.; Bhange, D. S.; Pradhan, S.; Ramaswamy, V., *Applied Catalysis a-General*, (2011) **400**, 176.

[53] Climent, M. J.; Corma, A.; Iborra, S.; Navarro, M. C.; Primo, J., *Journal of Catalysis*, (1996) **161**, 783.

[54] Climent, M. J.; Corma, A.; Guil-Lopez, R.; Iborra, S.; Primo, J., *Journal of Catalysis*, (1998) **175**, 70.

[55] Corma, A., *Chemical Reviews*, (1997) **97**, 2373.

[56] Zhang, D. S.; Wang, R. J.; Yang, X. X., *Catalysis Communications*, (2011) **12**, 399.

[57] Rac, B.; Molnar, A.; Forgo, P.; Mohai, M.; Bertoti, I., *Journal of Molecular Catalysis a-Chemical*, (2006) **244**, 46.

[58] Sheng, X. Y.; Gao, J. R.; Han, L.; Jia, Y. X.; Sheng, W. J., *Microporous and Mesoporous Materials*, (2011) **143**, 73.

[59] Ghiaci, M.; Aghabarari, B.; Rives, V.; Vicente, M. A.; Sobrados, I.; Sanz, J., *Catalysis Letters*, (2010) **136**, 141.

[60] Kraleva, E.; Saladino, M. L.; Spinella, A.; Nasillo, G.; Caponetti, E., *Journal of Materials Science*, (2011) **46**, 7114.

[61] Rachwalik, R.; Michorczyk, P.; Ogonowski, J., *Catalysis Letters*, (2011) **141**, 1384.

[62] Kozhevnikov, I. V.; Sinnema, A.; Jansen, R. J. J.; Pamin, K.; Vanbekkum, H., *Catalysis Letters*, (1995) **30**, 241.

[63] Corma, A.; Fornes, V.; Martinaranda, R. M.; Garcia, H.; Primo, J., *Applied Catalysis*, (1990) **59**, 237.

[64] Barthomeuf, D., *Catalysis Reviews-Science and Engineering*, (1996) **38**, 521.

[65] Kloetstra, K. R.; Vanbekkum, H., *Journal of the Chemical Society-Chemical Communications*, (1995), 1005.

[66] Albuquerque, M. C. G.; Jimenez-Urbistondo, I.; Santamaria-Gonzalez, J.; Merida-Robles, J. M.; Moreno-Tost, R.; Rodriguez-Castellon, E.; Jimenez-Lopez, A.; Azevedo, D. C. S.; Cavalcante, C. L.; Maireles-Torres, P., *Applied Catalysis a-General*, (2008) **334**, 35.

[67] Sun, H.; Han, J. X.; Ding, Y. Q.; Li, W.; Duan, J. Z.; Chen, P.; Lou, H.; Zheng, X. M., *Applied Catalysis a-General*, (2010) **390**, 26.

[68] Brunel, D.; Cauvel, A.; Fajula, F.; DiRenzo, F., MCM-41 type silicas as supports for immobilized catalysts, In *Zeolites: a Refined Tool for Designing Catalytic Sites*, (1995); Vol. 97, pp 173.

[69] Yokoi, T.; Kubota, Y.; Tatsumi, T., *Applied Catalysis a-General*, (2012) **421**, 14.

[70] Shang, F. P.; Sun, J. R.; Wu, S. J.; Liu, H.; Guan, J. Q.; Kan, Q. B., *Journal of Colloid and Interface Science*, (2011) **355**, 190.

[71] Shao, Y. Q.; Guan, J. Q.; Wu, S. J.; Liu, H.; Liu, B.; Kan, Q. B., *Microporous and Mesoporous Materials*, (2010) **128**, 120.

[72] Shylesh, S.; Thiel, W. R., *Chemcatchem*, (2011) **3**, 278.

[73] Yu, X. F.; Zou, Y. C.; Wu, S. J.; Liu, H.; Guan, J. Q.; Kan, Q. B., *Materials Research Bulletin*, (2011) **46**, 951.

[74] Shang, F. P.; Sun, J. R.; Wu, S. J.; Yang, Y.; Kan, Q. B.; Guan, J. Q., *Microporous and Mesoporous Materials*, (2010) **134**, 44.

[75] Shylesh, S.; Wagner, A.; Seifert, A.; Ernst, S.; Thiel, W. R., *Chemistry-a European Journal*, (2009) **15**, 7052.

[76] Clerici, M. G., *Applied Catalysis*, (1991) **68**, 249.

[77] Bellussi, G.; Carati, A.; Clerici, M. G.; Maddinelli, G.; Millini, R., *Journal of Catalysis*, (1992) **133**, 220.

[78] Huybrechts, D. R. C.; Debruycker, L.; Jacobs, P. A., *Nature*, (1990) **345**, 240.

[79] Blasco, T.; Camblor, M. A.; Corma, A.; Esteve, P.; Martinez, A.; Prieto, C.; Valencia, S., *Chemical Communications*, (1996), 2367.

[80] Corma, A.; Esteve, P.; Martinez, A.; Valencia, S., *Journal of Catalysis*, (1995) **152**, 18.

[81] Camblor, M. A.; Corma, A.; Martinez, A.; Perezpariente, J., *Journal of the Chemical Society-Chemical Communications*, (1992), 589.

[82] Corma, A.; Navarro, M. T.; Pariente, J. P., *Journal of the Chemical Society-Chemical Communications*, (1994), 147.

[83] Corma, A.; Iglesias, M.; Sanchez, F., *Catalysis Letters*, (1996) **39**, 153.

[84] Tanev, P. T.; Chibwe, M.; Pinnavaia, T. J., *Nature*, (1994) **368**, 321.

[85] Zhang, W. H.; Froba, M.; Wang, J. L.; Tanev, P. T.; Wong, J.; Pinnavaia, T. J., *Journal of the American Chemical Society*, (1996) **118**, 9164.

[86] Parvulescu, V.; Su, B. L., *Catalysis Today*, (2001) **69**, 315.

[87] Parvulescu, V.; Anastasescu, C.; Constantin, C.; Su, B. L., Highly selective oxidation of aromatic hydrocarbons (Styrene, Benzene and Toluene) with H2O2 over Ni, Ni-Cr and Ni-Ru modified MCM-41 catalysts, In *Impact of Zeolites and Other Porous Materials on the New Technologies at the Beginning of the New Millennium, Pts a and B*, Aiello, R.; Giordano, G.; Testa, F. Eds.; (2002); Vol. 142, pp 1213.

[88] Parvulescu, V.; Constantin, C.; Su, B. L., *Journal of Molecular Catalysis a-Chemical*, (2003) **202**, 171.

[89] Jia, L. H.; Zhang, S.; Gu, F. N.; Ping, Y.; Guo, X. F.; Zhong, Z. Y.; Su, F. B., *Microporous and Mesoporous Materials*, (2012) **149**, 158.

[90] Wang, G. J.; Zhang, S.; Huang, Y. H.; Kang, F. F.; Yang, Z. X.; Guo, Y. J., *Applied Catalysis a-General*, (2012) **413**, 52.

[91] Shukla, P.; Sun, H. Q.; Wang, S. B.; Ang, H. M.; Tade, M. O., *Catalysis Today*, (2011) **175**, 380.

[92] Carvalho, W. A.; Wallau, M.; Schuchardt, U., *Journal of Molecular Catalysis a-Chemical*, (1999) **144**, 91.

[93] Sakthivel, A.; Selvam, P., *Journal of Catalysis*, (2002) **211**, 134.

[94] Armengol, E.; Corma, A.; Fornes, V.; Garcia, H.; Primo, J., *Applied Catalysis a-General*, (1999) **181**, 305.

[95] Rana, R. K.; Viswanathan, B., *Catalysis Letters*, (1998) **52**, 25.

[96] Rana, S.; Mallick, S.; Parida, K. M., *Journal of Porous Materials*, (2012) **19**, 397.

[97] Bulanek, R.; Kaluzova, A.; Setnicka, M.; Zukal, A.; Cicmanec, P.; Mayerova, J., *Catalysis Today*, (2012) **179**, 149.

[98] Patel, A.; Shukla, P.; Rufford, T.; Wang, S. B.; Chen, J. L.; Rudolph, V.; Zhu, Z. H., *Applied Catalysis a-General*, (2011) **409**, 55.

[99] Chen, L. F.; Hu, J. C.; Qi, Z. W.; Fang, Y. J.; Richards, R., *Industrial & Engineering Chemistry Research*, (2011) **50**, 13642.

[100] Wang, X.; Chen, L. F.; Shang, M.; Lin, F.; Hu, J. C.; Richards, R. M., *Nanotechnology*, (2012) **23**,

[101] Raynor, S. A.; Thomas, J. M.; Raja, R.; Johnson, B. F. G.; Bell, R. G.; Mantle, M. D., *Chemical Communications*, (2000), 1925.

[102] Johnson, B. F. G.; Raynor, S. A.; Shephard, D. S.; Mashmeyer, T.; Thomas, J. M.; Sankar, G.; Bromley, S.; Oldroyd, R.; Gladden, L.; Mantle, M. D., *Chemical Communications*, (1999), 1167.

[103] Lasperas, M.; Bellocq, N.; Brunel, D.; Moreau, P., *Tetrahedron-Asymmetry*, (1998) **9**, 3053.

[104] Bellocq, N.; Abramson, S.; Lasperas, M.; Brunel, D.; Moreau, P., *Tetrahedron-Asymmetry*, (1999) **10**, 3229.

[105] Soai, K.; Niwa, S., *Chemical Reviews*, (1992) **92**, 833.

[106] Soai, K.; Ookawa, A.; Kaba, T.; Ogawa, K., *Journal of the American Chemical Society*, (1987) **109**, 7111.

[107] Bae, S. J.; Kim, S. W.; Hyeon, T.; Kim, B. M., *Chemical Communications*, (2000), 31.

[108] Piaggio, P.; McMorn, P.; Langham, C.; Bethell, D.; Bulman-Page, P. C.; Hancock, F. E.; Hutchings, G. J., *New Journal of Chemistry*, (1998) **22**, 1167.

[109] Amarasekara, A. S.; McNeal, I.; Murillo, J.; Green, D.; Jennings, A., *Catalysis Communications*, (2008) **9**, 2437.

[110] Ji, R. N.; Yu, K.; Lou, L. L.; Gu, Z. C.; Liu, S. X., *Journal of Inorganic and Organometallic Polymers and Materials*, (2010) **20**, 675.

[111] Kuzniarska-Biernacka, I.; Silva, A. R.; Carvalho, A. P.; Pires, J.; Freire, C., *Catalysis Letters*, (2010) **134**, 63.

[112] Lou, L. L.; Yu, Y.; Yu, K.; Jiang, S.; Dong, Y. L.; Liu, S. X., *Science in China Series B-Chemistry*, (2009) **52**, 1417.

[113] Luts, T.; Frank, R.; Suprun, W.; Fritzsche, S.; Hey-Hawkins, E.; Papp, H., *Journal of Molecular Catalysis a-Chemical*, (2007) **273**, 250.

[114] Roy, T.; Kureshy, R. I.; Khan, N.; Abdi, S. H. R.; Sadhukhan, A.; Bajaj, H. C., *Tetrahedron*, (2012) **68**, 6314.

[115] Perez, C.; Perez, S.; Fuentes, G. A.; Corma, A., *Journal of Molecular Catalysis a-Chemical*, (2003) **197**, 275.

[116] Lou, L. L.; Dong, Y. L.; Yu, K.; Jiang, S.; Song, Y.; Cao, S.; Liu, S. X., *Journal of Molecular Catalysis a-Chemical*, (2010) **333**, 20.

[117] Corma, A.; Garcia, H.; Moussaif, A.; Sabater, M. J.; Zniber, R.; Redouane, A., *Chemical Communications*, (2002), 1058.

[118] Park, J. K.; Kim, S. W.; Hyeon, T.; Kim, B. M., *Tetrahedron-Asymmetry*, (2001) **12**, 2931.

[119] Fakhfakh, F.; Baraket, L.; Ghorbel, A.; Fraile, J. M.; Herrerias, C. I.; Mayoral, J. A., *Journal of Molecular Catalysis a-Chemical*, (2010) **329**, 21.

[120] Thomas, J. M.; Maschmeyer, T.; Johnson, B. F. G.; Shephard, D. S., *Journal of Molecular Catalysis a-Chemical*, (1999) **141**, 139.

[121] Whiston, C., *X-Ray Method, John Wiley & Sons*, (1987) **1st ed**,

[122] Kruk, M.; Jaroniec, M., *Chemistry of Materials*, (2001) **13**, 3169.

[123] Brunauer, S.; Emmett, P. H.; Teller, E., *Journal of the American Chemical Society*, (1938) **60**, 309.

[124] Roque-Malherbe, R. M. A., *Adsorption and Diffusion in Nanoporous Materials, Taylor & Francis Group*, (2007) **1st ed**,

[125] Barrett, E. P.; Joyner, L. G.; Halenda, P. P., *Journal of the American Chemical Society*, (1951) **73**, 373.

[126] Braithwaite, A.; Smith, F. J., *Chromatographic Method, Chapman and Hall* (1985) **4th ed**,

[127] Ma, T. S.; Rittner, R. C., *Modern Organic Elemental Analysis, Marcel Dekker, Inc.*, (1979) **1st ed**,

[128] Scheinmann, F., *An Introduction to Spectroscopic Metrhods for the Identification of Organic Compounds, Pergamon Press*, (1970) **1st ed**,

[129] Alpert, N. L.; Keiser, W. E.; Szymanski, H. A., *Theory and Practice of Infrared Spectroscopy, Plentum Press*, (1970) **2nd ed**,

[130] Marcelli, A.; Cricenti, A.; Kwiatek, W. M.; Petibois, C., *Biotechnology Advances*,

[131] http://www.chemistry.oregonstate.edu/courses/ch361-464/ch362/irinstrs.htm, (2012),

[132] Abraham, R. J.; Fisher, J.; Lofus, P., *Introduction to NMR Spectroscopy, John Willey & Sons*, (1991) **2nd ed**,

[133] http://www.pharmacopeia.cn/v29240/usp29nf24s0_c761.html, (2012),

[134] Cai, Q.; Lin, W. Y.; Xiao, F. S.; Pang, W. Q.; Chen, X. H.; Zou, B. S., *Microporous and Mesoporous Materials*, (1999) **32**, 1.

[135] Huang, H. Y.; Yang, R. T.; Chinn, D.; Munson, C. L., *Industrial & Engineering Chemistry Research*, (2003) **42**, 2427.

[136] Huo, Q. S.; Leon, R.; Petroff, P. M.; Stucky, G. D., *Science*, (1995) **268**, 1324.

[137] Kim, M. J.; Ryoo, R., *Chemistry of Materials*, (1999) **11**, 487.

[138] Chen, C. Y.; Burkett, S. L.; Li, H. X.; Davis, M. E., *Microporous Materials*, (1993) **2**, 27.

[139] Huo, Q. S.; Margolese, D. I.; Ciesla, U.; Demuth, D. G.; Feng, P. Y.; Gier, T. E.; Sieger, P.; Firouzi, A.; Chmelka, B. F.; Schuth, F.; Stucky, G. D., *Chemistry of Materials*, (1994) **6**, 1176.

[140] Hyde, S. T., *Pure and Applied Chemistry*, (1992) **64**, 1617.

[141] Henriksson, U.; Blackmore, E. S.; Tiddy, G. J. T.; Soderman, O., *Journal of Physical Chemistry*, (1992) **96**, 3894.

[142] Diaz, I.; Perez-Pariente, J., *Chemistry of Materials*, (2002) **14**, 4641.

[143] Lin, H. P.; Cheng, S. F.; Mou, C. Y., *Journal of the Chinese Chemical Society*, (1996) **43**, 375.

[144] Lin, W. Y.; Cai, Q.; Pang, W. Q.; Yue, Y.; Zou, B. S., *Microporous and Mesoporous Materials*, (1999) **33**, 187.

[145] Mokaya, R.; Zhou, W. Z.; Jones, W., *Chemical Communications*, (1999), 51.

[146] Park, S. E.; Kim, D. S.; Chang, J. S.; Kim, W. Y., *Catalysis Today*, (1998) **44**, 301.

[147] Ryoo, R.; Ko, C. H.; Park, I. S., *Chemical Communications*, (1999), 1413.

[148] Sayari, A.; Liu, P.; Kruk, M.; Jaroniec, M., *Chemistry of Materials*, (1997) **9**, 2499.

[149] Cheng, C. F.; Park, D. H.; Klinowski, J., *Journal of the Chemical Society-Faraday Transactions*, (1997) **93**, 193.

[150] Mokaya, R.; Zhou, W. Z.; Jones, W., *Journal of Materials Chemistry*, (2000) **10**, 1139.

[151] Liu, S. Q.; Cool, P.; Collart, O.; Van der Voort, P.; Vansant, E. F.; Lebedev, O. I.; Van Tendeloo, G.; Jiang, M. H., *Journal of Physical Chemistry B*, (2003) **107**, 10405.

[152] Monnier, A.; Schuth, F.; Huo, Q.; Kumar, D.; Margolese, D.; Maxwell, R. S.; Stucky, G. D.; Krishnamurty, M.; Petroff, P.; Firouzi, A.; Janicke, M.; Chmelka, B. F., *Science*, (1993) **261**, 1299.

[153] Kruk, M.; Cao, L., *Langmuir*, (2007) **23**, 7247.

[154] Zhao, D. Y.; Feng, J. L.; Huo, Q. S.; Melosh, N.; Fredrickson, G. H.; Chmelka, B. F.; Stucky, G. D., *Science*, (1998) **279**, 548.

[155] Berquier, J. M.; Teyssedre, L.; Jacquiod, C., *Journal of Sol-Gel Science and Technology*, (1998) **13**, 739.

[156] Lin, H. P.; Wong, S. T.; Mou, C. Y.; Tang, C. Y., *Journal of Physical Chemistry B*, (2000) **104**, 8967.

[157] Horikawa, T.; Do, D. D.; Nicholson, D., *Advances in Colloid and Interface Science*, (2011) **169**, 40.

[158] Qiao, S. Z.; Bhatia, S. K.; Zhao, X. S., *Microporous and Mesoporous Materials*, (2003) **65**, 287.

[159] Ikeue, K.; Miyoshi, N.; Tanaka, T.; Machida, M., *Catalysis Letters*, (2011) **141**, 877.

[160] Kubota, Y.; Nishizaki, Y.; Ikeya, H.; Saeki, M.; Hida, T.; Kawazu, S.; Yoshida, M.; Fujii, H.; Sugi, Y., *Microporous and Mesoporous Materials*, (2004) **70**, 135.

[161] Peng, Y.; Wang, J. Y.; Long, J.; Liu, G. H., *Catalysis Communications*, (2011) **15**, 10.

[162] Linssen, T.; Cassiers, K.; Cool, P.; Vansant, E. F., *Advances in Colloid and Interface Science*, (2003) **103**, 121.

[163] Lim, M. H.; Blanford, C. F.; Stein, A., *Journal of the American Chemical Society*, (1997) **119**, 4090.

[164] Fowler, C. E.; Lebeau, B.; Mann, S., *Chemical Communications*, (1998), 1825.

[165] Udayakumar, S.; Son, Y. S.; Lee, M. K.; Park, S. W.; Park, D. W., *Applied Catalysis a-General*, (2008) **347**, 192.

[166] Wei, Q.; Nie, Z. R.; Hao, Y. L.; Chen, Z. X.; Zou, J. X.; Wang, W., *Materials Letters*, (2005) **59**, 3611.

[167] Mokaya, R.; Jones, W., *Chemical Communications*, (1997), 2185.

[168] Lasperas, M.; Llorett, T.; Chaves, L.; Rodriguez, I.; Cauvel, A.; Brunel, D., Amine functions linked to MCM-41-type silicas as a new class of solid base catalysts for condensation reactions, In *Heterogeneous Catalysis and Fine Chemicals Iv*, Blaser, H. U.; Baiker, A.; Prins, R. Eds.; (1997); Vol. 108, pp 75.

[169] Yoshitake, H.; Yokoi, T.; Tatsumi, T., *Chemistry of Materials*, (2002) **14**, 4603.

[170] Kubota, Y.; Sugi, Y.; Tatsumi, T., *Catalysis Surveys from Asia*, (2007) **11**, 158.

[171] Kister, O.; Roessner, F., *Journal of Porous Materials*, (2012) **19**, 119.

[172] Matsumoto, A.; Yeoh, F. Y.; Fujihara, S.; Tsutsumi, K.; Baba, T., *Adsorption Science & Technology*, (2006) **24**, 451.

[173] Popa, A.; Sasca, V.; Kiss, E. E.; Marinkovic-Neducin, R.; Holclajtner-Antunovic, I., *Materials Research Bulletin*, (2011) **46**, 19.

[174] Eddaoudi, M.; Kim, J.; Rosi, N.; Vodak, D.; Wachter, J.; O'Keeffe, M.; Yaghi, O. M., *Science*, (2002) **295**, 469.

[175] Walton, K. S.; Snurr, R. Q., *Journal of the American Chemical Society*, (2007) **129**, 8552.

[176] Wang, F.; Guan, Y. F.; Zhang, S.; Xia, Y., *Journal of Chromatography A*, (2012) **1246**, 76.

[177] Antochshuk, V.; Kruk, M.; Jaroniec, M., *Journal of Physical Chemistry B*, (2003) **107**, 11900.

[178] Chong, A. S. M.; Zhao, X. S.; Kustedjo, A. T.; Qiao, S. Z., *Microporous and Mesoporous Materials*, (2004) **72**, 33.

[179] Hodgkins, R. P.; Garcia-Bennett, A. E.; Wright, P. A., *Microporous and Mesoporous Materials*, (2005) **79**, 241.

[180] Hoffmann, F.; Cornelius, M.; Morell, J.; Froba, M., *Journal of Nanoscience and Nanotechnology*, (2006) **6**, 265.

[181] Hoffmann, F.; Cornelius, M.; Morell, J.; Froba, M., *Angewandte Chemie-International Edition*, (2006) **45**, 3216.

[182] Fan, J.; Yu, C. Z.; Gao, T.; Lei, J.; Tian, B. Z.; Wang, L. M.; Luo, Q.; Tu, B.; Zhou, W. Z.; Zhao, D. Y., *Angewandte Chemie-International Edition*, (2003) **42**, 3146.

[183] Kruk, M.; Antochshuk, V.; Matos, J. R.; Mercuri, L. P.; Jaroniec, M., *Journal of the American Chemical Society*, (2002) **124**, 768.

[184] Zapilko, C.; Anwander, R., *Chemistry of Materials*, (2006) **18**, 1479.

[185] Sakamoto, Y.; Kaneda, M.; Terasaki, O.; Zhao, D. Y.; Kim, J. M.; Stucky, G.; Shim, H. J.; Ryoo, R., *Nature*, (2000) **408**, 449.

[186] Garcia-Bennett, A. E.; Willliamson, S.; Wright, P. A.; Shannon, I. J., *Journal of Materials Chemistry*, (2002) **12**, 3533.

[187] Corriu, J. P.; Masse, J. P., *Journal of the Chemical Society-Chemical Communications*, (1972), 144.

[188] Tamao, K.; Sumitani, K.; Kumada, M., *Journal of the American Chemical Society*, (1972) **94**, 4374.

[189] Wright, M. E.; Jin, M. J., *Journal of Organometallic Chemistry*, (1990) **387**, 373.

[190] Li, G. Y.; Marshall, W. J., *Organometallics*, (2002) **21**, 590.

[191] Wolf, J.; Labande, A.; Daran, J. C.; Poli, R., *Journal of Organometallic Chemistry*, (2006) **691**, 433.

[192] Ackermann, L.; Born, R.; Spatz, J. H.; Meyer, D., *Angewandte Chemie-International Edition*, (2005) **44**, 7216.

[193] Lau, S. Y. W.; Hughes, G.; O'Shea, P. D.; Davies, I. W., *Organic Letters*, (2007) **9**, 2239.

[194] Liang, L. C.; Chien, P. S.; Lin, J. M.; Huang, M. H.; Huang, Y. L.; Liao, J. H., *Organometallics*, (2006) **25**, 1399.

[195] Saeki, T.; Takashima, Y.; Tamao, K., *Synlett*, (2005), 1771.

[196] Semeril, D.; Lejeune, M.; Jeunesse, C.; Matt, D., *Journal of Molecular Catalysis a-Chemical*, (2005) **239**, 257.

[197] Yoshikai, N.; Mashima, H.; Nakamura, E., *Journal of the American Chemical Society*, (2005) **127**, 17978.

[198] Lipshutz, B. H.; Tasler, S.; Chrisman, W.; Spliethoff, B.; Tesche, B., *Journal of Organic Chemistry*, (2003) **68**, 1177.

[199] Styring, P.; Grindon, C.; Fisher, C. M., *Catalysis Letters*, (2001) **77**, 219.

[200] Haswell, S. J.; O'Sullivan, B.; Styring, P., *Lab on a Chip*, (2001) **1**, 164.

[201] Phan, N. T. S.; Brown, D. H.; Adams, H.; Spey, S. E.; Styring, P., *Dalton Transactions*, (2004), 1348.

[202] Phan, N. T. S.; Brown, D. H.; Styring, P., *Green Chemistry*, (2004) **6**, 526.

[203] Richardson, J. M.; Jones, C. W., *Journal of Molecular Catalysis a-Chemical*, (2009) **297**, 125.

[204] Dreos, R.; Nardin, G.; Randaccio, L.; Siega, P.; Tauzher, G.; Vrdoljak, V., *Inorganic Chemistry*, (2003) **42**, 6805.

[205] Yeori, A.; Gendler, S.; Groysman, S.; Goldberg, I.; Kol, M., *Inorganic Chemistry Communications*, (2004) **7**, 280.

[206] Kim, J.; Bhattacharjee, S.; Jeong, K.-E.; Jeong, S.-Y.; Ahn, W.-S., *Chemical Communications*, (2009), 3904.

[207] Rosen, B. M.; Quasdorf, K. W.; Wilson, D. A.; Zhang, N.; Resmerita, A.; Garg, N. K.; Percec, V., *Chemical Reviews*, (2011) **111**,

[208] Bhattacharjee, S.; Jeong, K. E.; Jeong, S. Y.; Ahn, W. S., *New Journal of Chemistry*, (2010) **34**, 156.

[209] Li, J. S.; Miao, X. Y.; Hao, Y. X.; Zhao, J. Y.; Sun, X. Y.; Wang, L. J., *Journal of Colloid and Interface Science*, (2008) **318**, 309.

[210] Djakovitch, L.; Wagner, M.; Hartung, C. G.; Beller, A.; Koehler, K., *Journal of Molecular Catalysis a-Chemical*, (2004) **219**, 121.

[211] Glasnov, T. N.; Findenig, S.; Kappe, C. O., *Chemistry-a European Journal*, (2009) **15**, 1001.

[212] Joucla, L.; Cusati, G.; Pinel, C.; Djakovitch, L., *Applied Catalysis a-General*, (2009) **360**, 145.

[213] Lamblin, M.; Nassar-Hardy, L.; Hierso, J. C.; Fouquet, E.; Felpin, F. X., *Advanced Synthesis & Catalysis*, (2010) **352**, 33.

[214] Alcon, M. J.; Corma, A.; Iglesias, M.; Sanchez, F., *Journal of Organometallic Chemistry*, (2002) **655**, 134.

[215] Zhu, R. X.; Shen, J.; Wei, Y. Y.; Zhang, F., *New Journal of Chemistry*, (2011) **35**, 1861.

[216] Tasler, S.; Lipshutz, B. H., *Journal of Organic Chemistry*, (2002) **68**, 1190.

[217] Zhao, X. S.; Lu, G. Q., *Journal of Physical Chemistry B*, (1998) **102**, 1556.

[218] Guerrero, V. V.; Shantz, D. F., *Industrial and Enginering Chemistry Research*, (2009) **48**, 10375.

[219] Muller, C. A.; Maciejewski, M.; Mallat, T.; Baiker, A., *Journal of Catalysis*, (1999) **184**, 280.

[220] Liu, Y. R.; Tu, M. J.; Zhang, J.; Song, Z. R.; Tang, Y., *Microporous and Mesoporous Materials*, (2011) **145**, 182.

[221] Sutra, P.; Fajula, F.; Brunel, D.; Lentz, P.; Daelen, G.; Nagy, J. B., *Colloids and Surfaces a-Physicochemical and Engineering Aspects*, (1999) **158**, 21.

[222] Bendjeriou-Sedjerari, A.; Pelletier, J. D. A.; Abou-Hamad, E.; Emsley, L.; Basset, J. M., *Chemical Communications*, (2012) **48**, 3067.

[223] Yuan, H.; Xu, J. Q.; Xie, L. L., *Materials Chemistry and Physics*, (2011) **129**, 1195.

[224] Asefa, T.; Kruk, M.; MacLachlan, M. J.; Coombs, N.; Grondey, H.; Jaroniec, M.; Ozin, G. A., *Journal of the American Chemical Society*, (2001) **123**, 8520.

[225] Kubota, Y.; Ikeya, H.; Sugi, Y.; Yamada, T.; Tatsumi, T., *Journal of Molecular Catalysis a-Chemical*, (2006) **249**, 181.

[226] Matos, J. R.; Kruk, M.; Mercuri, L. P.; Jaroniec, M.; Zhao, L.; Kamiyama, T.; Terasaki, O.; Pinnavaia, T. J.; Liu, Y., *Journal of the American Chemical Society*, (2003) **125**, 821.

[227] Suzuki, T. M.; Nakamura, T.; Fukumoto, K.; Yamamoto, M.; Akimoto, Y.; Akimoto, Y.; Yano, K., *Journal of Molecular Catalysis a-Chemical*, (2008) **280**, 224.

[228] Bandyopadhyay, M.; Shiju, N. R.; Brown, D. R., *Catalysis Communications*, (2010) **11**, 660.

[229] Pirouzmand, M.; Amini, M. M.; Safari, N., *Journal of Colloid and Interface Science*, (2008) **319**, 199.

[230] Selvam, P.; Dapurkar, S. E., *Catalysis Today*, (2004) **96**, 135.

[231] Lv, C. W.; Xu, D. Q.; Wang, S. F.; Miao, C. X.; Xia, C. G.; Sun, W., *Catalysis Communications*, (2011) **12**, 1242.

[232] Lv, W. F.; Wang, Y. R.; Wu, B.; Yao, Y. M.; Shen, Q., *Zeitschrift Fur Anorganische Und Allgemeine Chemie*, (2012) **638**, 1167.

[233] Pandey, R.; Ribas, J.; Corbella, M.; Pandey, D. S., *Indian Journal of Chemistry Section a-Inorganic Bio-Inorganic Physical Theoretical & Analytical Chemistry*, (2011) **50**, 1450.

[234] Romero, M. J.; Pedrido, R.; Gonzalez-Noya, A. M.; Maneiro, M.; Fernandez-Garcia, M. I.; Zaragoza, G.; Bermejo, M. R., *Dalton Transactions*, (2012) **41**, 10832.

[235] Seth, P.; Das, L. K.; Drew, M. G. B.; Ghosh, A., *European Journal of Inorganic Chemistry*, (2012), 2232.

[236] Gu, L.; Zhang, A. F.; Hou, K. K.; Dai, C. Y.; Zhang, S. G.; Liu, M.; Song, C. S.; Guo, X. W., *Microporous and Mesoporous Materials*, (2012) **152**, 9.

[237] Li, Y.; Guan, Y. J.; van Santen, R. A.; Kooyman, P. J.; Dugulan, I.; Li, C.; Hensen, E. J. M., *Journal of Physical Chemistry C*, (2009) **113**, 21831.

[238] Song, H.; Rioux, R. M.; Hoefelmeyer, J. D.; Komor, R.; Niesz, K.; Grass, M.; Yang, P. D.; Somorjai, G. A., *Journal of the American Chemical Society*, (2006) **128**, 3027.

[239] Celer, E. B.; Jaroniec, M., *Journal of the American Chemical Society*, (2006) **128**, 14408.

[240] Celer, E. B.; Jaroniec, M., *Abstracts of Papers of the American Chemical Society*, (2007) **233**, 752.

[241] Chen, G. Q.; Zheng, Y.; Zheng, X. L.; Shen, X. N., *Journal of Porous Materials*, (2009) **16**, 361.

[242] Shironita, S.; Takasaki, T.; Kamegawa, T.; Mori, K.; Yamashita, H., *Catalysis Letters*, (2009) **129**, 404.

[243] Tian, B. Z.; Liu, X. Y.; Yang, H. F.; Xie, S. H.; Yu, C. Z.; Tu, B.; Zhao, D. Y., *Advanced Materials*, (2003) **15**, 1370.

[244] Furtado, A. M. B.; Liu, J.; Wang, Y.; Levan, M. D., *Journal of Materials Chemistry*, (2011) **21**, 6698.

[245] Huang, C. H.; Chang, K. P.; Ou, H. D.; Chiang, Y. C.; Wang, C. F., *Microporous and Mesoporous Materials*, (2011) **141**, 102.

[246] Lu, S.; Song, Z. H.; He, J., *Journal of Physical Chemistry B*, (2011) **115**, 7744.

[247] Okada, K.; Yoshizawa, A.; Kameshima, Y.; Isobe, T.; Nakajima, A.; Mackenzie, K. J. D., *Journal of Porous Materials*, (2011) **18**, 345.

[248] Wei, K.; Shu, L. J.; Guo, W. S.; Wu, Y. A.; Zeng, X. F., *Chinese Journal of Chemistry*, (2011) **29**, 143.

[249] Jang, K. S.; Kim, H. J.; Johnson, J. R.; Kim, W. G.; Koros, W. J.; Jones, C. W.; Nair, S., *Chemistry of Materials*, (2011) **23**, 3025.

[250] Li, X. S.; Su, X.; Zhu, G. T.; Zhao, Y.; Yuan, B. F.; Guo, L.; Feng, Y. Q., *Journal of Separation Science*, (2012) **35**, 1506.

[251] Paik, P.; Gedanken, A.; Mastai, Y., *Microporous and Mesoporous Materials*, (2010) **129**, 82.

[252] Wang, Z.; Fang, D. M.; Li, Q.; Zhang, L. X.; Qian, R.; Zhu, Y.; Qu, H. Y.; Du, Y. P., *Analytica Chimica Acta*, (2012) **725**, 81.

[253] Zhang, M.; Wu, Y. P.; Feng, X. Z.; He, X. W.; Chen, L. X.; Zhang, Y. K., *Journal of Materials Chemistry*, (2010) **20**, 5835.

[254] Bruzzoniti, M. C.; De Carlo, R. M.; Fiorilli, S.; Onida, B.; Sarzanini, C., *Journal of Chromatography A*, (2009) **1216**, 5540.

[255] Galarneau, A.; Lapichella, J.; Brunel, D.; Fajula, F.; Bayram-Hahn, Z.; Unger, K.; Puy, G.; Demesmay, C.; Rocca, J. L., *Journal of Separation Science*, (2006) **29**, 844.

[256] Mesa, M.; Sierra, L.; Lopez, B.; Ramirez, A.; Guth, J. L., *Solid State Sciences*, (2003) **5**, 1303.

[257] Wan, H. H.; Liu, L.; Li, C. M.; Xue, X. Y.; Liang, X. M., *Journal of Colloid and Interface Science*, (2009) **337**, 420.

[258] Jin, Z.; Zhang, X. B.; Xie, D. X.; Gong, Y. J.; Zhang, J.; Chen, X.; Shen, G. L.; Yu, R. Q., *Analytical Chemistry*, (2010) **82**, 6343.

[259] Lei, J. Y.; Wang, L. Z.; Zhang, J. L., *Chemical Communications*, (2010) **46**, 8445.

[260] Lu, D. L.; Yang, L. G.; Tian, Z. D.; Wang, L. Z.; Zhang, J. L., *Rsc Advances*, (2012) **2**, 2783.

[261] Wang, F. G.; Yang, J. Q.; Wu, K. B., *Analytica Chimica Acta*, (2009) **638**, 23.

[262] Xu, X. M.; Liu, Z.; Zhang, X.; Duan, S.; Xu, S.; Zhou, C. L., *Electrochimica Acta*, (2011) **58**, 142.

[263] Lu, J.; Li, Z. X.; Zink, J. I.; Tamanoi, F., *Nanomedicine-Nanotechnology Biology and Medicine*, (2012) **8**, 212.

[264] Mamaeva, V.; Rosenholm, J. M.; Bate-Eya, L. T.; Bergman, L.; Peuhu, E.; Duchanoy, A.; Fortelius, L. E.; Landor, S.; Toivola, D. M.; Linden, M.; Sahlgren, C., *Molecular Therapy*, (2011) **19**, 1538.

[265] Pan, L. M.; He, Q. J.; Liu, J. N.; Chen, Y.; Ma, M.; Zhang, L. L.; Shi, J. L., *Journal of the American Chemical Society*, (2012) **134**, 5722.

[266] Pang, J.; Luan, Y.; Yang, X.; Jiang, Y.; Zhao, L.; Zong, Y.; Li, Z., *Mini-Reviews in Medicinal Chemistry*, (2012) **12**, 775.

[267] Yang, P. P.; Gai, S. L.; Lin, J., *Chemical Society Reviews*, (2012) **41**, 3679.

[268] Yuan, L.; Tang, Q. Q.; Yang, D.; Zhang, J. Z.; Zhang, F. Y.; Hu, J. H., *Journal of Physical Chemistry C*, (2011) **115**, 9926.